Bonding Behavior of Biodegradable Films Composed of Hydrophobically Modified Gelatin on Soft Tissues under Wet Condition

KEIKO YOSHIZAWA
Doctoral Program in Materials Science and Engineering

Submitted to the Graduate School of
Pure and Applied Sciences
in Partial Fulfillment of the Requirements
for the Degree of Doctor of Philosophy
in Engineering

at the
University of Tsukuba

Content

Chapter 2

Bonding Behavior of Hydrophobically Modified Gelatin Films on the Intestinal Surface----------16-30

Chapter 3

Chapter 4

Enhance Angiogenesis of Growth Factor-Free Porous Biodegradable Adhesive Made by Hexanoyl Group Modified Gelatin----------47-69

Chapter 5

Pore Size Impact on Angiogenesis and Bonding Strength in Hexanoyl Group Modified Gelatin Adhesive Film---------- 70-91

Chapter 6

Chapter 1

General Introduction

1.1. Wound Care

1.1.1. Wound Dressing

Wound care after accidents and/or surgery requires quick hemostasis. In many cases, sutures are applied to occlude the wound; however, tissues with high fluid and/or gas pressure, such as the aorta and intestine, require further treatment to the prevent leakage from the area (Figure 1.1).

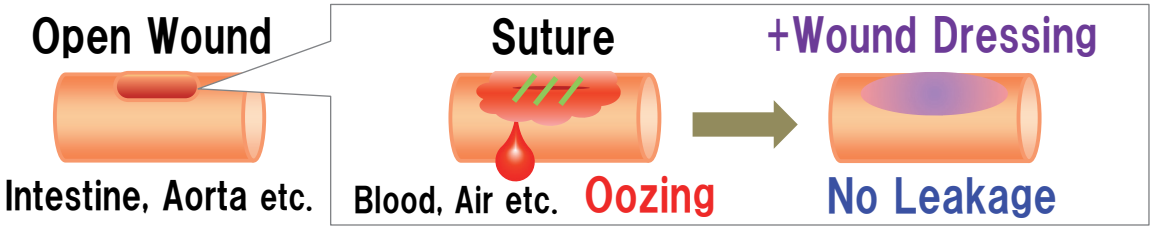

Figure 1.1. Wound care.

Wound dressing has been widely applied to quicken hemostasis, to supply a moist environment around the wounds, and to reinforce the sutured site. There are several wound dressings in practical use, including hydrocolloid, polyurethane foam, alginate, hydrogel, and hydropolymer materials[1]. Currently, the application of these manufactured products is not intended for use beyond hemostasis, and several aspects of their application can be improved upon.

1.2. Adhesives

Today, wound dressings with features beyond hemostasis and fluid/gas leakage prevention are being studied[1]. Dressings with strong adhesion to wet tissue, hemostasis, and reinforcement properties will eventually replace sutures and save time in the operating room (Figure 1.2A). Moreover, new materials under investigation can bind different tissues and can offer the appropriate environment for tissue/cell proliferation (Figure 1.2B).

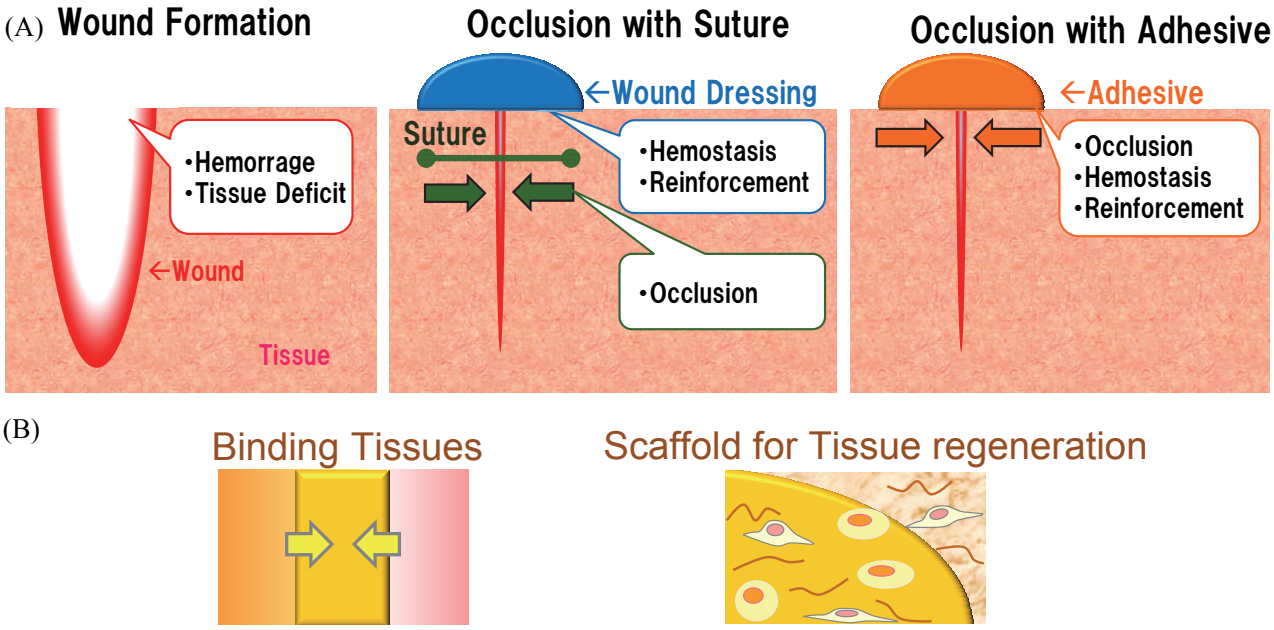

Figure 1.2. Wound dressing with adhesion ability (A) and the expected roles for adhesives (B).

1.2.1. Essences of Adhesives

Adhesives used for surgery have set requirements for their practical application (Table 1.1), and there are some critical points that must be improved: bulk strength (crosslinkings and crosslinkers), interfacial interaction strength, and composition (polymer morphology and polymer origin). The physical property of bonding strength and the following properties are the basic points for adhesion. Preventing infection and inflammation are two keys for biomaterials. Resolution of a wound cannot be attained without some immunogenic drawbacks *in vivo*. In addition, materials should possess appropriate biodegradability to not leave a scar upon healing. Finally, the handling and cost of the biomaterials must be taken into account.

Table 1.1. Essence for clinical adhesives

Requirements	Conditions to be improved
Bonding strength	Bulk strength (Crosslinking), Interfacial interaction etc.
Following property	Bulk strength (Crosslinking), Polymer morphology, etc.
Infection prohibition	Protein derived polymer, Sterilization, Application place etc.
Inflammation prohibition	Polymer morphology etc.
Degradability	Polymer morphology, Crosslinking etc.
Handling	Polymer origin, Crosslinker etc.
Cost	Polymer origin, Crosslinker etc.

1.2.1.1. Bonding Strength

Bonding strength depends on the bulk strength of adhesives and on the adhesive-tissue interfacial strength. These elements are crucial determinants of how adhesion failures occur. Appropriate bulk strength and interfacial strength results in cohesive failure inside the adhesive and adherend failure inside the adherend. In contrast, with inappropriate bulk strength and interfacial strength, interfacial failure should occur between the adhesive and the adherend. A combination of these three failures causes complex failure (Figure 1.3).

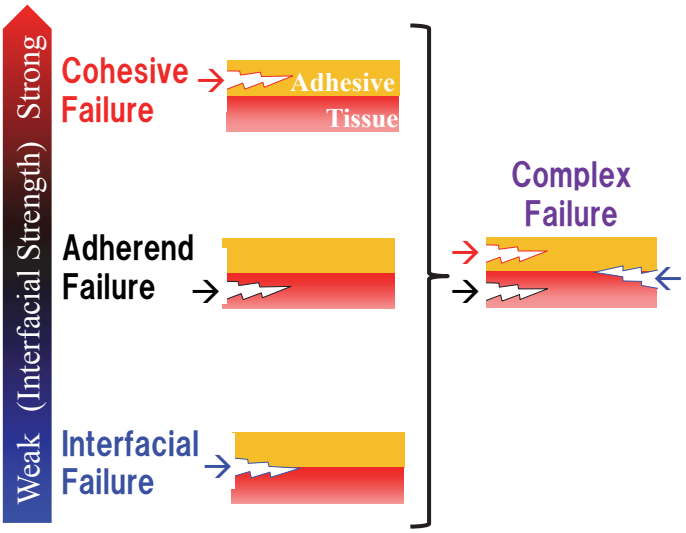

Figure 1.3. Bonding failure styles.

Adhesives also require similar bulk strength to the adherend, while inappropriate bulk strength induces weak adhesion (Table 1.2).

Table 1.2. Relation between bulk/interfacial strength and bonding failure

Bulk Strength	Interfacial Strength	Bonding Failure	Bonding Strength
Adherend > Adhesive	Weak	Interfacial	Weak
	Strong	Cohesive	Weak
Adherend = Adhesive	Weak	Interfacial	Weak
	Strong	**Complex**	**Strong**
Adherend < Adhesive	Weak	Interfacial	Weak
	Strong	Adherend	Weak

1.2.1.2. Bulk Strength

As described above, bulk strength is the critical element for adhesives, and bulk strength or material stiffness is influenced by the crosslinking level between the adhesive base molecules and by molecular structure.

Crosslinking is crucial for combining adhesive compositions and tissue surface. Moreover, the crosslinking level decides both adhesive properties that is required for elastic tissue/organ application and adhesive bulk strength (Figure 1.4). Moreover, as described above, bulk strength also results in strong bonding ability because strong adhesion requires equivalent stiffness between the adherent and adhesive.

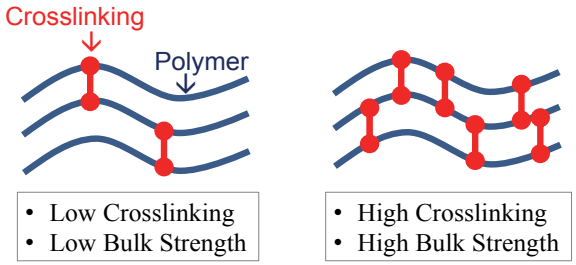

Figure 1.4. Crosslinking effect on bulk strength

Table 1.3. Crosslinking methods

Crosslinking Methods	Advantages	Disadvantages
Electronic beam crosslinking	Simple and easy Sterilization Low toxicity	Polymer denaturation Device requirement Difficult crosslinking regulation
Gamma ray crosslinking		
UV light crosslinking		
Cryogelation	Low polymer denaturation Low toxicity	Time consuming
Thermal crosslinking	Simple and easy Low toxicity	Polymer denaturation/degradation Device-requirement Difficult crosslinking regulation
Chemical crosslinking	Easy crosslinking regulation Easy functional modification	(High toxicity) Composition alteration

There are several major crosslinking methods such as electronic beam crosslinking, gamma ray crosslinking, UV light crosslinking, cryogelation, thermal crosslinking, and chemical crosslinking (Table 1.3). All of them have advantages as well as disadvantages.

Chemical crosslinkers can easily regulate the crosslinking level by altering the amount of crosslinker. In addition, functional modification of polymers by crosslinkers has been reported. The insertion of the chemical compounds and the subsequent generation of byproducts are potential disadvantages.

On the other hand, electronic beam crosslinking, gamma ray crosslinking, UV light crosslinking, and thermal crosslinking are simple to execute. These methods mainly release H_2O and CO_2, and are harmless. In addition, electronic beam crosslinking, gamma ray crosslinking, and UV light treatment sterilizes the materials.

However, difficulty in crosslinking level, denaturation of some polymers, and the requirement of devices are the disadvantages of these methods.

Cryogelation is superior in retaining polymer morphology and has low toxicity at levels reasonable in tissues and/or cells. The disadvantage of this method is that it is time consuming and the product has weak bulk strength[2].

As every method has drawbacks and advantages, the appropriate crosslinking method should be selected for each specific purpose[3].

1.2.1.3. Interfacial Strength

Interfacial interaction is also an important factor in creating strong bonding[4]. Stronger interfacial bonding results from strong interfacial interactions and large regions of interfacial interaction. Forces that drive the reinforcement of interface strength include chemical and physiological interactions. These are described in section 1.2.2.3.

1.2.2. Classification of Adhesives

Current medical adhesives under development can be classified by conformation, composition, and conception (Table 1.4). Choosing appropriate conformation and composition is important for effective wound treatment. Various conceptions for adhesives have been proposed and studied as follows:

Table 1.4. Classification of adhesives

Classification	Type
Conformation	Liquid/Splay
	Gel
	Powder
	Film
Composition	Polymer
	Crosslinker
Conception	Biomimetic
	Natural materials
	Nano materials

1.2.2.1. Adhesive Conformation

Adhesive conformation is crucial for handling under real-life circumstances. The important point is to select the conformation best for the purpose, which may include deep scars, superficial injuries, with/without

quantity requirement[5]. For instant, for small wound liquid adhesives can cover all the area, however, for large wound, solid adhesives will be handy to cover the surface.

Liquid/Splay Type Adhesives: Liquid and spray adhesives are superior in adhering with high infiltration properties[6], and are also the crosslinking level can be easily regulated. The disadvantage of the liquid/spray type adhesives is that their preparation is not trivial. All of the ingredients, including the solvent, base polymer, and crosslinker must be mixed in order. Effusion of the liquid/spray adhesives from the wound should be also avoided.

Gel Type Adhesives: Gel type adhesives are time-saving, and have the advantage of being already wet. However, have weak bulk strength. Gel type adhesives are dependent on crosslinkers for adhesion, and have mainly been researched for use in tissue engineering applications[7, 8].

Powder Type Adhesives: The powder type adhesives are easy to sterilize by UV treatment and have higher wettability compared to membrane type adhesives[9, 10]. In addition, when sustained in dried state, they are easier to store. However, for reaction initiation, these adhesives require a driving force such as body fluid, and too much body fluid may reduce bulk strength.

Membrane Type Adhesives: Membrane type adhesives are easy to handle at the time of application. Time is saved in the pre-mixing process, and these adhesives can be stored longer than others without adhesive base denaturation. The membranes can be readily regulated its 3D constitution. Two 3D types are well known—mesh structured and pore structured (Table 1.5).

Table 1.5. Spatial structure of membrane shaped materials

Membrane Style	**Flat**	**Pored**	**Meshed**
			
Wall Thickness	Very thick	Thin~Thick	Thin
Pore Size Control	-	Easy	Hard

In addition, its inner connection through holes considerably improves tissue reactions compared to flat adhesives[11-13]. Nutrients and wastes can be transferred through the membrane via the holes. Importantly, cells and cytokines can also pass through the holes and result in the establishment of a new extracellular matrix (ECM). The effect of the pores has also been studied in the context of clinical applications and tissue engineering.

1.2.2.2. Adhesive Composition

Adhesive Base: The adhesive base is classified into biopolymers and synthetic polymers (Table 1.6). Biopolymers include proteins and polysaccharides. The proteins can be further classified into human-derived and other animal-[14] or plant-derived. The origin of the adhesive base can influence infection, cost, and

biocompatibility. In an attempt to ameliorate the existing disadvantages, some polymers were blended and applied as an adhesive base[5].

Table 1.6. Adhesive bases and their origins

Adhesive Bases		Examples	Immunogenicity	Infection	Cost	Degradability
Biopolymers	Proteins	Collagen Gelatin Fibrin Albumin Keratin etc.	Low	High	High	High
	Poly saccharides	Chitosan Alginate Chondroitin sulfate Dextran aldehyde etc.	Low/Middle	Low	Middle	Low/Middle
Synthetic polymer		Polyurethane PCL Cyanoacrylate Dendrimer etc.	Middle/High	Low	Low	Low

Adhesive bases derived from proteins have high affinity for human tissues[15]. Collagen, which is composed of gelatin, is the most abundant resource in our body[16]. Cells can react to materials such as gelatin, elastin, and keratin via a binding site known the Arg-Gly-Glu (RGD) structure[17]. Fibrin and albumin are enriched in blood. Fibrin mediates thrombocyte adhesion facilitating hemostat: fibrin adhesives adopt the fibrin property of hemostat mechanism[18]. Albumin is the serum derived protein and the amino groups are used for crosslinking cite.

Adhesive bases derived from animals, especially from humans, show low immunogenicity, high biodegradability, and low inflammatory properties[19], although they carry high risk of infection. In contrast to proteins, synthesized bases are low/not biocompatible and are immunogenic with low biodegradability; however, they are economical and carry a low risk of infection. Polysaccharide derivatives[20, 21] show intermediate properties between the protein derivatives and synthetic polymers.

Crosslinker: Fibrin, cyanoacrylate, aldehyde, and EDC-NHS are the chemical crosslinkers frequently used in medical adhesives. Genipin, derived from plants, and citric acid derived crosslinker (trisuccinimidyl citrate: TSC) are promising crosslinkers with high biocompatibility and great bonding strength (Table 1.7).

Table 1.7. Chemical crosslinkers

Crosslinker	Immuno-genicity	Infection	Reaction	Adhesion	Notes
Cyanoacrylate	High	Low	Fast	Strong	By-product: formaldehyde
N-Hydroxysuccinimide(NHS)-ester					
Carbodiimide (EDC)	Low				
Glutaraldehyde	High				By-product: Aldehyde
Genipin	Low		Slow		Under Study
Fibrin		High	Middle	Weak	
Citric acid derived crosslinker (TSC)		Low	Fast	Strong	Commercially unavailable

Cyanoacrylate and aldehyde crosslinkers including glutaraldehyde, acetaldehyde, and formaldehyde are effective in crosslinking, are economical, and carry low risk of infection due to their synthetic origin[22]. However, cyanoacrylate leaves formaldehyde as a byproduct, and aldehyde crosslinkers leave aldehyde as a byproduct. These byproducts can induce inflammation *in vivo*. In spite of the toxicity, these crosslinkers are often used for clinical operations due to their superior adhesivity.

N-hydroxysuccinimide (NHS) ester and ethyl(dimethylpropyl)carbadiimide (EDC) are typically used simultaneously in crosslinker syntheses[23]. EDC shows low immunogenicity and destabilizes carboxyl groups, thereby improving effective NHS introduction. NHS stabilizes active esters and shows acridity owing to its acidity.

Genipin is a plant-derived crosslinker that shows low toxicity and strong adhesion but slower crosslinking that can occur over three days. Furthermore, its regulation of crosslinking level is still unclear[24].

Fibrin is applied in practical treatment. Derived from plasma, fibrin is less immunogenic and highly metabolic, but can be infectious and shows low bonding strength to tissue[25]..

1.2.2.3. Adhesive Conception

Current studies report several adhesives bonding strongly to tissues with little to no dependence on chemical crosslinker. These materials can be divided into three types of adhesives: biomimetic adhesives, naturally derived adhesives, and nanomaterials (Figure 1.6). The driving forces behind each adhesion can be categorized into van der Waals' force and hydrogen bonding between the materials and the tissues (Table 1.8).

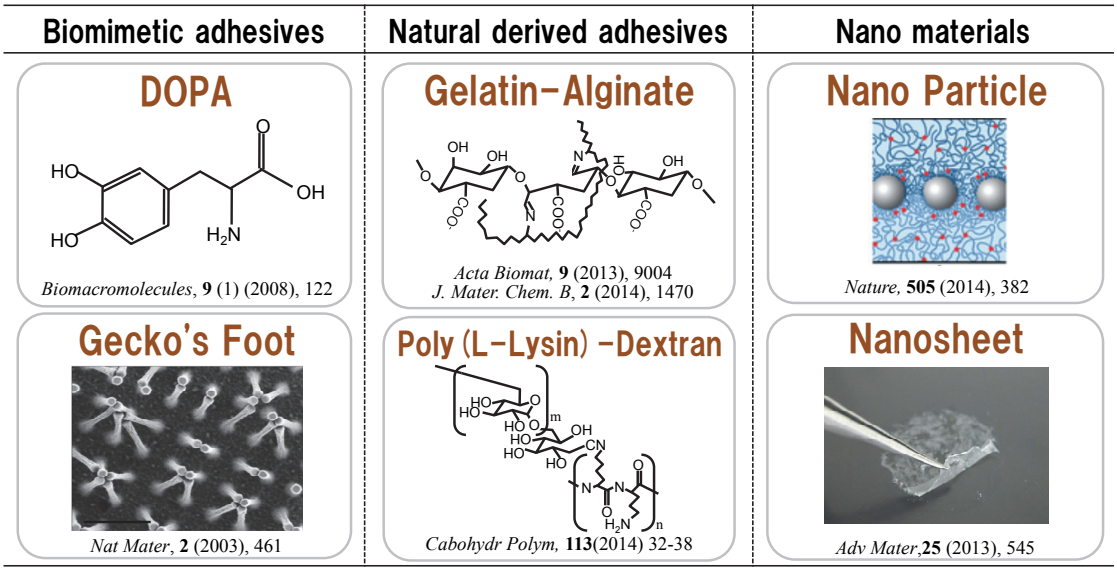

Figure 1.6. Conceptions of adhesives

Biomimetic Adhesives: The biomimetic adhesives include dihydroxyphenylalanine (DOPA) and Gecko's foot, both of which have high adhesion ability. The adhesion mainly depend s on the morphologies of the bonds.

DOPA is molecularly identical to mussel retinaculum[4,26]. Mussel adheres strongly to ship hulls by secreting adhesive substances, a property that could be attributed to its catechol molecular geometry. The water-resistant characteristic of DOPA has attracted much attention for its potential application to wet tissue[27-29].

Geckos climb walls without secreting any sticky substance from its limbs, under both wet and dry conditions. Besides, the stickiness is retained semi-permanently, while the stickiness of other adhesives is weaken owing to the condition and repeats of sticking and stripping. The adhesivity is due to its hand-like geometry at micro scale. The geometry imitations of the geckos foot are still under on-going research[4, 30, 31].

Natural Derived Adhesives: Natural resources with strong bonding properties also exist. They are different from biomimetic adhesives, and these natural derived adhesives are put into practice those original ingredients with some processing like mixing with other materials and qualifications to combine merits of the natural resources and the other materials. .

Alginate[32-34] is a component of seaweed and is widely used in medication, primarily as a hemostatic agent. Owing to its origin, the material shows low immunogenicity and low risk of infection. The solubility of original alginate is very low and it is neutralized by alkaline dosage. Therefore, alginate is used in controlled release medications.

Dextran is a polysaccharide produced by a lactic acid bacterium. Combining it with poly (L-lysine) causes it to undergo the Schiff reaction and results in gelation[35]. Dextran shows antibacterial properties owing to its ionic absorption and destructive interaction with the bacterial membrane.

Nanomaterials: Nanosheet[36-39] and Nano particles[40] comprise a class called nanomaterials. Their adhesive ability is mainly derived from van der Waals' forces. These materials can be fabricated from various polymers including artificial ones like PCL and natural ones like collagen[41]. Microneedle conception is a relatively new mechanism in which anchor the needles in tissue by needles-swelling at its stinging place[4, 42].

Table 1.8. Adhesives and those driving forces of tissue bonding

Driving Force	Material Examples
Van der Waals' force	Nano Sheet Nano Particle Gecko's Foot
Hydrogen bond	DOPA
Interlocking	Microneedle
Chemical bond	Crosslinker
Hydrophobical interaction Anchoring	Hydrophobically modified gelatin

1.3. Hydrophobically Modified Gelatin Solution and TSC Crosslinker

1.3.1. Hydrophobically Modified Gelatins

To develop materials with biocompatibility and strong bonding ability, hydrophobically modified gelatin (hm-Gltn) adhesives have been researched. The main source of gelatin is porcine skin. Gelatin is widely used and studied in clinical applications and is well known for its good biodegradability and lack of inflammatory response. The potency of hydrophobic group modification of polymers has been clarified to improve tissue interaction, and the hm-Gltns have been developed with a hypothesis such that combining them will result in new materials with superb adhesivity[43-46].

1.3.2. TSC Crosslinker

The citric acid-derived crosslinker TSC was also developed in an attempt to generate a material with low cytotoxicity and effective crosslinking. Citric acid is abundant in our bodies and is one of main components in the aerobic metabolism cycle, also known as the citric acid cycle. The molecular structure of this compound includes three carboxyl tails that are modified with highly reactive n-hydroxysuccinimide (NHS) groups. With these characteristics, TSC can effectively crosslink polymers through amino groups and can be smoothly metabolized after adhesive biodegradation (Figure 1.7) [47].

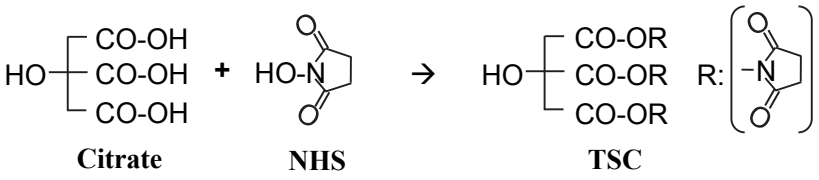

Figure 1.7. Citrate derived crosslinker: TSC.

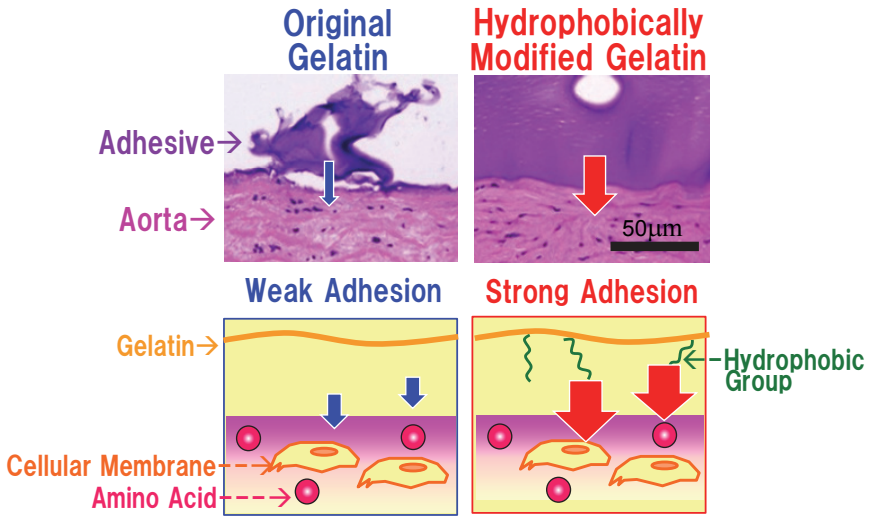

Figure 1.8. Adhesion between wet tissue and original/hydrophobically-modified gelatin-'liquid' adhesive.

Hm-Gltn 'liquid' adhesives crosslinked by TSC were reported to have superior bonding ability to wet tissue with suitable crosslinking speed and low inflammatory response *in vivo*. The bonding strength dependence on the hydrophobic group and the modification ratio are now clear. The hydrophobic interaction between hm-Gltn and cells or tissue combined with the anchoring effect of the hydrophobic group into lipid membranes are thought to be the driving forces of strong adhesion.

1.4. Purpose and Objective of This Study

Fabrication of an ideal adhesive with strong bonding ability, good biocompatibility, and effectiveness in wound treatment requires further molecular design. Achieving adhesiveness is also necessary. However, only few materials currently meet these requirements. As described above, the liquid adhesive composed of hm-Gltn base and the TSC crosslinker is good candidate with strong bonding ability to wet tissue, and shows superb biocompatibilities *in vitro* and *in vivo*.

Meanwhile, the bonding ability to wet tissues and other properties of the hydrophobically modified gelatin adhesive in film condition remains unclear. On the other hand, various studies of tissue regeneration using biomaterials been carried out. Cellular differentiation control by scaffold structures, angiogenesis induction by growth factor dosage, and material-cellular transplanting have all been examined. Therefore, further uses including tissue regeneration can be expected for film adhesives with previously arranged structures.

Given this background, the current research was focused on the bonding properties and the tissue reaction to 'film' adhesives fabricated with hm-Gltn. We investigated the hydrophobic group length effect, the bulk strength effect, and the special structure effect of the hm-Gltn films (Figure 1.9).

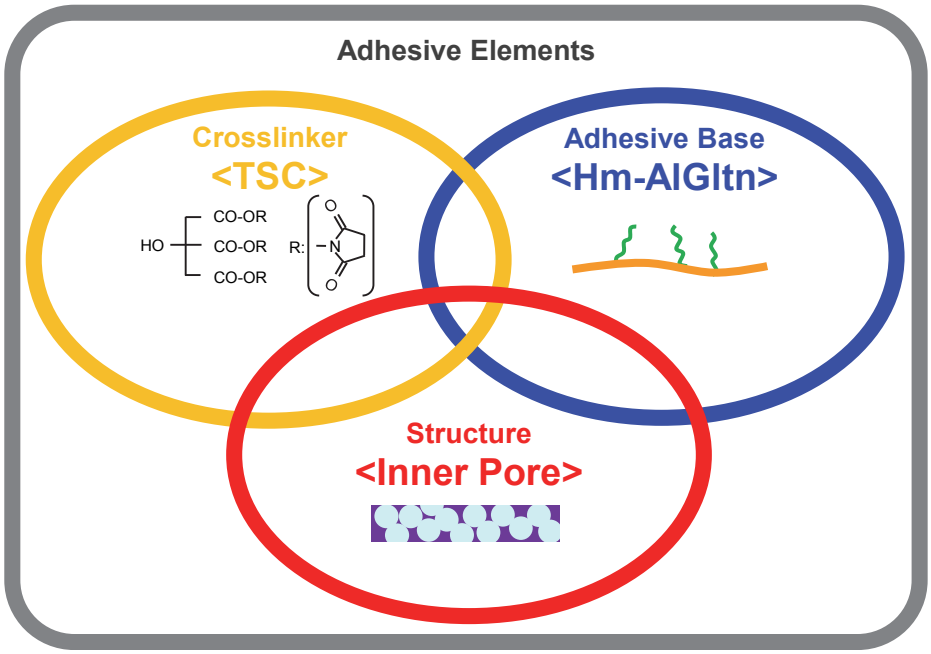

Figure 1.9. Adhesive elements and the candidates employed in this research.

1.5. References

1. Mayet N, Choonara YE, Kumar P, et al. A Comprehensive Review of Advanced Biopolymeric Wound Healing Systems. *J Pharmaceut Sci* **103**(8), 2211-2230 (2014).
2. Takei T, Nakahara H, Ijima H, Kawakami K. Synthesis of a chitosan derivative soluble at neutral pH and gellable by freeze–thawing, and its application in wound care. *Act Biomater* **8**(2), 686-693 (2012).
3. Hayashi T. Biomedicl Applications of Adhesives. *接着学会誌*. **70**(2), 19-23 (2001).
4. Bouten PJM, Zonjee M, Bender J, et al. The chemistry of tissue adhesive materials. *Prog Polym Sci* **39**(7), 1375–1405 (2014).
5. Peng HT, Shek PN. Novel wound sealants: biomaterials and applications. *Exp Rev Med Dev* **7**(5), 639-659 (2010).
6. Randall, Lyman MD, Edelman PG, Campbell PK. Evaluation of the SprayGel™ adhesion barrier in the rat cecum abrasion and rabbit uterine horn adhesion models. *Fertil Steril* **75**(2), 411-416 (2001).
7. Camci-Unal G, Cuttica D, Annabi N, Demarchi D, Khademhosseini A. Synthesis and characterization of hybrid hyaluronic acid-gelatin hydrogels. *Biomacromolecules* **14**(4), 1085-1092 (2013).
8. Park KM, Lee Y, Son JY, Oh DH, Lee JS, Park KD. Synthesis and characterizations of in situ cross-linkable gelatin and 4-arm-PPO-PEO hybrid hydrogels via enzymatic reaction for tissue regenerative medicine. *Biomacromolecules* **13**(3), 604-611 (2012).
9. Arnaud F, Teranishi K, Tomori T, Carr W, McCarron R. Comparison of 10 hemostatic dressings in a groin puncture model in swine. *J Vascul Surg* **50**(3), 632-639 (2009).
10. Oz MC, Rondinone JF, Shargill NS. Floseal Matrix. *J Card Surg***18**(6), 486-493 (2003).
11. Li CQ, Huang B, Luo G, Zhang CZ, Zhuang Y, Zhou Y. Construction of collagen II/hyaluronate/chondroitin-6-sulfate tri-copolymer scaffold for nucleus pulposus tissue engineering and preliminary analysis of its physico-chemical properties and biocompatibility. *J Mater Sci Mater Med* **21**(2), 741-751 (2010).
12. Messias AD, Lucchesi C, Coraça-Huber DC, Filho AP, Duek EAR. Lithograph-moulded poly-L-co-D,L lactide porous membranes for osteoblastic culture. *Mater Res* **17**, 7-15 (2014).
13. Lawrence BJ, Madihally SV. Cell colonization in degradable 3D porous matrices. *Cell Adhes Migrat* **2**(1), 9-16 (2008).
14. Bode F, da Silva MA, Drake AF, Ross-Murphy SB, Dreiss CA. Enzymatically cross-linked tilapia gelatin hydrogels: physical, chemical, and hybrid networks. *Biomacromolecules* **12**(10), 3741-3752 (2011).
15. Karim AA, Bhat R. Review Fish gelatin: properties, challenges, and prospects as an alternative to mammalian gelatins. *Food Hydrocol* **23**, 563-576 (2009).
16. Zaupa A, Neffe AT, Pierce BF, Nochel U, Lendlein A. Influence of tyrosine-derived moieties and drying conditions on the formation of helices in gelatin. *Biomacromolecules* **12**, 75-81 (2011).
17. Hersel U, Dahmen C, Kessler H. RGD modified polymers: biomaterials for stimulated cell adhesion and beyond. *Biomaterials***24**(24), 4385-4415 (2003).
18. Lang G. Efficacy and safety of topical application of human fibrinogen/thrombin-coated collagen patch (TachoComb) for treatment of air leakage after standard lobectomy. *Eur J Cardiothorac Surg* **25**(2),

160-166 (2004).

19. Thirupathi Kumara Raja S, Thiruselvi T, Sailakshmi G, Ganesh S, Gnanamani A. Rejoining of cut wounds by engineered gelatin-keratin glue. *Biochimica Biophysic Acta* **1830**(8), 4030-4039 (2013).
20. Jayakumar R, Prabaharan M, Sudheesh Kumar PT, Nair SV, Tamura H. Biomaterials based on chitin and chitosan in wound dressing applications. *Biotechnol Adv* **29**(3), 322-337 (2011).
21. Wang D, Varghese S, Sharma B, et al. Multifunctional chondroitin sulphate for cartilage tissue-biomaterial integration. *Nat Mater* **6**(5), 385-392 (2007).
22. Leonard F, Kulkarni RK, Nelson J, Brandes G. Tissue Adhesives and Hemostasis-Inducing Compounds. The Alkyl Cyanoacrylates. *J Biomed Mater Res* **1**, 3-9 (1967).
23. Wissink MJB, Beernink R, Pieper JS, et al. Immobilization of heparin to EDC/NHS-crosslinked collagen. Characterization and in vitro evaluation. *Biomaterials* **22**(2), 151-163 (2001).
24. Yunoki S, Hatayama H, Ohyabu Y. Temperature-responsive characteristics of injectable collagen gel with improved mechanical properties by the addition of genipin as a crosslinker. *東京都立産業技術研究センター研究報告* **9**, 30-33 (2014).
25. Dare EV, Griffith M, Poitras P, et al. Fibrin Sealants from Fresh or Fresh-Frozen Plasma as Scaffolds for In Vitro Articular Cartilage Regeneration. *Tissue Eng A* **15**(8), 2285-2297 (2009).
26. Zhang H, Bré LP, Zhao T, Zheng Y, Newland B, Wang W. Mussel-inspired hyperbranched poly(amino ester) polymer as strong wet tissue adhesive. *Biomaterials* **35**(2), 711-719 (2014).
27. Krogsgaard M, Behrens MA, Pedersen JS, Birkedal H. Self-healing mussel-inspired multi-pH-responsive hydrogels. *Biomacromolecules* **14**(2), 297-301 (2013).
28. Lee BP, Messersmith PB, Israelachvili JN, Waite JH. Mussel-Inspired Adhesives and Coatings. *Ann Rev Mater Res* **41**, 99-132 (2011).
29. Lee H, Dellatore SM, Miller WM, Messersmith PB. Mussel-inspired surface chemistry for multifunctional coatings. *Science* **318**(5849), 426-430 (2007).
30. Autumn K, Liang YA, Hsieh ST, et al. Adhesive force of a single gecko foot-hair. *Nature* **405**(6787), 681-685 (2000).
31. Bartlett MD, Croll AB, King DR, Paret BM, Irschick DJ, Crosby AJ. Looking beyond fibrillar features to scale gecko-like adhesion. *Adv Mater* **24**(8), 1078-1083 (2012).
32. Liu Y, Sakai S, Taya M. Impact of the composition of alginate and gelatin derivatives in bioconjugated hydrogels on the fabrication of cell sheets and spherical tissues with living cell sheaths. *Acta Biomater* **9**(5), 6616-6623 ()2013.
33. Dong Z, Wang Q, Du Y. Alginate/gelatin blend films and their properties for drug controlled release. *J Membr Sci* **280**(1-2), 37-44 (2006).
34. Cohen B, Pinkas O, Foox M, Zilberman M. Gelatin-alginate novel tissue adhesives and their formulation-strength effects. *Act Biomater* **9**(11), 9004-9011 (2013).
35. Matsumura K, Nakajima N, Sugai H, Hyon SH. Self-degradation of tissue adhesive based on oxidized dextran and poly-l-lysine. *Carbohydr Polym* **113**(0), 32-38 (2014).
36. Fujie T, Matsutani N, Kinoshita M, Okamura Y, Saito A, Takeoka S. Adhesive, Flexible, and Robust Polysaccharide Nanosheets Integrated for Tissue-Defect Repair. *Adv Funct Mater* **19**(16), 2560-2568 (2009).

37. Okamura Y, Kabata K, Kinoshita M, et al. Fragmentation of Poly(lactic acid) Nanosheets and Patchwork Treatment for Burn Wounds. *Adv Mater* **25**(4), 545-551 (2013).
38. Okamura Y, Kabata K, Kinoshita M, Saitoh D, Takeoka S. Free-Standing Biodegradable Poly(lactic acid) Nanosheet for Sealing Operations in Surgery. *Adv Mater* **21**(43), 4388-4392 (2009).
39. Miyazaki H, Kinoshita M, Saito A, et al. An ultrathin poly(L-lactic acid) nanosheet as a burn wound dressing for protection against bacterial infection. *Wound Repair Regener* **20**(4), 573-579 (2012).
40. Rose S, Prevoteau A, Elziere P, Hourdet D, Marcellan A, Leibler L. Nanoparticle solutions as adhesives for gels and biological tissues. *Nature* **505**(7483), 382-385 (2014).
41. Niwa D, Fujie T, Lang T, Goda N, Takeoka S. Heterofunctional nanosheet controlling cell adhesion properties by collagen coating. *J Biomater App* **27**(2), 131-141 (2010).
42. Yang SY, O'Cearbhaill ED, Sisk GC, et al. A bio-inspired swellable microneedle adhesive for mechanical interlocking with tissue. *Nature Commun* **4**, 1702 (2013).
43. Matsuda M, Inoue M, Taguchi T. Adhesive properties and biocompatibility of tissue adhesives composed of various hydrophobically modified gelatins and disuccinimidyl tartrate. *J Bioact Compat Polym* **27**(5), 481-498 (2012).
44. Matsuda M, Inoue M, Taguchi T. Enhanced bonding strength of a novel tissue adhesive consisting of cholesteryl group-modified gelatin and disuccinimidyl tartarate. *J Bioact Compat Polym* **27**(1), 31-44 (2012).
45. Matsuda M, Ueno M, Endo Y, Inoue M, Sasaki M, Taguchi T. Enhanced tissue penetration-induced high bonding strength of a novel tissue adhesive composed of cholesteryl group-modified gelatin and disuccinimidyl tartarate. *Colloid Surface B* **91**, 48-56 (2012).
46. Matsuda M, Taguchi T. In vitroevaluation of tissue adhesives composed of hydrophobically modified gelatins and disuccinimidyl tartrate. *Sci Technol Adv Mat* **13**(6), 064212 (2012).
47. Taguchi T, Saito H, Aoki H, et al. Biocompatible high-strength glue consisting of citric acid derivative and collagen. *Mat Sci Eng C* **26**(1), 9-13 (2006).

Chapter 2

Bonding Behavior of Hydrophobically Modified Gelatin Films on the Intestinal Surface

2.1. Summary

The bonding behavior was determined for hydrophobically modified alkaline-treated gelatin on wet porcine intestinal surfaces. The modified gelatin films were obtained by reacting the amino groups of alkaline-treated gelatin with fatty acid chlorides of different alkyl chain lengths, namely, hexanoyl (Hx: C_6) chloride, decanoyl (Dec: C_{10}) chloride, and stearoyl (Ste: C_{18}) chloride. Three kinds of the films were prepared, 32HxAlGltn, 24DecAlGltn, and 26SteAlGltn that had substitution ratios of hydrophobic groups to the amino groups of 32HxAlGltn, 24DecAlGltn, and 26SteAlGltn of 32%, 24%, and 26%, respectively. The 32HxAlGltn film had the strongest bonding to porcine intestinal surfaces. A thick 32HxAlGltn film remained on the intestinal surface even after the bonded film was scraped off for the measurement of bonding strength. In addition, the burst strength increased with an increase in the substitution ratio of the Hx group. Thus, the HxAlGltn film with the higher Hx modification ratio has a potential as a sealant material to prevent agglutination of intestinal surfaces.

2.2. Introduction

Agglutination is a major obstacle in successful post-surgical wound healing. The closure of the wounded surface with sutures may cause inflammation and subsequent accumulation of fibrin, microphages, and fibroblasts, causing agglutination of the wounded surface. In extreme cases, this process can even cause intestinal obstruction. The agglutinated site cannot be lysed with medications; instead, it has to be treated by physical dissection. Various methods have been reported for preventing the occurrence of conglutination, including surgical techniques, pharmacological approaches, and material-based barriers[1-3]. Among them, material-based barriers, especially anticoagulation film-based barriers, have a high reliability for preventing post-surgical agglutination[4-7]. Some commercially available barrier materials include Seprafilm®[8-13], Intercede®[14], Repel-CV®[15], Gore-Tex Surgical Membrane®[16], and Prevadh®[17]. These barrier materials are normally composed of cellulose derivatives, hyaluronic acid, poly(ethylene glycol), poly(lactic acid), hydrophilic collagen, or polytetrafluoroethylene. An efficient material-based barrier should be biocompatible, anti-adhesive, and biodegradable. In addition, the film must adhere tightly to wet tissues to prevent film detachment from the operation site.

Previously, we developed a liquid adhesive composed of hydrophobically modified gelatin (hm-Gltn), which improved the bonding ability to porcine arterial media compared with the conventional Gltn-based adhesives[18-21]. The bonding strength of the adhesive depended on the structure of the added hydrophobic groups[22,23]. It has been reported that the chain length of the adhesive can affect percutaneous absorption[24]. In addition, several ongoing studies including nanoparticle carriers have demonstrated great tissue absorbability[8,25,26]. Based on these findings, it appears that certain types of hydrophobic groups increase the bonding strength of adhesive materials.

In this study, hydrophobically modified alkaline-treated gelatins (hm-AlGltns) were synthesized by reacting the amino group of AlGltn with fatty acid chlorides of different chain lengths, including hexanoyl (Hx: C_6) chloride, decanoyl (Dec: C_{10}) chloride, and stearoyl (Ste: C_{18}) chloride. The resulting hm-AlGltns were molded into films, and their adhesion to wet intestinal surfaces was evaluated.

2.3. Materials and Methods

2.3.1. Materials

AlGltn derived from porcine skin (beMatrix™; molecular weight 100,000) was donated by Nitta Gelatin Inc. (Osaka, Japan). Ethanol (EtOH), 1,1,1,3,3,3-hexafluoroisopropanol (HFIP), dimethyl sulfoxide (DMSO), triethylamine (TEA), 2,4,6-trinitorobenzoylsurfonic acid (TNBS), hydrochloric acid (HCl), sodium dodecyl sulfate (SDS), 10% neutral-buffered formalin, and glycine were purchased from Wako Pure Chemical Industries, Ltd (Osaka, Japan). Hx chloride, Dec chloride, and Ste chloride were purchased from Sigma Chemical Co. (St Louis, MO, USA). The porcine intestine was obtained from Funakoshi Corporation (Tokyo, Japan). All chemicals were used without further purification.

2.3.2. Synthesis of hm-AlGltns

Hm-AlGltns were prepared by following the procedure reported[19-21]. Briefly, 10 g of AlGltn was dissolved in 99 mL of dehydrated DMSO at 80°C. Then, 1 mL of TEA was added to the AlGltn/DMSO solution to produce 100 mL of 10% (w/v) AlGltn/DMSO solution under a dry nitrogen atmosphere. Subsequently, each fatty acid chloride (i.e. Hx, Dec, or Ste chloride) was added to the AlGltn solution, which was then stirred for 17 h at room temperature. The resulting hm-AlGltn/DMSO solution was added to 300 mL of cold EtOH, followed by stirring for 1 h. The hm-AlGltn precipitate was washed three times with 300 mL of cold EtOH to remove unreacted fatty acid chlorides. The hm-AlGltn was obtained under vacuum as a white precipitate.

2.3.3. Characterization of hm-AlGltns

Light absorbance measurement can determine the amount of TNBS molecules that react with the amino group residues on the hm-AlGltn molecules (i.e. unsubstituted amino groups). Therefore, the modification ratios of the hydrophobic groups on the AlGltn molecules were quantified by using the TNBS method[27]. Briefly, 0.05% (w/v) hm-AlGltn in DMSO and AlGltn in DMSO solution were prepared. Next, 100 μL of 0.1% (w/v) TEA/DMSO, 50 μL of 0.1% (w/v) SDS/DMSO, and 100 μL of 0.1% (w/v) TNBS/DMSO were added to 100 μL of AlGltn/DMSO or hm-AlGltn/DMSO solution. The solution was incubated at 37°C for 2 h under light-shielding conditions, and 50 μL of 2 N HCl/DMSO was added to the solution to terminate the TNBS reaction. Finally, spectrophotometrical measurement of light absorbance intensity was performed on a microplate reader (GENios A-5082; Tecan Japan, Kanagawa, Japan) at 340 nm. Based on the intensities of hm-AlGltns, the substitution ratios of the amino groups with fatty acid chlorides were calculated by using the following equation (n = 3)

$$\text{Substitution ratio}(\%) = 100 \times \left(\begin{array}{l} \text{Absorbance of AlGltn} \\ -\text{Absorbance of hm-AlGltn} \end{array} \right) / \text{Absorbance of AlGltn}$$

The introduction of fatty acids to AlGltn was also confirmed by the spectra obtained from proton nuclear magnetic resonance (^{1}H-NMR) spectroscopic (AL300; JEOL, Tokyo, Japan) and Fourier-transform infrared (FT-IR) spectroscopic (FTIR-8400S; Shimadzu, Kyoto, Japan) analyses.

The thermal behavior of the hm-AlGltn solution was characterized by using differential thermal analysis (differential scanning colorimetry (DSC); DSC8230; Rigaku, Tokyo, Japan), where a 70% (w/v) hm-AlGltn/water solution was prepared and heated from 0°C to 100°C at 5°C/min under a nitrogen atmosphere (n = 3).

2.3.4. Fabrication of hm-AlGltn Films

To fabricate hm-AlGltn films, a 10% (w/v) hm-AlGltn/HFIP solution was prepared, and 2.5 mL of the solution was poured into 4cm x 4cm x 0.5cm molds with a glass-bottom plate and silicon wall and dried at room temperature for 12 h. After that, hm-AlGltn films were obtained and then dried in vacuum at room temperature for 2 days to remove HFIP.

2.3.5. Measurement of Water-Contact Angles of hm-AlGltn Films

The water-contact angle of each hm-AlGltn and AlGltn film was measured with a contact angle meter (DM800; Kyowa Interface Science Co., Ltd., Saitama, Japan). Ultrapure water (Milli-Q, 2 mL) was deposited on each film, and the contact angle between the water droplet and film substrate was evaluated 5 s after sample mounting. Data were analyzed by the FAMAS software (Kyowa Interface Science Co., Ltd, Saitama, Japan). Three points per film were measured to determine the mean value of the water-contact angle (n = 3).

2.3.6. Measurement of Bonding Strength of hm-AlGltn Films to the Intestinal Surface

Bonding strengths were measured using the apparatus shown in Figure 2.3(A). The porcine intestine was dissected into circular shapes with a diameter of 4 mm using a dermal punch. The inner surface of the dissected intestine was bonded onto the probe by using a cyanoacrylate-type adhesive or GelBoy® (LOCTITE; Henkel Japan, Tokyo, Japan). The hm-AlGltn films were cut into 7-mm-diameter circular forms, and each film sample was fixed onto a heated plate (37°C) by a piece of Scotch tape (3M, Tokyo, Japan) with a central hole of 4 mm in diameter. The bonding strength was measured by Texture Analyzer (TA-XT2i; Stable Micro Systems, Surrey, UK) under the following conditions: contact time, 180 s; applied force, 20 g/mm^2; and tracking speed, 10 mm/min. Three samples per film (n = 3) were tested for determining the average bonding strength.

2.3.7. Measurement of Pressure Durability of hm-AlGltn Films on the Intestinal Surface

Burst testing was performed by using the American Society for Testing and Materials (ASTM) method (F2392-04)[28]. Briefly, the hm-AlGltn films were cut out into circular shapes with a diameter of 1.5 cm. The porcine intestine was dissected into 3.0-cm circular shapes with 3-mm central holes. The intestine sample was mounted between the metal components and the O-ring of the burst testing system. After that, each film sample was placed over the intestine, and physiological saline was induced into the system at a flow rate of 2 mL/min at 37°C for measuring the pressure durability.

2.3.8. Visualization of the hm-AlGltn Film–Intestine Interface

After measuring the bonding strength, all samples were fixed with 10% neutral-buffered formalin solution and stained with hematoxylin and eosin (H&E). The cross section of the stained interfaces was then inspected under a light microscope (BX51; Olympus, Tokyo, Japan).

2.3.9. Statistical Analysis

Statistical analysis was performed using the Aspin–Welch t-test. A value of $p < 0.05$ was considered statistically significant. The data are presented as mean ± standard deviation (SD).

2.4. Results and Discussion

2.4.1. Synthesis and Characterization of hm-AlGltns

Hm-AlGltns with various hydrophobic chain lengths were obtained via the nucleophilic reaction of the amino groups of AlGltn with fatty acid chlorides (Figure 2.1(a)). We used three types of fatty acid chlorides: Hx (C_6) chloride, Dec (C_{10}) chloride, and Ste (C_{18}) chloride to evaluate the effect of hydrophobic chain length on the film adhesion to intestinal surfaces. Summarized in Table 2.1 are the characteristics of hm-AlGltns with various hydrophobic chain lengths. The substitution of the amino groups with fatty acid chlorides was determined by the spectrophotometric method using TNBS and confirmed that Hx, Dec, and Ste groups were successfully introduced into AlGltn molecules. The modification ratio of 32HxAlGltn, 24DecAlGltn, and 26SteAlGltn was 32%, 24%, and 26%, respectively. The amount of Dec chloride required for generating DecAlGltn was higher than of Hx and Ste for generating HxAlGltn and SteAlGltn, respectively. The introduction of an octanoyl group (C_8) into gelatin has been reported to be slightly more difficult than that of lauryl (C_{12}) and butyl groups (C_4). 29 This result indicates that the reaction of fatty acid chlorides with medium-long alkyl groups is more difficult than those of short or long alkyl groups. Therefore, the reaction of the Dec group (C_{10}) with the AlGltn molecules was probably more difficult than the reactions of the Hx (C_6) and Ste (C_{18}) groups.

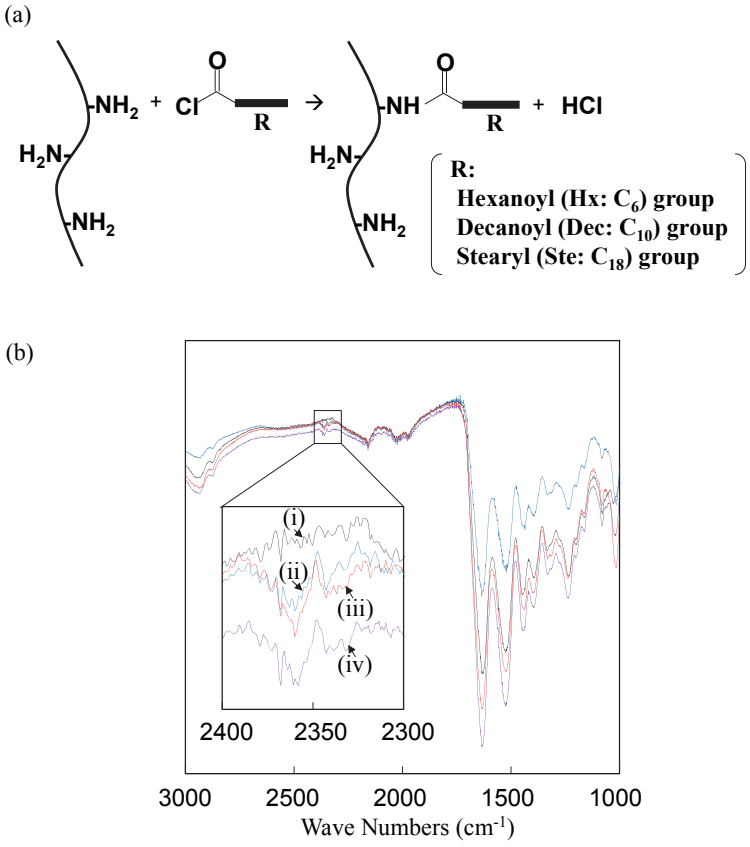

Figure 2.1. Preparation of hm-AlGltns with various hydrophobic groups: (a)chemical reaction between the fatty acid chlorides and the amino groups of AlGltn and (b) FT-IR spectra of AlGltn (blacki), 32HxAlGltn (blueii), 24DecAlGltn (purpleiv), and 26SteAlGltn (iii). hm-AlGltn: hydrophobically modified alkaline-treated gelatin; FT-IR: Fourier-transform infrared.

Table 2.1. Hm-AlGltns with different modification ratios

Compound	Number of carbon	Fatty acid chloride		Modification (%)	Yield (%)	T_d (°C)
		In feed (mL)	In amino groups of AlGltn (%)			
AlGltn	–	–	–	–	–	38.7 ± 1.2
32HxAlGltn	6	49	30	32	93	34.2 ± 1.8*
24DecAlGltn	10	818	100	24	78	35.4 ± 0.8*
26SteAlGltn	18	330	30	26	55	36.5 ± 0.2

Hm-AlGltn: hydrophobically modified alkaline-treated gelatin. In T_d measurements, all the measurement was under $n = 3$ condition. The asterisks mean $p < 0.05$ compared with 32HxAlGltn under Student's *t*-test.

The thermal denaturation temperature (T_d) of hm-AlGltns increased with an increase in alkyl chain length (Table 2.1). Thus, the aggregation of hm-AlGltn with longer alkyl groups through hydrophobic interaction is much easier than that of hm-AlGltn modified with shorter alkyl groups. However, the T_d of AlGltn was greater than that of the other hm-AlGltns, indicating that the hydrogen bonding among the AlGltn molecules, without the loss of amino groups, was stronger than that among the hm-AlGltn molecules.

The ^{1}H-NMR spectra of hm-AlGltns before and after the modification with hydrophobic groups were obtained by following the procedure described previously[30]. The peak at 1.3 ppm was assigned to the alkyl chain, indicating the successful introduction of the hydrophobic groups into the AlGltn molecules. The spectra displayed pronounced sharp peaks, especially that of 26SteAlGltn, suggesting that the longer hydrophobic chains in SteAlGltn were easier to be detected than the shorter chains in the other hm-AlGltns and AlGltn.

Shown in Figure 2.1(b) are the FT-IR spectra of the hm-AlGltns. Typical peaks were found at 2357 cm^{-1} (C = O of long-chain fatty acids) and 2332–2323 cm^{-1} (C–N of amino bond between fatty acids and the amino groups of AlGltn molecules), which were characteristic bands of hydrocarbons.

2.4.2. Measurement of Water-Contact Angles of hm-AlGltn Films

A new wound area is usually moist with body fluids, such as blood or lymph. Thus, the films should have a high affinity for wet organ surfaces. In order to assess the surface wettability, the water-contact angles of all the hm-AlGltn films fabricated were measured. Shown in Figure 2.2 is the water-contact angle for each hm-AlGltn film measured 5 s after the application of a water droplet onto the film substrate at room temperature. The water-contact angle of the films increased with an increase in the alkyl chain length, and it was 56.8°, 56.2°, 60.0°, and 97.5° for AlGltn, 32HxAlGltn, 24DecAlGltn, and 26SteAlGltn, respectively. In addition, the water-contact angle of 12HxAlGltn, 18HxAlGltn, and 36HxAlGltn was 52.9°, 55.6°, and 54.6°, respectively. The angle was 51.7°, 60.0°, and 53.8° for 9DecAlGltn, 24DecAlGltn, and 38DecAlGltn, respectively; and it was 78.9°, 97.5°, and 104.7° for 10SteAlGltn, 26SteAlGltn, and 44SteAlGltn, respectively. Among the tested samples, 24DecAlGltn had similar hydrophobicity to those of AlGltn and HxAlGltns; however, the hydrophobicity of 26SteAlGltn was 1.7 times greater than that of all other samples. This result indicated that when hm-AlGltn was modified with shorter hydrophobic groups such as Hx and Dec, however, the hydrophobicity was not significantly

different from the initial value. In other words, the film surfaces obtain with enhanced hydrophobicity when modified with long alkyl chains. It is known that the chemicals composed of longer alkyl chains melt at higher temperatures than with those composed of shorter alkyl chains; and the melting temperature of hexanoic acid (or caproic acid, $C_5H_{11}COOH$), decanoic acid (or capric acid, $C_9H_{19}COOH$), and stearic acid ($C_{17}H_{35}COOH$) is –3°C, 31°C, and 69.6°C, respectively. This indicated that the Hx group on HxAlGltn molecules can easily penetrate the film to avoid contacting the water droplet at 37°C, which is above its melting temperature. In contrast, the Dec or Ste groups on the hm-AlGltn molecules rarely moved at the same temperature, due to their relatively high melting temperatures. However, due to low surface tension, long hydrophobic chain–modified gelatins tend to be more hydrophobic, as compared with short chain–modified gelatins[29,31,32]. In this study, HxAlGltn with short hydrophobic chains had lower hydrophobicity compared with other samples, due to its high surface tension; it also had greater wettability than DecAlGltn and SteAlGltn.

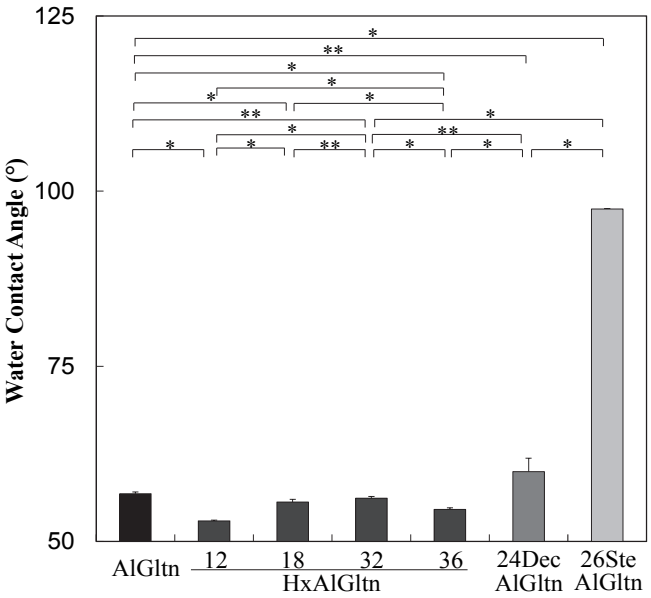

Figure 2.2. Measurement of water-contact angles of AlGltn, HxAlGltns with various introduction ratios, 24DecAlGltn, and 26SteAlGltn films. Data are presented as mean ± SD of three samples, n = 3 (*$p < 0.05$, **$p \geq 0.05$). AlGltn: alkaline-treated gelatin; SD: standard deviation.

2.4.3. Bonding Behavior of hm-AlGltn Films onto the Intestinal Surface

The bonding strengths of all hm-AlGltn films were comparable to or greater than that of the original AlGltn film (Figure 2.3(B)). In particular, the bonding strength of 32HxAlGltn film was approximately 1.4 times greater than that of the original AlGltn film. The 24DecAlGltn and 26SteAlGltn films exhibited similar bonding strengths to that of the original AlGltn film. After the measurements, the interfaces between the films and intestinal surfaces were stained with H&E and visualized for evaluating the bonding or delamination of the hm-AlGltn films. The thickness of AlGltn, 32HxAlGltn, 24DecAlGltn, 26SteAlGltn, and TachoSil® films was 9.4, 30.6, 15.6, 3.1, and 6.3μm, respectively. Among them, the comparatively thick 32HxAlGltn film remained on the

intestinal surface (Figure 2.3(C) (b)); in contrast, only thin layers of 24DecAlGltn and 26SteAlGltn films were observed after the tests (Figure 2.3(C) (c, d)). Moreover, the thickness of the remaining AlGltn film was between that of the thin 24DecAlGltn and 26SteAlGltn films and the thick 32HxAlGltn film (Figure 2.3(C) (a)). These results suggested that the 32HxAlGltn film had the highest bonding strength to the intestinal surface among all tested films.

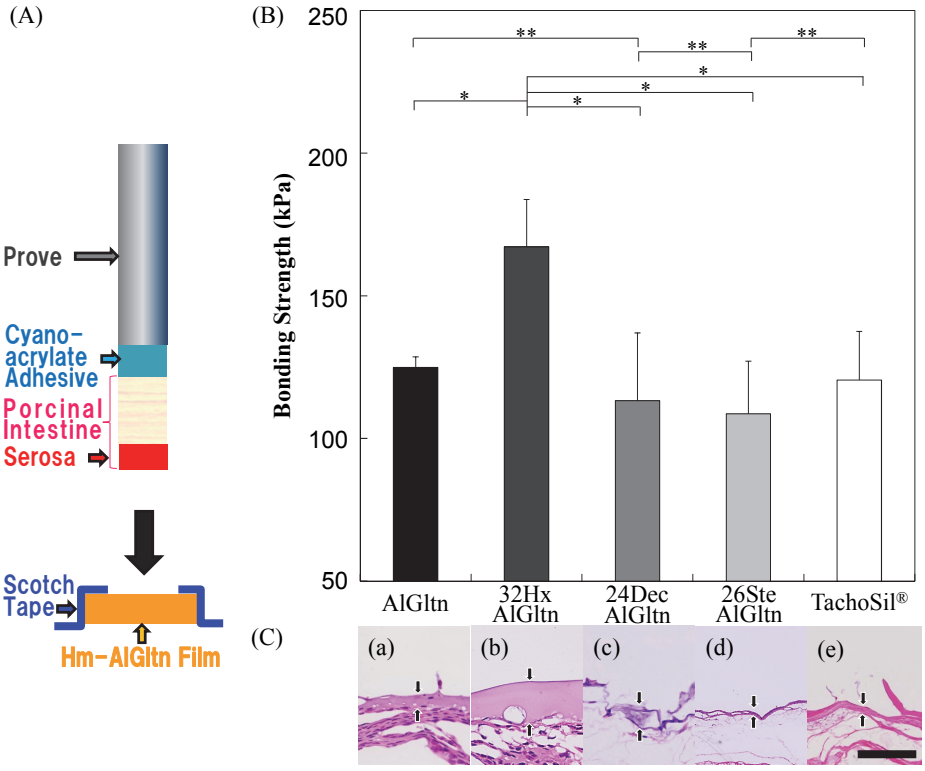

Figure 2.3. Evaluation of bonding behaviors of the hm-AlGltn films to the porcine intestine surface: (A) schematic illustration of the apparatus used for bonding strength measurement and (B) bonding strengths of hm-AlGltns to the porcine intestinal surfaces. Data are presented as mean ± SD of three samples; $n = 3$ (*$p < 0.05$, **$p \geq 0.05$). (C) Histological visualization of the film–intestine interface stained with HE after the measurement of bonding strength. Black arrows indicate (a) AlGltn, (b) 32HxAlGltn, (c) 24DecAlGltn, (d) 26SteAlGltn, and (e) TachoSil® layers that remained on the intestinal surfaces (scale bar = 50 μm). hm-AlGltn: hydrophobically modified alkaline-treated gelatin; SD: standard deviation.

The tensile strengths of the hm-AlGltn films were measured (data not shown) to characterize the bonding behavior of the hm-AlGltn films to intestinal surfaces. The 26SteAlGltn film had the highest tensile strength among all the hm-AlGltn films, probably because the Ste hydrophobic group induced significantly more physical cross-linking in the film. In other words, long alkyl chains could enhance the mechanical strength of the hm-AlGltn films, although they did not promote the interpenetration between the films and intestinal surface layers. The stronger mechanical strength of 26SteAlGltn may result in weaker bonding to the intestinal surface, compared to other films; because rigid materials cannot maintain a conformable attachment to the large surface area of the adherent, this results in dramatically reduced adhering or bonding behaviors. On the other hand, soft materials are capable of creating stronger bonding as compared with rigid materials. In this study, the 32HxAlGltn

film, which exhibited similar mechanical strength to that of blood vessels, had significantly greater bonding strength to the intestinal surfaces compared with other films.

2.4.4. Pressure Durability of hm-AlGltn Films on the Intestinal Surface

As body fluids and digested food materials flow through the intestines, the hm-AlGltn films should be able to sustain external pressure to maintain their intactness. A burst test was performed to investigate the pressure durability of the prepared films (Figure 2.4(A)). Shown in Figure 2.4(B) is the effect of the Hx modification ratio on the burst strength, and the HxAlGltn films with low modification ratios had lower burst strengths compared with those with high modification ratios.

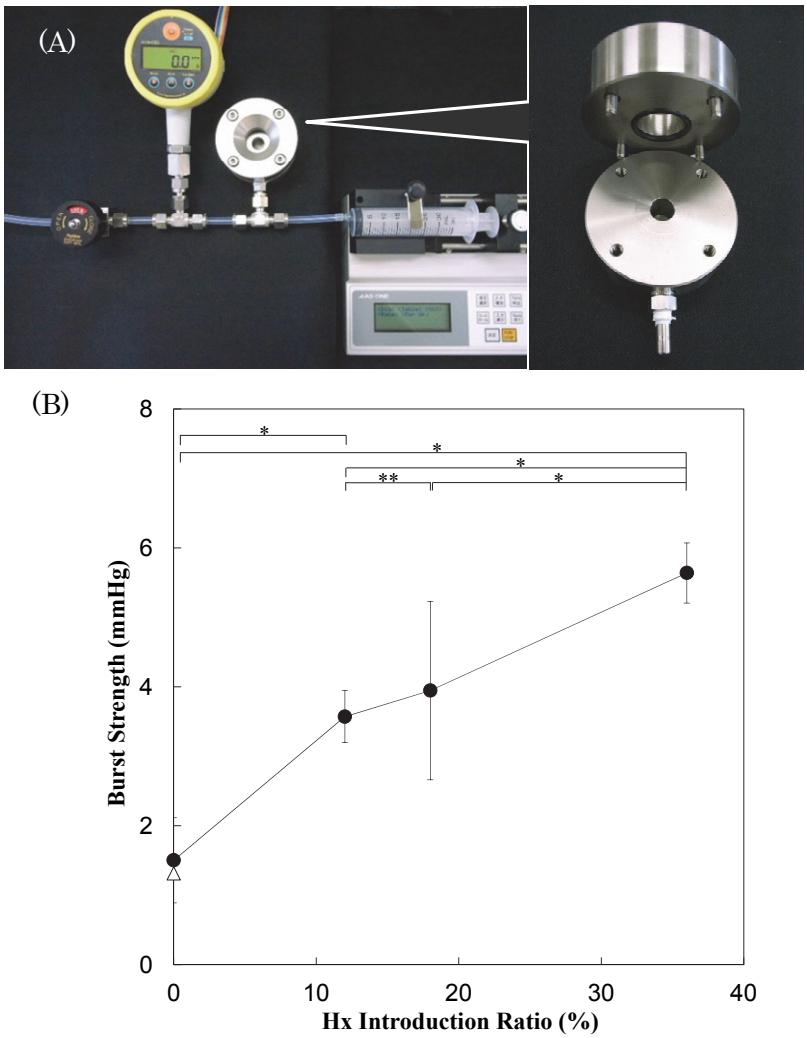

Figure 2.4. Durability test of the HxAlGltn films on the intestinal surfaces against saline-flow pressure. (A) The overall view of the (a) burst test system and (b) film-mounting device. (B) Comparison of the burst durability of the HxAlGltn films (●) and TachoSil® (Δ) on the intestinal surface. Data are presented as mean ± SD of three samples; $n = 3$ (*$p < 0.05$, **$p \geq 0.05$). hm-AlGltn: hydrophobically modified alkaline-treated gelatin; SD: standard deviation.

The hydrophobic groups introduced into the AlGltn molecules can promote the penetration of hm-AlGltn in the intestinal serosa (Figure 2.3). In particular, the Hx group demonstrated the most effective interpenetration among all the reaction groups. Dec and Ste groups have longer hydrophobic chains than the Hx group and induced severe hydrophobic aggregation of the hm-AlGltn molecules in the films. Moreover, the melting temperature of the hydrophobic groups is an important determinant of the ability of hm-AlGltn to penetrate the intestinal surface. Since hexanoic acid has the lowest melting temperature among hexanoic acid, decanoic acid, and stearic acid, Hx may have higher mobility and interact more easily with the intestine at physiological temperature (37°C) as compared with other hydrophobic groups (Figure 2.5).

Histologically, the surface layer of the intestine is composed of extracellular matrix proteins, including elastin and type IV collagen. Collagen is one of the most abundant components in all organs and presents in a triple helix in its natural state[19]. AlGltn can be obtained by the denaturation of collagen molecules. Therefore, the formation of partial triple helices with hm-AlGltn and collagen molecules of the intestinal tissues, in addition to the interpenetration between the hydrophobic groups and intestinal surface, is highly probable. Furthermore, the hydrophobic groups of hm-AlGltn may interact with the hydrophobic amino acids or cellular phospholipid bilayers in the intestinal tissues[33]. These components also contribute to the enhanced bonding strength of the hm-AlGltn film to the intestinal surface, as compared with the bonding of original AlGltn film.

Agglutination can occur not only to the intestinal surfaces but also to other organs in the human body. Agglutination is a complicated process that includes inflammatory reactions between inflamed and healthy organs after contact. To avoid possible contact between the inflamed tissues around the wounded site and other healthy tissues or organs, anti-adhesive materials are widely used in clinical surgeries. The adhesive bonding of the film material to the wounded site provides an effective solution for preventing the direct contact with unaffected sites; however, frequent delamination and detachment of the anti-adhesive films are the major obstacles for their effective usage. The bonding abilities of the hm-AlGltn films prepared in this study to the porcine aorta were tested (data not shown), and they had enhanced bonding behaviors compared with conventional films. HxAlGltn film had stronger bonding to the aorta as compared with DecAlGltn and SteAlGltn films, and the increase in the bonding strength of various HxAlGltn films was in accordance to their Hx group introduction ratio. In this study, the bonding behaviors of the films to the intestinal surfaces were investigated, and the evaluation of their bonding strengths to other organs, including the uterus and liver, will be conducted in the future.

Increased bulk strength is required to obtain hm-AlGltn films with high bonding strengths without compromising the mobility of hm-AlGltn. Although the hm-AlGltn films prepared in this study were fabricated by using the solvent-evaporation method, it has been suggested that the optimum cross-linking of the hm-AlGltn films with some biocompatible cross-linkers[34–36] or heat treatment could increase both the bonding and bulk strengths[30].

Ideally, the anti-adhesive films should gradually degrade with the progression of the wound healing process. Thus, the biodegradability of the 25HxAlGltn film formed by the citrate acid–derived cross-linker in rat subcutaneous tissues was tested in a previous study, and it was found that the film completely degraded within 28 days (data not shown). Therefore, we assumed that this degradation period could be controlled by the cross-link density and hydrophobicity of the hm-AlGltn films.

The bonding of anti-adhesive materials has been reported to not only prevent agglutination but also promote the cellular activities through cellular adhesion in in vitro studies[37–39]. This indicated that the hm-AlGltn films have

great promise for use not only as clinical anti-adhesive materials but also as scaffold substrates for cellular functionalization.

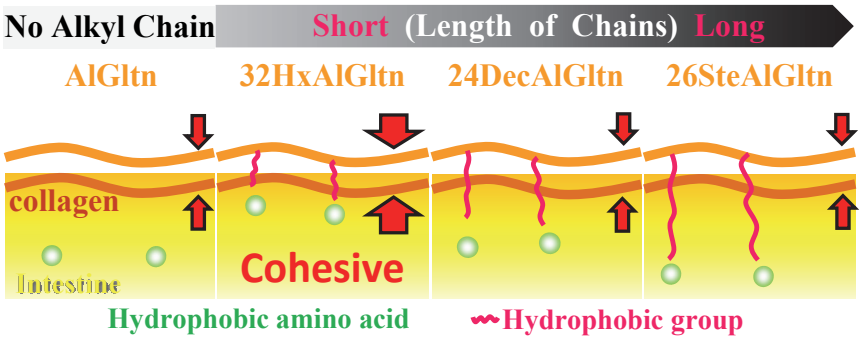

Figure 2.5. Schematic representation of the bonding behaviors of the hm-AlGltns films containing various hydrophobic groups to the intestinal surfaces (AlGltn: C_0; 32HxAlGltn:C_6; 24DecAlGltn: C_{10}; and 26SteAlGltn: C_{18}). hm-AlGltn: hydrophobically modified alkaline-treated gelatin.

2.5. Conclusion

In this study, the bonding behavior of hm-AlGltn films onto the porcine intestinal surface was investigated for post-surgical wound healing. The HxAlGltn film had higher bonding strength onto the intestinal surface compared to DecAlGltn and SteAlGltn films. A thick HxAlGltn film remained at the bonding interface, whereas only thin layers of the DecAlGltn and SteAlGltn films remained on the intestinal surface after the measurement of their bonding strengths. The burst strength of HxAlGltn on the intestinal surface increased with the increase in the Hx modification ratio. These results indicated that the hm-AlGltn films could be used as potent anti-adhesive materials for preventing organ agglutination after clinical surgeries.

2.6. References

1. Brochhausen C, Schmitt VH, Planck CN, et al. Current strategies and future perspectives for intraperitoneal adhesion prevention. *J Gastroint Surg* **16**(6), 1256–1274 (2012).
2. Liakakos T, Thomakos N, Fine P, et al. Peritoneal adhesions: etiology, pathophysiology, and clinical significance. *Dig Surg* **18**, 260–273 (2001).
3. Tsujimoto H, Anzawa A, Matoba M, et al. The anti-adhesive effect of thermally cross-linked gelatin film and its influence on the intestinal anastomosis in canine models. *J Biomed Mater Res* **101**, 99-109 (2013).
4. Chang SJ, Kuo SM, You JL, et al. Physical and biological effects of gellan gum on decreasing postoperative adhesion in a rat model. *J Bioact Compat Polym* **28**(2), 178–187 (2013).
5. Peng HH, Chen JW, Yang TP, et al. Polygalacturonic acid hydrogel with shortchain hyaluronate cross-linker to prevent postoperative adhesion. *J Bioact Compat Polym* **26**(6), 552–564 (2011).
6. Okuyama N, Wang C, Rose E, et al. Reduction of retrosternal and pericardial adhesions with rapidly resorbable polymer films. *Ann Thorac Surg* **68**, 913–918 (1999).
7. Ellis H. Intraabdominal and postoperative peritoneal adhesions. *J Am Coll Surg* **200**(5), 641–644 (2005).
8. Yuan S, Xiong G, Roguin A, et al. Immobilization of gelatin onto poly(glycidyl methacrylate)-grafted polycaprolactone substrates for improved cell-material interactions. *Biointerphases* **7**, 30 (2012).
9. Sasaki T, Shimura H, Tanaka T, et al. Protection of trocar sites from gallbladder cancer implantation by sodium hyaluronate carboxymethyl carboxymethylcellulose-based bioresorbable membrane (Seprafilm) in a murine model [corrected]. *Surg Endosc* **18**(2), 246–251 (2004).
10. Fazio VW, Cohen Z, Fleshman JW, et al. Reduction in adhesive small-bowel obstruction by Seprafilm adhesion barrier after intestinal resection, Diseases of the colon and rectum. *Diseas Colon Rect* **49**, 1-11 (2006).
11. Inoue M, Uchida K, Miki C, et al. Kusunoki, Efficacy of Seprafilm for reducing reoperative risk in pediatric surgical patients undergoing abdominal surgery. *J Pediat Surg* **40**, 1301-1306 (2005).
12. Zeng Q, Yu Z, You J, et al. Efficacy and safety of Seprafilm for preventing postoperative abdominal adhesion: systematic review and meta-analysis. *World J Surg* **31**(11), 2125–2131, discussion 2132 (2007).
13. Vrijland W, Tseng L, Eijkman H, et al. Fewer intraperitoneal adhesions with use of hyaluronic acid-carboxymethylcellulose membrane. *Ann Surg* **235**(2), 193–199 (2002).
14. Franklin RR, Diamond MP, Malinak LR, et al. Reduction of ovarian adhesions by the use of interceed. *Obstet Gynecol* **86**(3), 335-340 (1995).
15. Morales DL, Zafar F, Arrington KA, et al. Repeat sternotomy in congenital heart surgery: no longer a risk factor. *Ann Thorac Surg* **86**(3), 897–902 (2008).
16. Goldberg JM, Toledo AA and Mitchell DE. An evaluation of the Gore-Tex surgical membrane for the prevention of postoperative peritonieal adhesions. *Obstet Gynecol* **70**, 846-848 (1987).
17. Karacam V, Onen A, Sanli A, et al. Prevention of pleural adhesions using a membrane containing polyethylene glycol in rats. *Int J Med Sci* **8**(5), 380–386 (2011).
18. Lang G. Efficacy and safety of topical application of human fibrinogen/thrombin-coated collagen patch (TachoComb) for treatment of air leakage after standard lobectomy. *Eur J Cardiothorac Surg* **25**(2), 160–166

(2004).

19. Matsuda M, Inoue M and Taguchi T. Enhanced bonding strength of a novel tissue adhesive consisting of cholesteryl group-modified gelatin and disuccinimidyl tartrate. *J Bioact Compat Polym* **27**(1), 31–44 (2012).
20. Matsuda M, Inoue M and Taguchi T. Adhesive properties and biocompatibility of tissue adhesives composed of various hydrophobically modified gelatins and disuccinimidyl tartrate. *J Bioact Compat Polym* **27**(5), 481–498 (2012).
21. Matsuda M, Ueno M, Endo Y, et al. Enhanced tissue penetration-induced high bonding strength of a novel tissue adhesive composed of cholesteryl group-modified gelatin and disuccinimidyl tartrate. *Colloids Surface B* **91**, 48–56 (2012).
22. Zhu A, Zhao F and Ma T. Photo-initiated grafting of gelatin/N-maleic acyl-chitosan to enhance endothelial cell adhesion, proliferation and function on PLA surface. *Acta Biomater* **5**(6), 2033–2044 (2009).
23. Aewsiri T, Benjakul S, Visessanguan W, et al. Surface activity and molecular characteristics of cuttlefish skin gelatin modified by oxidized linoleic acid. *Int J Biol Macromol* **48**(4), 650–660 (2011).
24. Liu R, Masters KS and Gellman SH. Polymer chain length effects on fibroblast attachment on nylon-3-modified surfaces. *Biomacromolecules* **13**(4), 1100–1105 (2012).
25. Pabla D, Akhlaghi F and Zia H. Intestinal permeability enhancement of levothyroxine sodium by straight chain fatty acids studied in MDCK epithelial cell line. *Eur J Pharm Sci* **40**, 466–472 (2010).
26. Yodoya E, Uemura K, Tenma T, et al. Enhanced permeability of tetragastrin across the rat intestinal membrane and its reduced degradation by acylation with various fatty acids. *J Pharmacol Exp Ther* **271**(3), 1509–1513 (2012).
27. Morcol T, Subramanian A and Velander WH. Dot-blot analysis of the degree of covalent modification of proteins and antibodies at amino groups. *J Immunol Methods* **203**, 45–53 (1997).
28. F2392-04:2004. Standard test method for burst strength of surgical sealants.
29. Ofer T and Shlomo M. Formation of surface active gelatin by covalent attachment of hydrophobic chains. *J Colloid Interface Sci* **193**, 172–177 (1997).
30. Yoshizawa K and Taguchi T. Enhanced bonding strength of hydrophobically modified gelatin films on wet blood vessels. *Int J Mol Sci* **15**(2), 2142–2156 (2014).
31. Lin L-H and Chen K-M. Preparation and surface activity of gelatin derivative surfactants. *Colloids Surface A* **272**(1–2), 8–14 (2006).
32. Aewsiri T, Benjakul S, Visessanguan W, et al. Enhancement of emulsifying properties of cuttlefish skin gelatin by modification with N-hydroxysuccinimide esters of fatty acids. *Food Bioproc Tech* **6**(3), 671–681 (2011).
33. Kolodgie FD, Farb A and Virmani R. Local delivery of ceramide for restenosis. *Circ Res* 2000, **87**, 264–267.
34. Taguchi T, Saito H, Iwasashi M, et al. Biodegradable adhesives composed of human serum albumin and organic acid-based crosslinkers with active ester groups. *J Bioact Compat Polym* **24**(6), 546–559 (2009).
35. Saito H, Murabayashi S, Mitamura Y, et al. Unusual cell adhesion and antithrombogenic behavior of citric acid-cross-linked collagen matrices. *Biomacromolecules* **8**, 1992–1998 (2007).
36. Inoue M, Sasaki M, Nakasu A, et al. An antithrombogenic citric acid-crosslinked gelatin with endothelialization activity. *Adv Healthc Mater* **1**(5), 573–581 (2012).
37. Delio M, Pope K, Wang T, et al. Spectrum of elastin sequence variants and cardiovascular phenotypes in 49

patients with Williams-Beuren syndrome. *Am J Med Genet A* **161**(3), 527–533 (2013).

38. Wu S-C, Chang W-H, Dong G-C, et al. Cell adhesion and proliferation enhancement by gelatin nanofiber scaffolds. *J Bioact Compat Polym* **26**(6), 565–577 (2011).
39. Liu W, Cai Q, Zhang F, et al. Dose-dependent enhancement of bone marrow stromal cells adhesion, spreading and osteogenic differentiation on atmospheric plasma-treated poly(L-lactic acid) nanofibers. *J Bioact Compat Polym* **28**(5), 453–467 (2013).

Chapter 3

Enhanced Bonding Strength of Hydrophobically Modified Gelatin Films on Wet Blood Vessels

3.1. Summary

The bonding behavior between hydrophobically modified alkaline-treated gelatin (hm-AlGltn) films and porcine blood vessels was evaluated under wet conditions. Hexanoyl (Hx: C_6), decanoyl (Dec: C_{10}), and stearyl (Ste: C_{18}) chlorides were introduced into the amino groups of AlGltn to obtain HxAlGltn, DecAlGltn, and SteAlGltn, respectively, with various modification percentages. The hm-AlGltn was fabricated into films and thermally crosslinked to obtain water-insoluble films (t-hm-AlGltn). The 42% modified t-HxAlGltn (t-42HxAlGltn) possessed higher wettability than the 38% modified t-DecAlGltn (t-38DecAlGltn) and the 44% modified t-SteAlGltn (t-44SteAlGltn) films, and the t-42HxAlGltn film showed a high bonding strength with the blood vessel compared with all the hm-AlGltn films. Histological observations indicated that t-42HxAlGltn and t-38DecAlGltn remained on the blood vessel even after the bonding strength measurements. From cell culture experiments, the t-42HxAlGltn films showed significant cell adhesion compared to other films. These findings indicate that the Hx group easily interpenetrated the surface of blood vessels and effectively enhanced the bonding strength between the films and the tissue.

3.2. Introduction

Wound closure is one of the fundamental requirements in surgical operations. A suture is usually employed to close the wounded region. However, the use of sutures prolongs operation time and is not suitable for some complicated areas such as the junction site of a blood vessel and a lung. Therefore, tissue adhesives have been developed and used in the clinical field for shortening the operation time and for the closure of wounds with complicated structures[1]. However, these adhesives still possess some disadvantages in terms of bonding strength and biocompatibility[2–11]. For example, TachoSil® (CSL Behring K.K., Tokyo, Japan) is a common clinically available adhesive composed of equine collagen and fibrin; it, however, has several shortcomings. Xenogeneic product collagen and allogeneic fibrin may result in infection, and the fibrin-induced adhesivity is not very strong. Especially in terms of bonding strength, adhesives bonded on soft tissues are exposed to adverse environments because about 70% of our body is made of water. In addition, body fluids such as blood plasma and lymph fluid spill out from the wound area after a surgical operation.

To overcome these obstacles, molecular design of tissue adhesive materials that show good bonding behavior even on moisture-containing tissues is required. We recently developed a hydrophobically modified gelatin (hm-Gltn)-based adhesive and showed that the resulting hm-Gltn adhesive with a low modification percentage formed a stronger bond on porcine arterial media as compared to the original Gltn-based adhesives[12–16]. Our results suggest that films composed of hm-Gltn have the ability to bond to soft tissues even under wet conditions. However, the detailed adhesive properties of these hm-Gltn films have not yet been clarified.

For this purpose, hydrophobically modified alkali-treated Gltns (hm-AlGltns) were prepared by the modification of the amino groups of AlGltn with fatty acid chlorides with various chain lengths, including hexanoyl (Hx: C_6) chloride, decanoyl (Dec: C_{10}) chloride, and stearyl (Ste: C_{18}) chloride. We selected those fatty acid chlorides because our previous research showed that a longer hydrophobic group such as Ste resulted in good adhesivity to tunica media [13,15]. Therefore, the longest fatty acid is Ste in this research, and together we used a tunica blood vessel as an adherend, so, the fatty acid chlorides with different chain lengths could be compared with Ste. The obtained hm-AlGltns with various modification percentages were cast to fabricate films; these were then thermally crosslinked to prepare water-insoluble hm-AlGltn (t-hm-AlGltn) films. Using the t-hm-AlGltn films, surface wettability and bonding behavior on porcine blood vessels were evaluated.

3.3. Materials and Methods

3.3.1. Materials

BeMatrix™, an alkaline-treated gelatin (AlGltn) derived from porcine skin, was kindly donated by Nitta Gelatin Inc. (Osaka, Japan). Ethanol (EtOH), 1,1,1,3,3,3-hexafluoroisopropanol (HFIP), dimethylsulfoxide (DMSO), triethylamine (TEA), 2,4,6-trinitrobenzoylsulfonic acid (TNBS), hydrochloric acid (HCl), sodium dodecyl sulfide (SDS), calcium chloride, 10% formalin neutral buffer solution, 4',6-diamidino-2-phenylindole (DAPI), tris(hydroxymethyl)aminomethane, tert-butylalcohol, and glycine were purchased from Wako Pure Chemical Industries, Ltd. (Osaka, Japan). Hexanoyl (Hx: C_6) chloride, decanoyl (Dec: C_{10}) chloride, and stearyl (Ste: C_{18}) chloride were purchased from Sigma Chemical Co. (St. Louis, MO, USA). A porcine aorta was purchased from Funakoshi Corporation (Tokyo, Japan). RPMI was purchased from Lonza ((Basel, Switzerland)). L929 cells were purchased from RIKEN (Bio Resource Center Cell Bank, RBRC-RCB2619, Ibaraki, Japan). All chemicals were used without further purification.

3.3.2. Synthesis of hm-AlGltns

Based on former reports[13–16], hm-AlGltns with various chain lengths and densities were prepared by the reaction between fatty acid chlorides and primary amino groups of AlGltn. The employed fatty acid chlorides were hexanoyl (Hx: C_6), decanoyl (Dec: C_{10}), and stearyl (Ste: C_{18}) chloride. First, AlGltn (10 g) was fully dissolved into 99 mL of dried DMSO at 80 °C. Then, one mL of TEA was added into the AlGltn/DMSO solution to obtain 100 mL of 10 w/v% AlGltn/DMSO solution under a dry N_2 atmosphere. The fatty acid chloride was subsequently added to the AlGltn solution and stirred for 17h at room temperature. The resulting hm-AlGltn/DMSO solution was then poured into 300 mL of cold EtOH and stirred for 1h. Subsequently, the precipitate of hm-AlGltn was washed twice with 300 mL of cold EtOH followed by evaporation under vacuum to leave a white cake of which the yield was calculated.

3.3.3. Characterization of hm-AlGltns

The modification percentages of the hydrophobic groups in AlGltn were quantified by the method previously reported using TNBS[13–17]. Briefly, each hm-AlGltn and the original AlGltn were dissolved in DMSO to obtain 0.05 w/v% solutions. Then, 100 μL of 0.1v/v% TEA/DMSO, 50 μL of 0.1 w/v% SDS/DMSO, and 100 μL of 0.1w/v% TNBS/DMSO were added to 100 μL of each (hm-) AlGltn/DMSO solution, followed by incubation at 37 °C for 2h under light-shielding conditions. Then, 50 μL of the 2 N-HCl/DMSO solution was added to stop the reaction. Finally, the intensity of light absorbance was measured spectrophotometrically at 340 nm using a microplate reader (GENios A-5082, Tecan Japan, Kanagawa, Japan). The substitution percentage of amino groups

with the fatty acid chlorides was then calculated from the intensities of hm-AlGltn compared with the original AlGltn.

The modification of the fatty acid in AlGltn was confirmed by ^{1}H-NMR (AL300, JEOL, Tokyo, Japan) and FT-IR (FTIR-8400S, Shimadzu, Kyoto, Japan) measurements. The typical peaks were found at 2357 cm^{-1} (C=O bond of long-chain fatty acids) and 2332–2323 cm^{-1} (C–N bond of amino bonding between fatty acids and the amino groups of the AlGltn molecules).

Thermogravimetry (TG) analysis was executed to analyze thermal behavior of obtained hm-AlGltns (TG8120, Rigaku, Tokyo, Japan). Heating was conducted from 30 to 300 °C at a heating rate of 10 °C/min. Aluminium oxide was employed as control.The thermal behavior of the hm-AlGltn solution was also analyzed by differential thermal analysis (DSC) (DSC8230, Rigaku, Tokyo, Japan). The hm-AlGltns were dissolved in ultrapure water (Merck Millipore, Tokyo, Japan) to prepare 70 w/v% samples. Heating was conducted from 0 to 100 °C at a heating rate of 5 °C/min under nitrogen atmosphere.

3.3.4. Preparation and Characterization of Thermally Crosslinked hm-AlGltn Films

Each hm-AlGltn was first dissolved in HFIP to prepare a 10w/v% solution. Each solution (2.5 mL) was then cast on a 4 × 4 × 0.5 cm^3 mold with a glass plate bottom and a silicone wall and was dried for 12h, followed by drying overnight under vacuum at room temperature. The resulting films were placed between two thin silicone sheets and sandwiched between metal plates. Thermal treatment was then performed under vacuum at 140 °C for 24h.

In order to determine the residual amino group amount in t-hm-AlGltn, each film was cut into a disk 4mm in diameter and then immersed in 300 μL of ultrapure water. Then, 300 μL of a 4 w/v% $NaHCO_3$ aqueous solution and 300 μL of a 0.1 w/v% TNBS aqueous solution were added. After incubation for 2h, 600 μL of 6 N-HCl was added to stop the reaction. Then, 300 μL of each sample was placed into each well of a 96-well plate and the absorbance was measured at 340 nm using a microplate reader (GENios A-5082, Tecan Japan, Kanagawa, Japan).

3.3.5. Measurement of Water Content of Thermally Crosslinked hm-AlGltn Films

The thermally crosslinked hm-AlGltn films were cut into disks 4mm in diameter and were immersed in 1μL of ultrapure water at 37 °C. The weights of the swollen films after various time periods were gravimetrically determined. The water content of the films was calculated using the following equation:

$$\text{Water content (\%)} = (W' - W)/W' \times 100 \quad \ldots(1)$$

(W': weight of swollen film, W: weight of dried film.)

The water contents of the films after 5 min immersion in water were compared.

3.3.6. Determination of Surface Wettability of Thermally Crosslinked hm-AlGltn Films

In order to determine the surface wettability of the thermally crosslinked hm-AlGltn films, the water contact angle of each film was measured using a contact angle meter (DM800, Kyowa Interface Science Co., Ltd., Saitama, Japan). Briefly, 2 μL of ultrapure water was placed on the t-hm-AlGltn films and the time dependent change in the static water contact angle was measured after 3, 10, 30, 60, 120 and 180s. The resulting data were analyzed using FAMAS software (Kyowa Interface Science Co., Ltd., Saitama, Japan).

3.3.7. Measurement of the Mechanical Strength of Thermally Crosslinked hm-AlGltn Films

Each film was cut out into 5 mm × 1 cm rectangular shapes and both sides were bonded on 5 mm × 1 cm plastic sheets by GelBoy (LOCTITE, Henkel Japan, Tokyo, Japan) in a 2.5 mm × 5 mm area. After drying at room temperature, the plastic sites were clipped to probes and tensile tests were performed for all samples before and after thermal crosslinking at a rate of 10 mm/min (n = 3).

3.3.8. Measurement of Bonding Strength between Thermally Crosslinked hm-AlGltn Films and Blood Vessel

There was no existing protocol in place to evaluate the bonding strength between the tissue surface and the film; therefore, the following measurement method was applied. The porcine blood vessel was dissected with a dermal punch into disks 4mm in diameter. The dissected blood vessel was bonded onto a probe with GelBoy. The t-hm-AlGltn films were also punched out into 7 mm diameter disks and placed on a heated plate at 37 °C. They were fixed to the heated plate with scotch tape (3M, Tokyo, Japan) with a hole 4 mm in diameter. The bonding strength was then measured using a Texture Analyzer (TA-XT2i, Stable Micro Systems, Godalming, UK) (n = 3) with the following conditions: 180s contact time, 20 g/mm^2 applied force, and 10 mm/min tracking speed.

3.3.9. Observation of Thermally Crosslinked hm-AlGltn Film–Blood Vessel Interfaces

After the bonding strength measurement, each sample was fixed with a 10% formalin neutral buffer solution followed by hematoxylin and eosin (HE) staining. Cross sections of the stained samples were observed with an optical microscope (BX51, Olympus, Tokyo, Japan).

3.3.10. Cell Adhesion onto Thermally Crosslinked hm-AlGltn Film

A mouse fibroblast cell line, L929, was used to evaluate cell adhesion onto the t-hm-AlGltn films. The L929s were first cultured in a medium (RPMI-1640 (R8758, Sigma-Aldrich, St. Louis, MO, USA)) containing 2 v/v% fetal bovine serum. The t-hm-AlGltn films were placed on 24-well plates and a glass ring was put on each film. L929 cells (5.0×10^4 cells) were seeded onto each film for 5min and the films were rinsed with 2 mL of phosphate buffered saline (PBS, pH 7.4). Then the cells were fixed with 10% formalin neutral buffer solution for 60min and permeabilized in 0.2 v/v% Triton-X 100 in PBS for 2 min followed by 0.1% DAPI in PBS for 10 min in light-shielding conditions at room temperature. The adhered cells were observed with an IX81 inverted fluorescence microscope (Olympus Co. Ltd., Tokyo, Japan). The counted number of adhered cells was calculated from the area of the microscopic field (n = 3).The cells were then observed with a scanning electron microscope (SEM). In brief, the cells were gradually dehydrated with a 50–99 v/v% ethanol/water solution. Then, the cells were immersed in tert-butylalcohol twice followed by freeze drying at −80 °C. The cells were then observed by SEM.

3.3.11. Statistical Analysis

Statistical analysis was carried out using Student's t-test with Microsoft Excel software. Statistically significant differences were accepted when $p < 0.05$. The data are shown as mean ± standard deviation (S.D.).

3.4. Results and Discussion

3.4.1. Synthesis and Characterization of hm-AlGltns

As shown in Figure 3.1A, three different fatty acid chlorides, hexanoyl (Hx) chloride, decanoyl (Dec) chloride, and stearyl (Ste) chloride, were reacted with the amino groups of the AlGltn molecules by nucleophilic reactions to obtain HxAlGltn, DecAlGltn, and SteAlGltn.

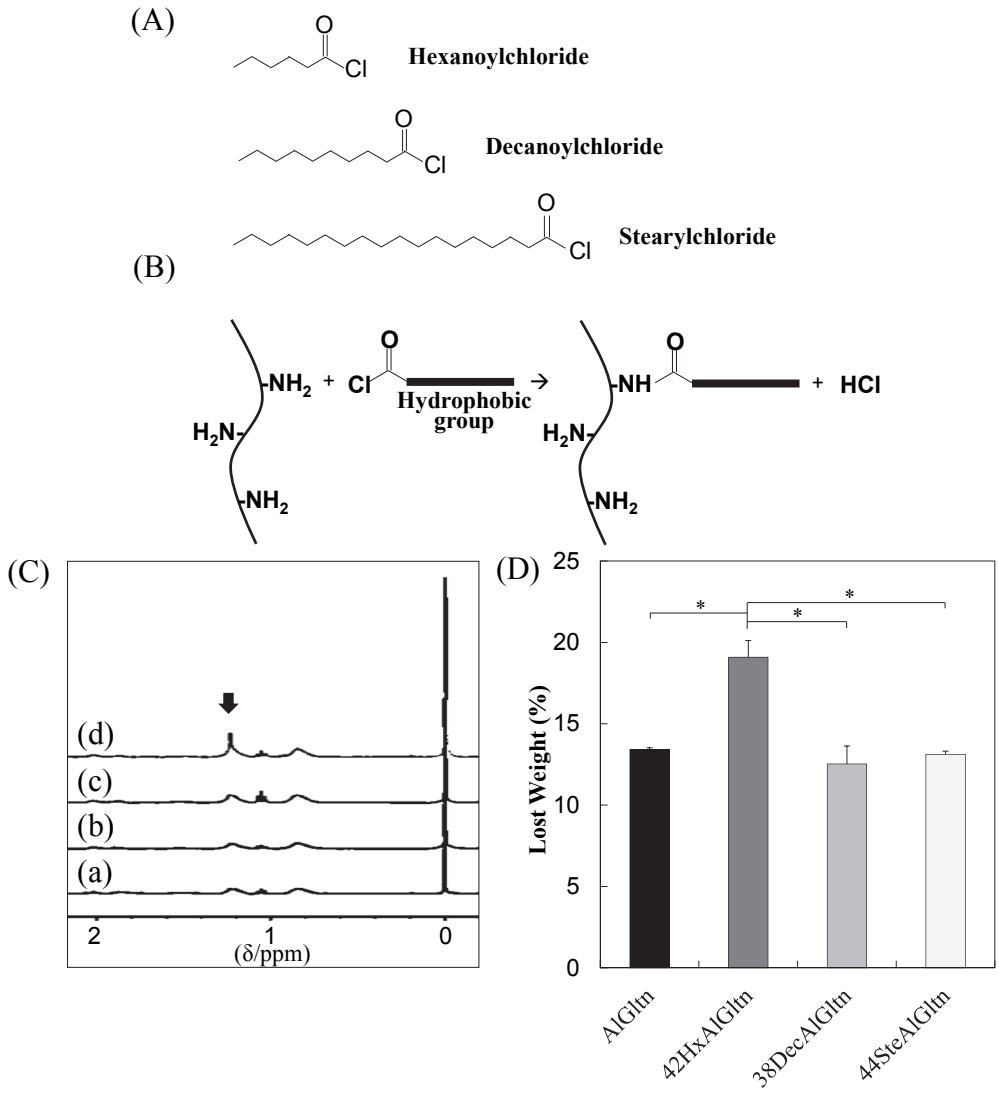

Figure 3.1. Modification of alkaline-treated gelatin (AlGltns) with hydrophobic groups using fatty acid chlorides and verification of the introduction. (A) Chemical formulas of fatty acid chlorides; and (B) nucleophilic substitution reaction between an amino group of the AlGltn molecule and a fatty acid chloride; (C) H1-NMR spectra of (a) AlGltn; (b) 42HxAlGltn; (c) 38DecAlGltn; and (d) 44SteAlGltn (the arrow indicates the peak derived for the methyl group of the alkyl chains); (D) Weight loss of hydrophobically modified alkaline-treated gelatin films (hm-AlGltns). Data are shown as the average ± S.D. of three samples (* $p < 0.05$).

Table 3.1 notes the characteristics of the hm-AlGltns after the nucleophilic substitution reactions of the amino groups of AlGltn with the fatty acid chlorides. The substituted quantities of amino groups with fatty acid chlorides were determined by the 2,4,6-trinitrobenzenesulfonic acid (TNBS) method[13–17]. Through this reaction, each hydrophobic group (Hx, Dec, Ste) was successfully introduced into each AlGltn with amide bonds to form hm-AlGltns, whose modification percentages ranged from 10% to 44%. Table 3.1 also lists the independent thermal denaturation temperature (T_d) of each hm-AlGltn. The value of T_d of the 30% hm-AlGltns was lower than that of both the 10% and 40% hm-AlGltns. In addition, the hm-AlGltns with longer side chains exhibited a lower T_d. The result may indicate that interaction between and coagulation of the introduced hydrophobic side chains together with the modest introduction ratio for crystallization, affected each T_d.

Table 3.1. Hydrophobically modified alkaline-treated gelatin films (hm-AlGltns) with various modification ratios

Abbreviation	Number of carbons	Fatty acid chloride		Modification (%)	Yield (%)	T_d (°C)
		in feed (μL)	in amino groups of AlGltn (%)			
12HxAlGltn	6	16	10	12	91	36.2
32HxAlGltn	6	49	30	32	93	34.2
42HxAlGltn	6	82	50	42	95	36.5
10DecAlGltn	10	409	50	10	76	36.8
24DecAlGltn	10	818	100	24	78	35.4
38DecAlGltn	10	409	50	38	89	36.9
10SteAlGltn	18	110	10	10	85	37.1
26SteAlGltn	18	330	30	26	55	36.5
44SteAlGltn	18	550	50	44	91	39.6

The prefixes of the abbreviations indicate the substituted ratio of amino group of AlGltn molecule and the introduced Hx, Dec, or Ste group (12HxAlGltn means 12 % Hx group introduced hm-AlGltn).

Figure 3.1(C) shows the ^{1}H-NMR spectra of the hydrophobic group of the molecule on the AlGltn or hm-AlGltns. The peak of the alkyl chain appears at 1.3ppm. The peak intensities of the original AlGltn, 32HxAltn, 24DecAlGltn, and 26SteAlGltn at 1.3 ppm were 0.14, 1.48, 1.98, and 1.69. Therefore, each hydrophobic group was successfully introduced into each hm-AlGltn. On the other hand, the hm-AlGltns with longer side chains showed sharper ^{1}H-NMR peaks.

The hydrated carbons of the longer side chains were easily detectable. Therefore, the 44SteAlGltn showed the sharpest peak as compared with other hm-AlGltns.

Weight losses of AlGltn, 42HxAlGltn, 38DecAlGltn, and 44SteAlGltn under heating from 25–300 °C were compared in Figure 3.1(D). 42HxAlGltn showed the highest weight loss from 35 to 115°C indicating that there is more bound water in 42HxAlGltn than AlGltn, 38DecAlGltn, and 44SteAlGltn. The higher weight loss means a looser network structure, each (hm-)AlGltn resulting from the AlGltn molecule of (hm-)AlGltn has higher flexibility.

3.4.2. Preparation and Characterization of Thermally Crosslinked hm-AlGltn Films

Ten w/v% hm-AlGltn/HFIP solutions were cast and transparent hm-AlGltn films were fabricated. The films were subsequently heated at 140 °C in vacuo for thermal crosslinking. It is known that covalent amide crosslinks form between amino groups and carboxyl groups in Gltn molecules after thermal treatment of the gelatin membranes in vacuo[18–20], resulting in water-insoluble Gltn films. To evaluate the amino group amounts used for the thermal crosslinking, the 2,4,6-trinitrobenzenesulfonic acid (TNBS) method was employed and the results are given in Table 3.2. The hm-AlGltns with short side chains, such as 12HxAlGltn and 10DecAlGltn, consumed more amino groups than the original AlGltn during the thermal-crosslinking. The hm-AlGltns with dense and long side chains consumed fewer amino groups.

These results indicate that shorter side chains did not inhibit amide bond formation among the hm-AlGltns, whereas dense and longer side chains did because the amino group and carboxyl group on a Gltn molecule of an hm-AlGltn cannot exist owing to volume exclusion by inactive long side chains.

Table 3.2. T-hm-AlGltns with various modification percentages.

Abbreviation	Number of carbons	Amino groups used for thermal crosslinking (%)	Stiffness in dried state (MPa)
t-AlGltn	0	14.9±6.3	4.66±0.22
t-12HxAlGltn	6	30.7±5.9	5.39±0.05
t-32HxAlGltn	6	11.0±4.9	4.39±0.20
t-42HxAlGltn	6	10.1±1.9	3.68±0.60
t-10DecAlGltn	10	20.0±2.6	5.06±0.11
t-24DecAlGltn	10	3.5±0.5	4.24±0.29
t-38DecAlGltn	10	0.2±2.0	3.06±0.06
t-10SteAlGltn	18	2.9±0.9	4.01±0.11
t-26SteAlGltn	18	7.2±0.1	3.49±0.42
t-44SteAlGltn	18	3.5±1.4	2.19±0.24

3.4.3. Mechanical Strength of Thermally Crosslinked hm-AlGltn Films

As shown in Table 3.2, the mechanical strength of the t-hm-AlGltns decreased with increasing modification percentage. Among t-hm-AlGltns with similar modification percentages but different alkyl chain lengths, the mechanical strength of films with longer side chains decreased. However, the t-12HxAlGltn and t-9DecAlGltn films were both stronger than the original t-AlGltn film.

It is hypothesized that with thermal crosslinking, the hm-AlGltn films acquired amide bonding between each hm-AlGltn molecule, thus becoming resistant to hydrolysis, even though dense hydrophobic groups inhibit the accessibility of the amino groups to the carboxyl groups of each hm-AlGltn molecule by volume exclusion. Amide bonds are more difficult to form in hm-AlGltns with dense hydrophobic groups than in hm-AlGltns with sparse hydrophobic groups.

These results are due to the fact that long hydrophobic groups inhibit the approach of amino groups to carboxyl groups, resulting in decreased crosslinking density in the t-hm-AlGltn films. As compared to the original AlGltn, hm-AlGltn molecules with low modification percentages can easily assemble by hydrophobic interaction. Therefore, the t-12HxAlGltn and t-9DecAlGltn films showed high stiffness as compared to the t-AlGltn film.

3.4.4. Water Content of Thermally Crosslinked hm-AlGltn Films

Figure 3.2 shows the water content of each t-hm-AlGltn film after 5min water immersion, at which point all the films reached a plateau. The water content of the films with dense side chains was lower compared to films with sparse side chains. On the other hand, the films with longer side chains showed higher water content compared to films with shorter side chains. The water content in t-9DecAlGltn and t-10SteAlGltn was high compared to the original t-AlGltn film. In all the prepared t-hm-AlGltn films, t-42HxAlGltn possessed the lowest water content. These results indicate that long hydrophobic groups prevented the agglomeration of Gltn molecules due to volume exclusion, resulting in greater retention of water molecules. In contrast, the higher mobility of short hydrophobic groups promoted the agglomeration of Gltn molecules, leaving less room for water molecules in the film.

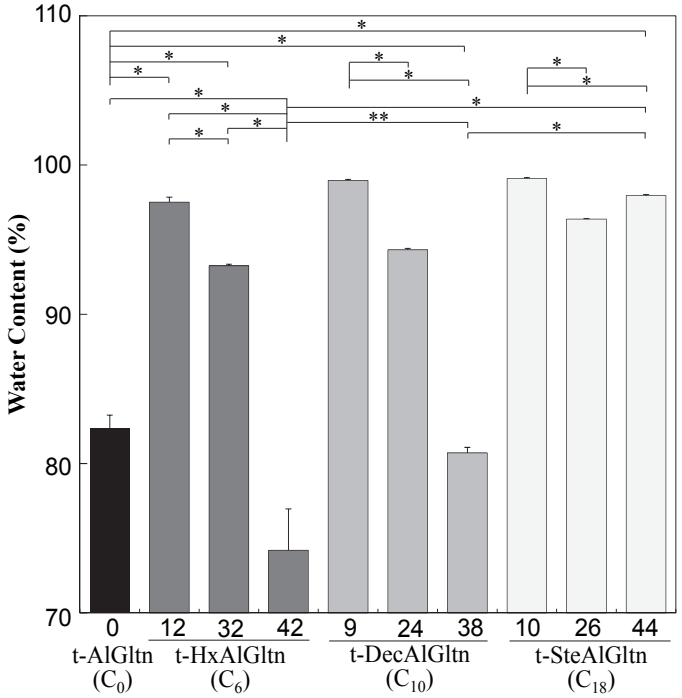

Figure 3.2. Water content of t-hm-AlGltn films after immersion in water at 37 °C for 5 min. Data are shown as the average ± S.D. of three samples (* $p < 0.05$, ** $p \geq 0.05$).

3.4.5. Surface Wettability of Thermally Crosslinked hm-AlGltn Films

When a film is applied for surgical use to close areas on organs, such areas will be in a wet condition because body fluids such as blood or lymph fluids ooze from the wound. Therefore, the films need to possess a high affinity for wet organ surfaces for use in surgical applications.

For the evaluation of wettability of t-hm-AlGltn films, the time dependence of the water contact angle was compared. In this experiment, films whose modification percentages were approximately 40%, i.e., t-42HxAlGltn, t-38DecAlGltn, and t-44SteAlGltn, were used. As can be seen from Figure 3.3, the water contact angles of the samples decreased with time. Additionally each film shows independent wettability indicating that t-42HxAlGltn showed excellent wettability even though the amino groups of AlGltn were partially substituted by Hx. However, the wettability of t-38DecAlGltn and t-44SteAlGltn was quite low compared to t-AlGltn and t-42HxAlGltn.

Hx, the shortest chain possessing a low melting point of −3 °C, can move freely at 37 °C. Therefore, Hx can move more easily from the outside to the inside of the films to escape from the aqueous surface than can longer hydrophobic groups such as Dec and Ste, whose melting points are 31 °C and 69.6 °C, respectively.

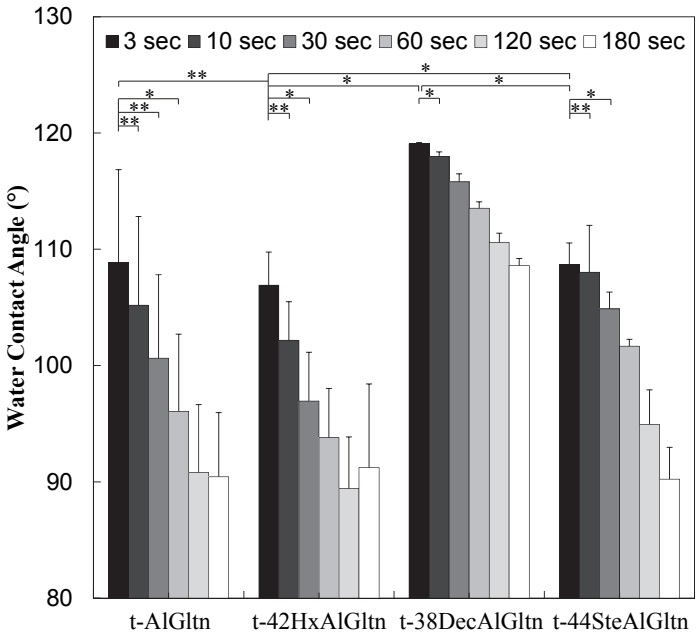

Figure 3.3. Surface wettability of t-hm-AlGltn films. Transition of static water contact angle on t-hm-AlGltn films (t-42HxAlGltn, t-38DecAlGltn, t-44SteAlGltn, and t-AlGltn). Data are shown as the average ± S.D. of three samples (* $p < 0.05$, ** $p \geq 0.05$).

3.4.6. Bonding Behavior of Thermally Crosslinked hm-AlGltn Films on the Porcine Blood Vessel

The bonding strength between the porcine blood vessel and t-hm-AlGltn films with various modification percentages is shown in Figure 3.4A. The bonding strength of all the t-hm-AlGltn films increased after the modification of the hydrophobic groups compared to the original t-AlGltn. In the case of the t-HxAlGltn films, the bonding strength increased with increasing modification percentage. The t-32HxAlGltn and t-42HxAlGltn films in particular had bond strengths that were 2.5 times greater than that of the t-AlGltn film. The modification percentages of t-DecAlGltn and t-SteAlGltn did not show sufficient enhancement of bond strength

even though their bonding strengths were greater than that of the t-AlGltn film. This result indicates that the Hx group is the most effective side chain for blood vessel adhesion among the three hydrophobic groups, Hx, Dec, and Ste. The Hx group could easily interpenetrate the hydrophobic region of the extracellular matrix (ECM) or the hydrophobic amino acid and cell membrane of the tissue because of its low melting point, resulting in its higher mobility. This interpenetration of Hx contributed to the high bonding strength of t-42HxAlGltn to the porcine blood vessel. Furthermore, Gltn molecules in t-42HxAlGln have the ability to partially form a triple helix with the Gltn molecule collagen on the surface of the blood vessel.

After measurement of the bonding strength, all of the tissue-film interfaces were fixed and hematoxylin and eosin (HE) staining was applied to observe the bonding/destruction behavior of the t-hm-AlGltn films on porcine blood vessels. By HE staining, the film remaining on the tissue surface and the tissue itself were colored dark purple and pink, respectively. Figure 3.4Ba and d show that no t-AlGltn or t-44SteAlGltn film remained on the blood vessel surfaces. However, the t-42HxAlGltn and t-38DecAlGltn films (Figure 3.4Bc and d), indicated by red arrows and dashed rectangles) clearly remained after the bonding strength measurement. Additionally, the remaining t-42HxAlGltn was thicker and broader than the t-38DecAlGltn, indicating the higher penetration ability of the Hx group into the blood vessel as compared with the Dec group.

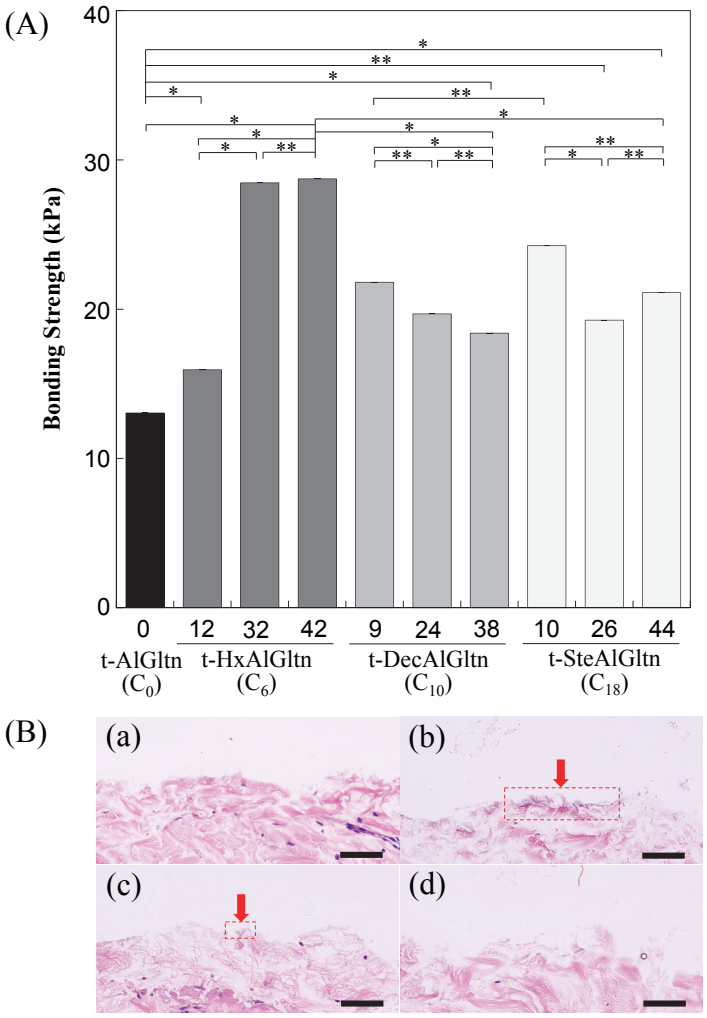

Figure 3.4. Bonding strength of t-hm-AlGltn films on the porcine blood vessel. (A) Effect of chain length and density of hm-AlGltns on the bonding strength. Data are shown as the average ± S.D. of three samples (* $p < 0.05$,

** $p \geq 0.05$); (B) Cross-sectional views of the film-tissue interface after bonding strength measurement of (a) t-AlGltn; (b) t-42HxAlGltn; (c) t-38DecAlGltn; and (d) t-44SteAlGltn. Scale bar: 50μm. Red arrows show the sites t-hm-AlGltn remained.

Recently, we reported that a tissue adhesive composed of cholesteryl group-modified Gltn and disuccinimidyl tartrate showed excellent bonding ability onto porcine arterial media[14–16]. From histological observations, a thick adhesive layer was found on the media surface even after the bonding strength measurement. In the present case, only a thin adhesive layer was observed. The t-hm-AlGltn films seemed to be much stiffer than the cholesteryl group-modified Gltn-based adhesive; therefore, film remaining on the blood vessel surface could be hard even when the films were bonded strongly.

3.4.7. Cell Adhesion onto Thermally Crosslinked hm-AlGltn Films

To compare cell adhesivity onto the films, L929 cells were seeded onto t-AlGltn, t-42HxAlGltn, t-38DecAlGltn, and t-44SteAlGltn films. After being cultured for 5 min, the number of adhered cells was counted. Also, the morphology of the adhered cells was observed using a scanning electron microscope (SEM).

Figure 3.5 shows SEM images of L929 cells adhered onto t-hm-AlGltn films or culture plate dishes after being cultured for 5 min. The cells on the tissue culture plate show a spherical shape (Figure 3.5e). However, the cells on each t-(hm-)AlGltn surface, especially on t-42HxAlGltn surface, spread more extensively on the t-42HxAlGltn surface (Figure 3.5a–d), indicating that short side chains such as Hx could easily interact with the cell membrane.

Many more L929 cells adhered on t-42HxAlGltn than on t-AlGltn, t-38DecAlGltn, and t-44SteAlGltn (data is not shown). The obvious difference may come from the easy Hx interpenetration into the cell membrane due to its low melting point.

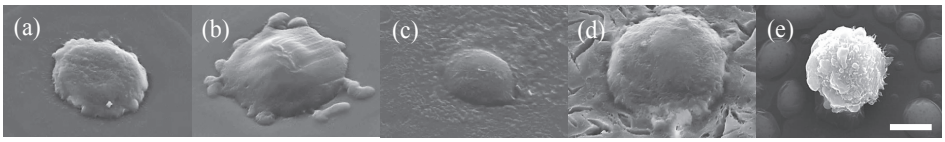

Figure 3.5. L929 adhesion onto t-hm-AlGltn films after being cultured for 5min. Morphology of L929 cells on t-hm-AlGltn films ((a) t-AlGltn; (b) t-42HxAlGltn; (c) t-38DecAlGltn; (d) t-44SteAlGltn and (e) tissue culture plate). Scale bar: 5 μm.

The results indicate that the introduced hydrophobic group Hx interacts with the tissue components, including collagen and the cell membrane. This means that the Hx group penetrated into the hydrophobic domains of the tissue, such as the hydrophobic amino acid residue and the phospholipids of the cell membrane. Figure 3.6 shows the effect of the chain length and the density on the ability of t-hm-AlGltn molecules to bond onto a blood vessel. When long chains such as those of the Ste and Dec groups are introduced into the AlGltn molecules, the resulting hm-AlGltn cannot easily interact with collagen molecules on the surface of the blood vessel because of their higher melting points and volume exclusion. Also, longer chains with lower mobility can hardly interact with hydrophobic groups because of hydrophobic amino acids in blood vessels. On the other hand, t-42HxAlGltn

molecules with dense and short chains with a lower melting point easily interact with blood vessels and form stronger bonds.

In this study, t-24DecAlGltn and t-38DecAlGltn were employed for comparison. If DecAlGltns with a slightly higher introduction ratio like t-30DecAlGltn and t-40DecAlGltn were compared, the bonding strength would be weaker than t-24DecAlGltn and t-38DecAlGltn. The hypothesis is from our previous data that hm-Gltns with a much higher introduction ratio, over 50% introduction ratios, bonded more weakly than t-hm-Gltns with appropriate introduction ratios. The higher amount of alkyl chains can agglomerate by hydrophobic interaction in the film, therefore, there will be less hydrophobic group which can interact with the hydrophobic group in the ECM of the blood vessel.

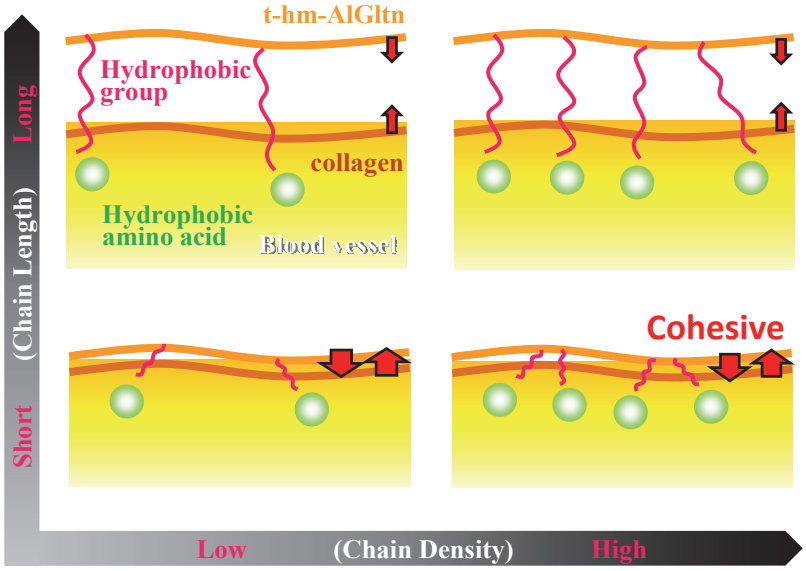

Figure 3.6. Schematic illustration of the bonding behavior of t-hm-AlGltns with various hydrophobic chain lengths and densities.

3.5. Conclusion

Thermally crosslinked film adhesives composed of hydrophobically modified AlGltn with Hx (C_6), Dec (C_{10}), or Ste (C_{18}) were fabricated and their bonding behaviors on porcine blood vessels were evaluated. The t-42HxAlGltn film with short and dense hydrophobic groups showed higher wettability, lower water content, and stronger bonding to the blood vessel compared to the other t-hm-AlGltn films.

The t-42HxAlGltn and t-38DecAlGltn films remaining after bonding strength measurement were confirmed by histological observation. L929 cells rapidly adhered and extended onto the t-42HxAlGltn film compared with other films. These results indicate that the t-42HxAlGltn film has potential for biomedical applications as a film adhesive.

3.6. References

1. Creton C, Hooker J. Bulk and Interfacial Contributions to the debonding mechanisms of soft adhesives: Extension to large strains. *Langmuir* **17**, 4948–4954 (2001).
2. Taguchi T, Saito H, Uchida Y, Sakane M, Kobayashi H, Kataoka K, Tanaka J. Bonding of soft tissues using a novel tissue adhesive consisting of a citric acid derivative and collagen. *Mater Sci Eng C* **24**, 775–780 (2004).
3. Taguchi T, Saito H, Aoki H, Uchida Y, Sakane M, Kobayashi H, Tanaka J. Biocompatible high-strength glue consisting of citric acid derivative and collagen. *Mater Sci Eng C* **26**, 9–13 (2006).
4. Iwasashi M, Sakane M, Saito H, Taguchi T, Tateishi T, Ochiai N. In vivo evaluation of bonding ability and biocompatibility of a novel biodegradable glue consisting of tartaric acid derivative and human serum albumin. *J Biomed Mater Res* **90**, 543–548 (2007).
5. Ito M, Taguchi T. Enhanced insulin secretion of physically crosslinked pancreatic β-cells by using a poly (ethylene glycol) derivative with oleyl groups. *Acta Biomater* **5**, 2945–2952 (2009).
6. Taguchi T, Rao Z, Ito M, Matsuda M. Induced albumin secretion from HepG2 spheroids prepared using poly (ethylene glycol) derivative with oleyl groups. *J Mater Sci Mater Med* **22**, 2357–2363 (2011).
7. Iwata H, Matsuda S, Mitsuhashi K, Itoh E, Ikada Y. A novel surgical glue composed of gelatin and N-hydroxysuccinimide activated poly (L-glutamic acid): Part 1. Synthesis of activated poly (L-glutamic acid) and its gelation with gelatin. *Biomaterials* **19**, 1869–1876 (1998).
8. Fukunaga S, Karck M, Harringer W, Cremer J, Rhein C, Haverich A. The use of gelatin-resorcin-formalin glue in acute aortic dissection type A. *Eur J Cardiothorac Surg* **15**, 564–570 (1999).
9. Bingley JA, Gardner AHM, Stafford EG, Mau TK, Pohlner PG, Tam RKW, Jalali H, Tesar PJ, O'Brien MF. Late complications of tissue glues in aortic surgery. *Ann Thorac Surg* **69**, 1764–1768 (2000).
10. Chao H, Torchiana D. BioGlue: Albumin/glutaraldehyde sealant in cardiac surgery. *J Card Surg* **18**, 500–503 (2003).
11. Shahbazi J, Marcal H, Watson S, Wakefield D, Sarris M, Foster LJ. Sutureless sealing of penetrating corneal wounds using a laser-activated thin film adhesive. *Lasers Surg Med* **43**, 490–498 (2011).
12. Taguchi T, Saito H, Iwasashi M, Sakane M, Ochiai N. Biodegradable adhesives composed of human serum albumin and organic acid-based crosslinkers with active ester groups. *J Bioact Compat Polym* **24**, 546–559 (2009).
13. Matsuda M, Taguchi T. In vitro evaluation of tissue adhesives composed of hydrophobically modified gelatins and disuccinimidyl tartrate. *Sci Technol Adv Mat* **13**, 064212 (2012).
14. Matsuda M, Ueno M, Endo Y, Inoue M, Sasaki M, Taguchi T. Enhanced tissue penetration-induced high bonding strength of a novel tissue adhesive composed of cholesteryl group-modified gelatin and disuccinimidyl tartarate. *Colloids Surf B* **91**, 48–56 (2012).
15. Matsuda M, Inoue M, Taguchi T. Adhesive properties and biocompatibility of tissue adhesives composed of various hydrophobically modified gelatins and disuccinimidyl tartrate. *J Bioact Compat Polym* **27**, 481–498 (2012).
16. Matsuda M, Inoue M, Taguchi T. Enhanced bonding strength of a novel tissue adhesive consisting of cholesteryl group-modified gelatin and disuccinimidyl tartarate. *J Bioact Compat Polym* **27**, 31–44 (2012).

17. Morcol T, Subramanian A, Velander WH. Dot-blot analysis of the degree of covalent modification of proteins and antibodies at amino groups. *J Immunol Met* **203**, 45–53 (1997).
18. Tanzawa A, Tsujimoto H, Matoba M, Hashimoto A, Suzuki S, Morita S, Ikada Y, Hagiwara A. Physical and biological properties of a novel anti-adhesive material made of thermally cross-linked gelatin film-preliminary study for the mechanism of the anti-adhesive effect. *Sci Eng Rev Doshisha Univ* **52**, 149–155 (2011).
19. Esposito E, Cortesi R, Nastruzzi C. Gelatin microspheres: Influence of preparation parameters and thermal treatment on chemico-physical and biopharmaceutical properties. *Biomaterials* **17**, 2009–2020 (1996).
20. Welz MM, Ofner CM. III Examination of self-crosslinked gelatin as a hydrogel for controlled release. *J Pharm Sci* **81**, 85–90 (1992).

Chapter 4

Enhanced Angiogenesis of Growth Factor-Free Porous Biodegradable Adhesive Made with Hexanoyl Group-Modified Gelatin

4.1. Summary

The bonding behavior of hexanoyl (Hx: C_6) group-modified alkaline-treated gelatin (HxAlGltn) porous films ((P)HxAlGltn) on the porcine intestine was evaluated. (P)HxAlGltns with various porosities were prepared by the salt-leaching method for various solid-liquid ratios. (P)HxAlGltns bonded more strongly to porcinal intestine surfaces than did porous AlGltn films ((P)AlGltns). L929 cells cultured on (P)HxAlGltns showed adhesivity than cells cultured on (P)AlGltns. Faster tissue infiltration and a shorter degradation time of highly porous (P)HxAlGltns were observed after implantation in rat subcutaneous tissues. The angiogenic markers CD34 and α-SMA were highly expressed around (P)HxAlGltns that had high porosity. These results indicated that highly porous (P)HxAlGltns have advantages with respect to not only bonding strength on wet soft tissues, but also angiogenesis.

4.2. Introduction

Fast and effective wound care requires the promotion of processes involved in the acute inflammatory and growth phases, including angiogenesis and tissue migration. Biomaterials for wound care should demonstrate strong tissue adhesion under wet conditions to close the wound and tissue regeneration properties, including cell adhesion, angiogenic activity, and appropriate porosity.

Biomaterials that are developed for strong adhesion to soft tissues under wet conditions are classified into three types: nanomaterials, biomimetic materials, and naturally derived polymer-based materials. Nanomaterials include nanoparticles1 and nanosheets[2] and are driven mainly by van der Waals' forces. Biomimetic materials are typically prepared by introducing a catechol moiety[3,4], which is the major component of the marine mussel adhesion protein, into biocompatible polymers under wet conditions. Gecko feet[5] have been reported to adhere to tissue/organ surfaces with fibrous structures exhibiting strong bonding ability on solid substrates. Naturally derived polymers including gelatin[6], alginate[7], and albumin[8-11] have been employed as basic components of tissue adhesive materials.

Highly porous materials[12] have been proposed for faster tissue regeneration and for their ability to release angiogenic factors[13-22]; however, angiogenic factors such as basic fibroblast growth factor (bFGF)[23-27] and vascular endothelial growth factor (VEGF)[28-30] are expensive cytokines and are not stable in physiological environments[31-34].

Hexanoyl (Hx: C_6) group-modified heparin has a high binding constant with bFGF[35], indicating that Hx-modified heparin can be a reservoir for bFGF. Furthermore, we recently reported that a liquid tissue adhesive containing hydrophobically modified gelatin (hm-Gltn) shows higher interfacial bonding strength to soft tissues under wet conditions than an adhesive containing non-modified, original Gltn[36-38]. Moreover, film-type adhesives composed of hm-Gltn, especially Hx-Gltn, bond strongly to soft tissue under wet conditions[39,40]. These results suggest that biopolymers combined with the Hx group will show high affinity with angiogenic factors such as bFGF and VEGF.

Hx group-modified alkali-treated Gltn (HxAlGltn) films with porous structures were fabricated using NaCl as a porogen to evaluate soft tissue bonding under wet conditions. Furthermore, the angiogenic properties and mechanisms of the resulting films were clarified.

4.3. Materials and Methods

4.3.1. Materials

Alkaline-treated gelatin (AlGltn) named BeMatrix® derived from porcine skin was kindly donated by Nitta Gelatin Inc. (Osaka, Japan). Ethanol (EtOH), dimethyl sulfoxide (DMSO), triethylamine (TEA), 2,4,6-trinitrobenzenesulfonic acid (TNBS), hydrochloric acid (HCl), sodium dodecyl sulfide (SDS), 10% formalin neutral buffer solution, tert-butyl alcohol, sodium chloride (NaCl), L-lactic acid (LA) and vascular endothelial growth factor (VEGF) were purchased from Wako Pure Chemical Industries, Ltd. (Osaka, Japan). Hexanoyl (Hx: C_6) chloride was purchased from Sigma Chemical Co. (St. Louis, MO, USA). Porcine intestine and anti CD34 Rat (Goat) antibody was purchased from Funakoshi Corporation (Tokushima, Japan). L929 cells were purchased from RIKEN BRC CELL BANK, RBRC-RCB2619 (Ibaraki, Japan). Fetal bovine serum (FBS), phosphate buffered saline (PBS) and RPMI-1640 (SIGMA, R8758) were purchased from Lonza (Basel, Switzerland). WST-8 was purchased from Dojindo Laboratories (Kumamoto, Japan). Fibronectin (FN) and bFGF were purchased from Sigma-Aldrich (St. Louis, MO, USA). Citrate acid derived crosslinker (TSC) was synthesized as previously reported18. All chemicals were used without further purification.

4.3.2. Synthesis and Characterization of HxAlGltn

Following previously reported methods[39,40], Hx group-introduced hm-AlGltn (HxAlGltn) was prepared by the reaction between Hx chloride and primary amino groups of AlGltn. First, AlGltn (10 g) was fully dissolved into 99 mL of DMSOat 80 °C. Then, 1 mL of hexanoyl (Hx: C_6) chloride was added to the AlGltn/DMSO solution to obtain 100 mL of 10 w/v% AlGltn/DMSO solution under a dry N_2 atmosphere at room temperature. One milliliter of TEA was subsequently added to the AlGltn solution and stirred for 17 h at room temperature. The resulting HxAlGltn/DMSO solution was poured into 300 mL of cold EtOH and stirred for 1 h. Subsequently, the HxAlGltn precipitate was washed twice with 300 mL of cold EtOH followed by evaporation under a vacuum to leave a white cake, and the yields were calculated.

The modification ratio for Hx groups in HxAlGltn was quantified using a previously reported method with TNBS[36,37,55-57]. Briefly, HxAlGltns or the original AlGltn was dissolved into DMSO to obtain 0.05 w/v% solutions. Then, 100 μL of 0.1 v/v% TEA/DMSO, 50 μL of 0.1 w/v% SDS/DMSO, and 100 μL of 0.1 w/v% TNBS/DMSO were added to 100 μL of the HxAlGltn or AlGltn/DMSO solution followed by incubation at 37 °C for 2 h under light-shielding conditions. Then, 50 μL of 2N HCl/DMSO was added to stop the reaction. Finally, the intensity of light absorbance was measured spectrophotometrically at 340 nm using a microplate reader (GENios A-5082, Tecan Japan, Kanagawa, Japan). The percentage of amino groups substituted with Hx chloride was then calculated based on the relative intensities of HxAlGltn compared with the original AlGltn.

4.3.3. Preparation and Characterization of (P)HxAlGltns and (P)AlGltns

HxAlGltn was dissolved in 10% LA-DMSO solvent to prepare 25 w/v% HxAlGltn solutions, and TSC (a citrate acid-derived crosslinker synthesized as previously reported[58]) was added to 10 mL of the HxAlGltn/LA-DMSO solution to match the amount of NHS group in TSC and the amount of amino group residues of the HxAlGltn molecule, and the TSC-HxAlGltn/DMSO was stirred quickly. The required amount of NaCl (for liquid-solid ratios of 1/1, 2/1, 3/1, 4/1, or 5/1 (w/w)) was added to the solution and mixed to disperse the NaCl uniformly. The solutions were packed into zipper bags (Unipack, Seisannipponsha Ltd., Tokyo, Japan) and the compounds were put between glass plates with 1-mm thick silicone spacers. After overnight crosslinking, the obtained NaCl-HxAlGltn gels were immersed in 4 °C ultra-pure water for 3 days with frequent water changes to remove LA-DMSO, NaCl, NHS, and unreacted TSC. The hydrogels were frozen at -80 °C and were lyophilized for 3 days to obtain the (P)HxAlGltn film. The (P)AlGltns were fabricated following the same method.

The porosity of each porous film was determined by a water content calculation considering the weight of water absorbed for porous films with cold water filled-pores (W_f) and the weight of water absorbed for porous films with empty pores (W_e). The porosity was calculated using the following formula:

$$\text{Porosity (\%)} = (W_f - W_e)/W_f \times 100.$$

4.3.4. Measurement of the Mechanical Strength of (P)HxAlGltns and (P)AlGltns

Each film was cut out into 5 mm × 10 mm rectangle shape, and both ends in 2.5 mm × 5 mm were bonded on the end of 10 mm × 20 mm plastic sheets by GelBoy (LOCTITE, Japan Henkel, Japan). Then, both ends of the plastics of the samples were attached to probes and tensile tests were performed by 10 mm/minute speed. For tensile test of swollen films, the samples were swollen in 37 ºC ultra-pure water for 5 min (n = 3).

4.3.5. Measurement of the Bonding Strength Between the Intestine and (P)HxAlGltns or (P)AlGltns and Observations of the Peeling Interface of Porous Film-Intestines

Porcinal intestine was dissected into disks 4 mm in diameter with a dermal punch. The dissected intestine was bound to the top of the probe with a cyanoacrylate adhesive, GelBoy. The porous films were also punched out into circles 7 mm in diameter and fixed on a 37 °C heated plate with scotch tape (3M, Tokyo, Japan) with a hole that was 4 mm in diameter. The bond strength was then measured using a Texture Analyzer (TA-XT2i, Stable Microsystems, Surrey, UK) (n = 3) under the following conditions: 180 sec contact time, 40 g/mm^2 applied force, and 10 mm/min tracking speed.

After the measurement, samples were fixed in a 10% formalin neutral buffer solution and stained with hematoxylin and eosin (H&E). The cross sections of the peeling interfaces were observed under an optical microscope (BX51, Olympus, Japan).

4.3.6. Cell Cultures on (P)HxAlGltns and (P)AlGltns

A murine fibroblast cell line, L929, was used to evaluate cell adhesion and viability on (P)HxAlGltns and (P)AlGltns. L929s were first cultured in a medium (RPMI-1640, SIGMA, R8758) containing 2 v/v% fetal bovine serum. Each (P)AlGltn or (P)HxAlGltn disc, 1 cm in diameter, was placed on 24-well plates and a glass ring was put on each film. All samples were swollen with RPMI without FBS. Then, L929 cells (5.0×10^4 cells) were cultured for 1, 4, 8, or 24 h. After incubation with 10 μL/well of WST-8 for 1 h, light absorbance was measured at 450 nm (n = 3). The films were rinsed with 2 mL of PBS twice, and the cells were fixed with 10% formalin neutral buffer solution.

After drying, the L929 cell morphologies were observed with a scanning electron microscope (SEM, JSM-5600, JEOL, Tokyo, Japan). In brief, the cells and the porous films were gradually dehydrated with a 50 to 99 v/v% ethanol/water solution followed by one wash with 50 v/v% tert-butyl alcohol/EtOH and two 100% tert-butyl alcohol immersions and freeze-drying at -80 °C. Then, the cells were sputtered with Pt and observed by SEM.

4.3.7. Subcutaneous Implantation of (P)HxAlGltns and (P)AlGltns

Each porous film was cut into a disk, 1 cm in diameter, and sterilized with ethylene-oxide gas. The disks were implanted subcutaneously in rats (Wistar, 7-week-old males) for 3, 7, 14, and 28 days. After the term, each tissue including the porous film disk was removed, fixed in 10% formalin neutral buffer solution, and subjected to H&E staining.

4.3.8. Angiogenesis Evaluation around the Porous Films with CD34 and α-SMA Immunostaining

The 10% formalin neutral buffer solution-fixed samples at 7, 14, and 28 days after implantation were immunostained with anti-CD34 rat (goat) antibody and for α-SMA. The number and area of CD34 or α-SMA regions per unit area and the densely marked area per unit area were calculated using ImageJ (n = 3).

4.3.9. Determination of dissociation constants between HxAlGltn/AlGltn and FN/bFGF/VEGF

Either HxAlGltn or AlGltn was fixed onto the carboxymethyl-fixed sensor chip (CM5) (GE Healthcare Japan Corp., Tokyo, Japan) by the amine coupling method. The carboxyl group was activated by NHS to fix the Gltn molecules via its amino group, and ethanolamine was then used for NHS residue blocking. The fixation process was performed with an amine coupling kit (BR-1000-50, GE Healthcare Japan Corp.) including EDC (N-ethyl-N'-(3-dimethylaminopropyl) carbodiimide hydrochloride), NHS, and 1 M ethanolamine hydrochloride solution (pH 8.5). A flow of 1000 μg/mL of HxAlGltn/10 mM acetic acid buffer (pH 4.0) for 7 min at 5 μL/min speed was used for amine coupling. The procedure was also implemented with 5, 50, and 100 μg/mL of FN/PBS

solution, 10, 25, and 50 μg/mL of bFGF/PBS solution, or 5, 7.5, and 10 μg/mL of VEGF/PBS for 3 min at a flow rate of 20 μL/min. After the interaction, the association and dissociation constants were calculated using a program (n = 3).

4.3.10. Statistical Analysis

Statistical analysis was carried out using Welch's t-tests. Statistically significant differences were accepted when $p < 0.05$. The data are shown as means ± standard deviation (SD).

4.4. Results and Discussion

4.4.1. Synthesis and Characterization of HxAlGltn

Following our previous method, HxAlGltn was synthesized by a reaction between the amino groups of AlGltn molecules and Hx chloride (Figure 4.1A)[39,40]. The degree of substitution of amino groups with Hx groups was 27%, as determined using the 2,4,6-trinitrobenzosulfonic acid (TNBS) method[40].

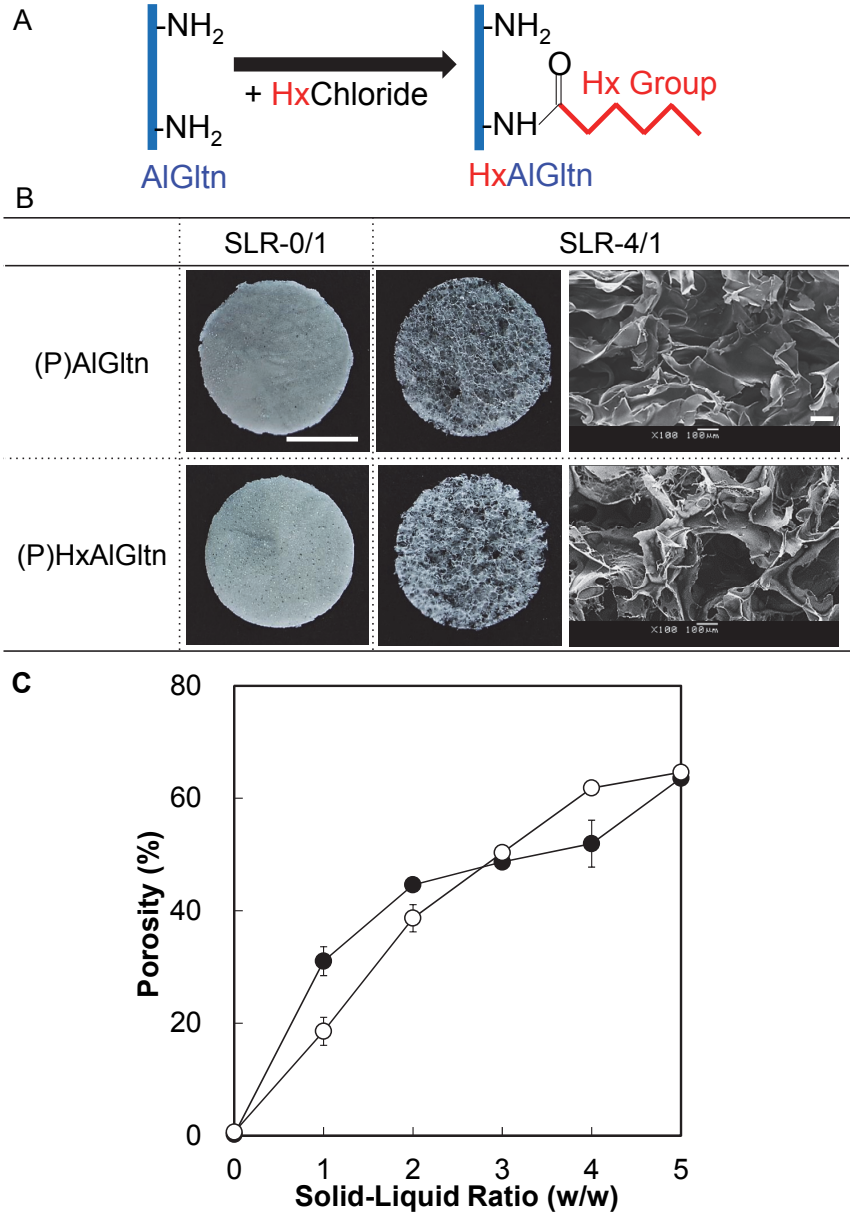

Figure 4.1. Preparation of the porous films. (A) HxAlGltn synthesis after the reaction between AlGltn and Hx chloride. (B) Macro/microscopic images of tissue-adhesive porous bodies fabricated without/with NaCl using AlGltn/HxAlGltn. Scale bars: 5 mm in macroscopic and 100 μm in microscopic. (c) Porosity of (P)AlGltns or (P)HxAlGltns with various amounts of NaCl (●(P)AlGltns and ○(P)HxAlGltns). Data represent the means ± SD of three samples (n = 3).

4.4.2. Preparation of porous films

The porous AlGltn or HxAlGltn films ((P)AlGltns and (P)HxAlGltns, respectively) were fabricated using the salt-leaching method with NaCl particles as a porogen. To crosslink AlGltn or HxAlGltn, trisuccinimidyl citrate (TSC) was employed[41] (Figure 4.1B). Solid-liquid ratios (SLR) of NaCl and AlGltn or HxAlGltn/(10% lactic acid (LA)-dimethyl sulfoxide (DMSO)) ranged from 0/1 to 5/1, and the porosity of each porous film was regulated with an accuracy of 1% to 65% (Figure 4.1C).

4.4.3. Mechanical Strength of the (P)HxAlGltns and the (P)AlGltns

The tensile strength of the porous films declined in accordance with the porosity-increase. Under both wet and dry condition, (P)HxAlGltns were lower in mechanical strength compared with (P)AlGltn (Figure 4.2). In dried state, the strength declining was outstanding between SLR0/1 to 1/1, however, those over SLR1/0 were not outstanding (Figure 4.2A). In wet state, there was rather gradual mechanical strengths declining from SLR0/1 to 1/1 and over 1/1 (Figure 4.2B). Under both wet and dry state, (P)HxAlGltns were weaker compared with (P)AlGltns with each SLR.

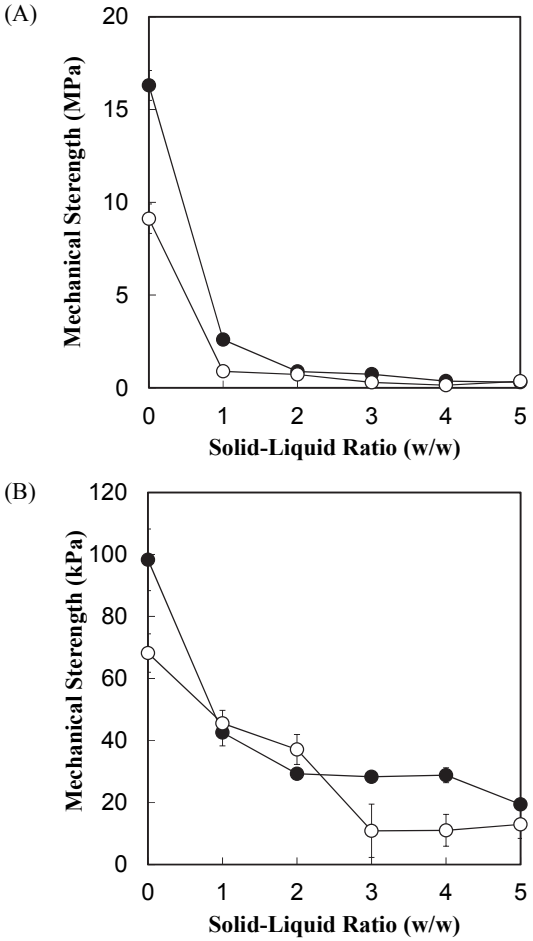

Figure 4.2. Bulk strength of the porous films. Tensile strength of (P)AlGltns (●) and (P)HxAlGltns (○) under dry (a) or wet (b) state. n=3.

Each Gltn molecule can interact with other Gltn molecules, however, Hx group inhibited HxAlGltn interaction with other HxAlGltn moiety by volume exclusion. The inhibition resulted in weaker bulk strength in both wet- and dry- (P)HxAlGltns than (P)AlGltns. The SLR dependent declining of the bulk strength was derived from inner wall thickness, and over SLR3/1, there were little space for packing NaCl particles in the solution and slight amount of holes without any NaCl particles and liquid were inserted resulted in gradual increasing through hole, or declining of the beam thickness. Under the wet state, all the pores were full with water and the HxAlGltn and AlGltn molecules can move more freely compared with those under dried state, therefore, the interaction between each molecule got weaker resulted in rather weak bulk strengths.

4.4.4. Bonding Strength of the (P)HxAlGltns and (P)AlGltns on the Intestine Surface

Before measuring bonding strength, the loading weight/moment was optimized using (P)AlGltn-SLR4/1. Pressure applied at 40 g/mm^2 for 3 min was found to be the optimum condition (Figure 4.3). Therefore, these conditions were applied to all further experiments. The same conditions were optimal for the (P)HxAlGltn-SLR4/1-intestine bonding measurements (Figure 4.4.).

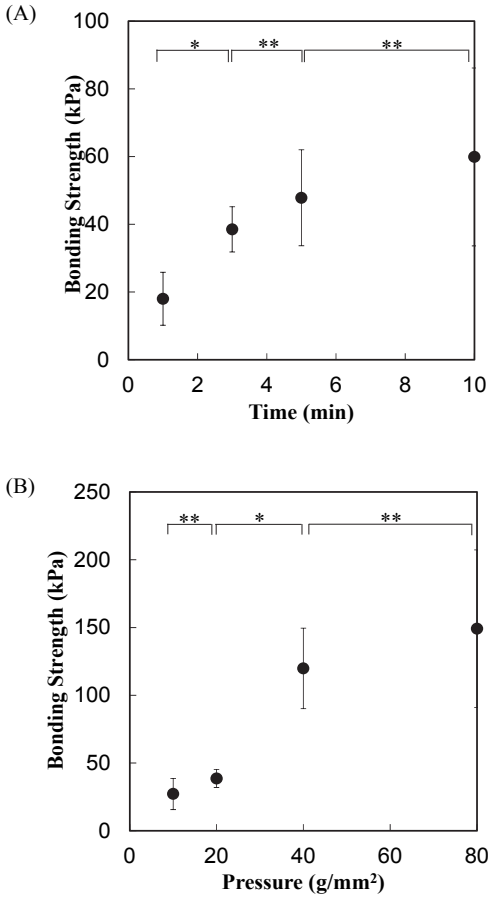

Figure 4.3. Optimization of loading weight and time for bonding strength measurements. The dependence on loading time and loading pressure on measurements of bonding strength between (P)AlGltns and the porcinal intestine. (A) Loading time effect on bonding strength for 20 g/mm^2 at 37 °C (B) Loading pressure effect on bond strength for 3 min-loading at 37 °C. Data are the means ± SD of three samples (n = 3), *p < 0.05, **p > 0.05.

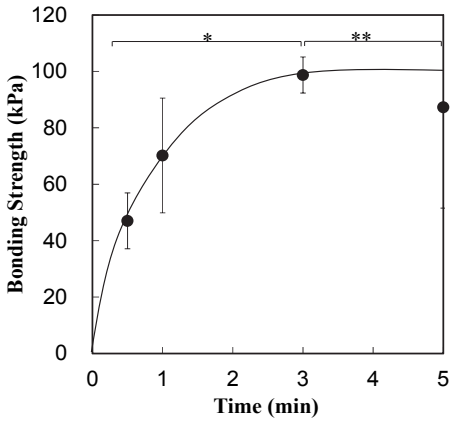

Figure 4.4. Determination of loading conditions for (P)HxAlGltn-intestine bonding strength measurements. Dependence on loading time of the bond strength between the (P)HxAlGltn film fabricated with 4/1-SLR and the porcinal intestine. Time-dependent bonding strength for 40 g/mm^2 at 37 °C. Data are the means ± SD of three samples (n = 3), *p < 0.05, **p > 0.05.

The bonding strength between porous films and the porcinal intestine indicated an advantage of (P)HxAlGltns relative to (P)AlGltns; for each SLR except SLR0/1, it had 2 to 3 times greater bonding strength (Table 4.1). In particular, (P)HxAlGltn bonded the strongest (98.7 ± 6.4 kPa) to the intestine surface in porous films when the porosity was 62%. In contrast, the bonding strength of (P)AlGltn to the intestine surface was below 40 kPa for all porosities.

Table 4.1. Bonding strength between porous membrane and intestine

Abbreviation	Solid-Liquid Ratio (w/w)	Porosity (%)	Bonding Strength (kPa)
(P)AlGltn-SLR0/1	0/1	0	25.2 ± 1.0
(P)AlGltn-SLR1/1	1/1	31	38.9 ± 2.4
(P)AlGltn-SLR2/1	2/1	45	40.1 ± 6.7
(P)AlGltn-SLR3/1	3/1	49	39.0 ± 9.3
(P)AlGltn-SLR4/1	4/1	52	31.2 ± 1.3
(P)AlGltn-SLR5/1	5/1	64	26.6 ± 15.6
(P)HxAlGltn-SLR0/1	0/1	1	25.6 ± 1.0*
(P) HxAlGltn-SLR1/1	1/1	17	77.8 ± 12.3*
(P) HxAlGltn-SLR2/1	2/1	39	94.9 ± 9.4*
(P) HxAlGltn-SLR3/1	3/1	50	73.2 ± 16.1*
(P) HxAlGltn-SLR4/1	4/1	62	98.7 ± 6.4*
(P) HxAlGltn-SLR5/1	5/1	65	77.0 ± 4.1*

(P)AlGltn: porous alkaline-treated gelatin film.
(P)HxAlGltn: porous hexanoyl group modified AlGltn film.
All the measurement was under n=3 condition.
The asterisks mean p < 0.05 compared with 45% porous AlGltn under Aspin-Welch's t-tests.

Figure 4.5 shows that the intestine tissue remained on the porous films after the bonding strength was measured. Thin tissue was found on the (P)AlGltn-SLR4/1 surface (Figure 4.5A); however, thick tissue remained on (P)HxAlGltn-SLR4/1 (Figure 4.5B) , indicating that the strong bonding of highly porous (P)HxAlGltn caused tissue destruction. These results showed that tissue destruction was highly correlated with bonding strength corresponded with the bonding strength.

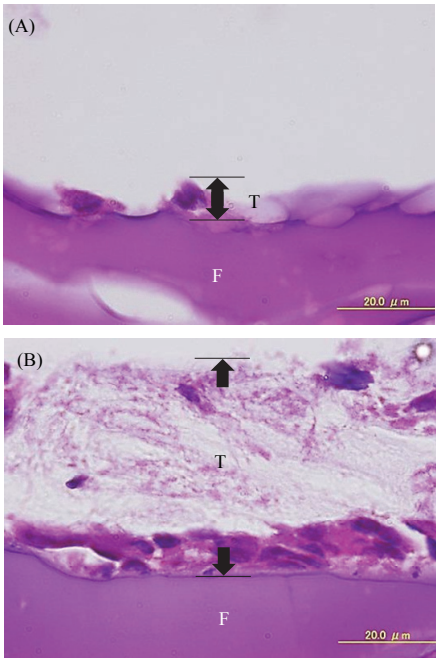

Figure 4.5. Bonding behavior between porous films and porcinal intestine surfaces. Hematoxylin and eosin-stained intestine remnants remained on the (P)AlGltn-SLR4/1 (A) or (P)HxAlGltn-SLR4/1 (B) interfaces after peeling strength measurements were taken. F: Film, T: tissue, arrows: the limb of attached tissue. Scale bars: 20 μm.

(P)HxAlGltns-SLR1/1 to SLR5/1 bonded approximately 3 times more strongly than (P)AlGltns for each SLR. This result indicates that the porous structure effected wet tissue bonding when the Hx group was included. Hematoxylin and eosin staining after bonding strength was measured indicated that film remnants (dark purple) remained on the tissue surfaces (pink purple) and vice versa (Figure 4.6). Tissue remnants could be observed on the (P)HxAlGltns surfaces (Figure 4.6i-l); however, little (P)HxAlGltn remained on the tissue surface (Figure 4.6m-p). In the case of (P)AlGltns, there was no remnant on the tissue surfaces (Figure 4.6e-h) and no tissue remained on (P)AlGltns (Figure 4.6a-d). These results suggest that strong binding of (P)HxAlGltns results in adherence failure. Compared with flat-structured surfaces, porous surfaces facilitate moisture absorption from wet tissue surfaces. The Hx group penetrated the cell membrane of the tissue surface and easily interacted with the hydrophobic region of the extracellular matrix including hydrophobic amino acids owing to its low melting point and resulting high mobility. Without the Hx group, (P)AlGltns could not strongly bind to the tissue surface, irrespective of SLR.

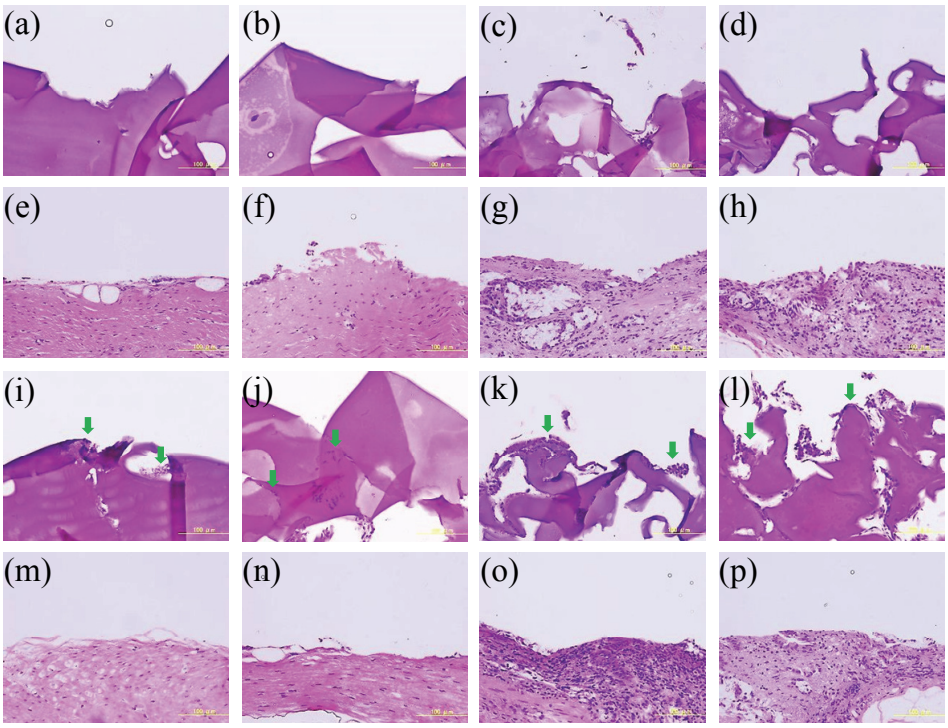

Figure 4.6. Peeling interface after bonding strength measurements. Hematoxylin and eosin-stained cross sections of the interfaces between porcinal intestines and porous films after bonding strength was measured. (a–d) (P)AlGltn surfaces, (e–h) (P)AlGltn-peeled intestine surfaces, (i–l) (P)HxAlGltn surfaces and (m–p) (P)HxAlGltn-peeled intestine surfaces. The solid-liquid ratio of each film was 0/1 (a, i), 1/1 (b, j), 4/1 (c, k), or 5/1 (w/w) (d, l).

4.4.5. Cellular Proliferation and the Morphology on the (P)HxAlGltns and (P)AlGltns

For fast tissue regeneration, cell adhesion to the material is also an important property. The initial cell adhesion and subsequent viability on the porous films were investigated by culturing L929 on (P)AlGltns and (P)HxAlGltns without FBS. The number of cells on (P)AlGltn-SLR1/1 was constant after culturing for 24h; on (P)AlGltn-SLR4/1, it increased until 8 h and decreased by 24h of culture. In contrast, a large number of L929 cells were found on the (P)HxAlGltns after 24h, especially on (P)HxAlGltn-SLR4/1 (Figure 4.7A). Throughout the cultivation period, the cultured L929 cells extended more widely on the (P)HxAlGltns than on the (P)AlGltns (Figure 4.7B). The expansion of cells on the (P)HxAlGltns depended on the culturing time. The cells on (P)AlGltns showed minimal differences among culturing times. Cells on (P)HxAlGltn-SLR4/1 were flatter than those on (P)HxAlGltn-SLR1/1.

The duplication time of L929 is 14h, and the culture period was sufficient for comparisons. The transition in cell number and cell morphology indicated that the cells proliferated easily on highly porous (P)HxAlGltns. It is well known that the stiffness of the scaffold effects the reaction of cells, including proliferation[44,45]. A shorter carbon chain acts as surfactant, inducing inflammation. As shown in Figure 4.7B, the softness of (P)HxAlGltn-SLR4/1 in wet conditions and the shorter carbon chain of the Hx group effected cellular

activation via a signaling pathway resulting in high proliferation. In addition, the Hx group facilitated reactions or insertions to the cellular membrane, resulting in elongation of the pseudopodia.

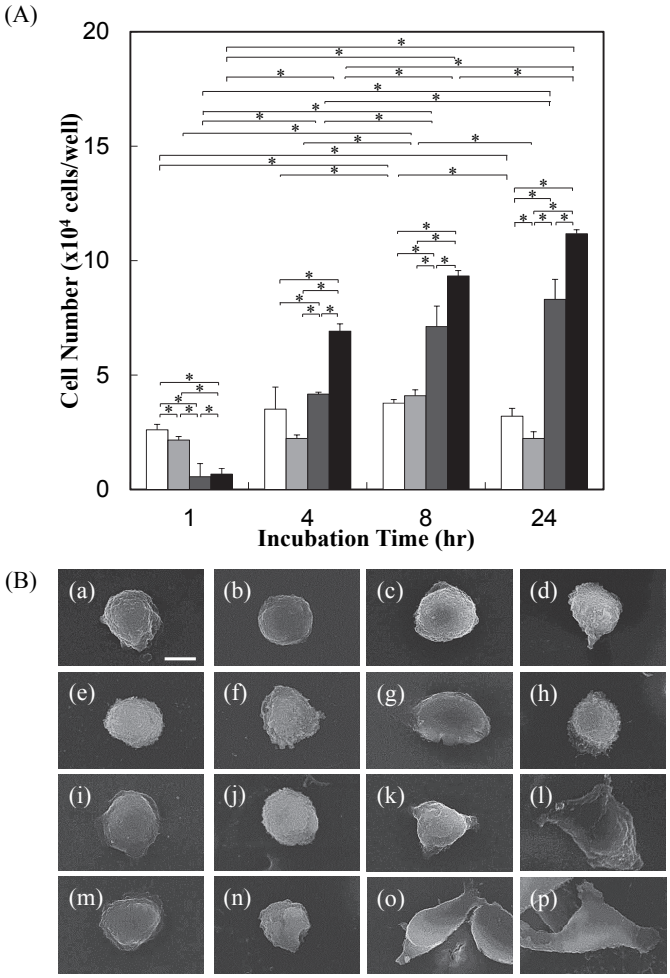

Figure 4.7. L929 cell proliferation and cell morphology. (A) L929 cell viability for 1-, 4-, 8-, and 24-h cultures on the porous films fabricated with various solid-liquid ratios. White column: (P)AlGltn-SLR0/1, light gray column: (P)AlGln-SLR4/1, dark gray column: (P)HxAlGltn-SLR0/1, black column: (P)HxAlGltn-SLR4/1. n = 3, * $p < 0.05$. (B) L929 cell morphology after 1 h (a~d), 4 h (e~h), 8 h (i~l), or 24 h (m~p) of culturing on (P)AlGltn-SLR0/1 (a, e, i, m), (P)AlGltn-SLR4/1 (b, f, j, n), (P)HxAlGltn-SLR0/1 (c, g, k, o), or (P)HxAlGltn-SLR4/1 (d, h, l, p) surfaces. Scale bar is 5 μm.

4.4.6. Tissue reaction for (P)HxAlGltns and (P)AlGltns

The disc-shaped porous films with diameters of 1 cm were subcutaneously implanted in the back of rats for 3, 7, 14, and 28 days to evaluate biodegradation, tissue infiltration, and angiogenesis. For all porosities, (P)HxAlGltns degraded faster than (P)AlGltns. Specifically, (P)HxAlGltn with a porosity of 62% degraded within 28 days, and its degradation was faster than that of (P)HxAlGltns with different porosities (Figure 4.8A).

Tissue infiltration into (P)HxAlGltns was also detected at an earlier stage, and the surrounding tissue was completely infiltrated 7 days after implantation (Figure 4.8B). Moreover, more red blood cells were found around (P)HxAlGltns than (P)AlGltns.

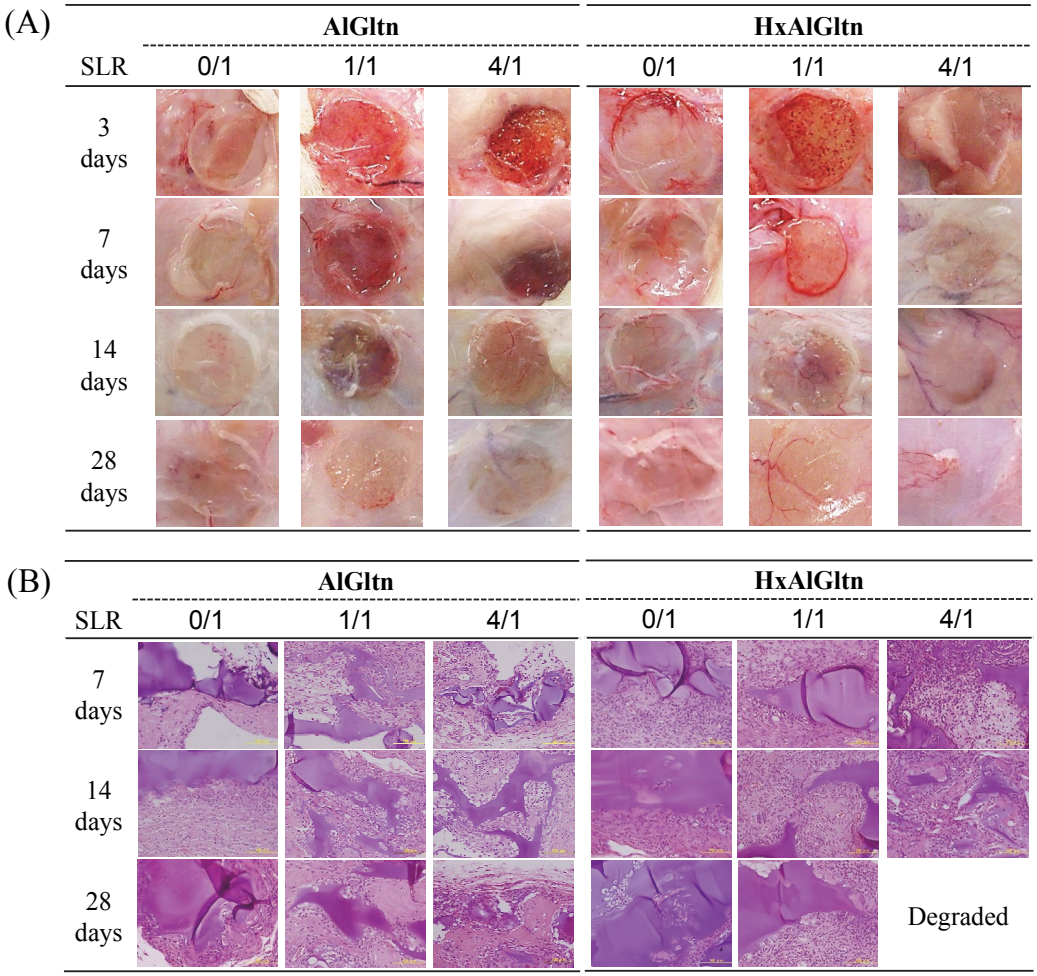

Figure 4.8. Behavior of the porous films under rat subcutaneous. (A) Biodegradation of (P)AlGltns and (P)HxAlGltns fabricated with various solid-liquid ratios under rat subcutaneous after 3 to 28 days implantation. (B) H&E stained tissue and (P)AlGltns or (P)HxAlGltns fabricated with various solid-liquid ratios implanted under rat subcutaneous for 7 to 28days.

The faster degradation of (P)HxAlGltn-SLR4/1 could be related to its lower bulk strength and cell proliferation/infiltration ability. Matrix metalloproteinases (MMPs), splitting enzymes that degrade the extracellular matrix, is widely expressed in fibroblasts[46-48]. Therefore, fibroblast proliferation and the accessibility of AlGltn molecules accelerated (P)HxAlGltn-SLR4/1 degradation via MMPs. Moreover, the highly porous structure and Hx group-derived cellular activation resulted in faster tissue infiltration.

4.4.7. Angiogenesis Evaluation around the Porous Films Based on CD34 and α-SMA Immunostaining

valuate angiogenesis after the implantation of porous films, CD34 and α-smooth muscle actin (α-SMA) immunostaining was performed. A larger positive area indicating CD34, which is a marker of immature endothelial cells or early vascularization, was found around (P)HxAlGltn than around (P)AlGltn (Figure 4.9A) with SLR 0/1 and 4/1. Quantitative data analyzed using ImageJ indicated more CD34 expression around (P)HxAlGltn in the early stage (i.e., the first 7 days), especially for a porosity of 62% (Figure 4.9Ba). However, the area of the vascular holes was constant from 7 to 28 days (Figure 4.9Bb) for almost all the implanted materials. The number of vascular areas marked by CD34 staining did not clearly differ between the porous films (Figure 4.9Bc).

The marker of mature endothelial cells or late vascularization, α-SMA, was also observed around both (P)AlGltn and (P)HxAlGltn (Figure 4.10A and Ba). Furthermore, the α-SMA-positive area decreased over time when (P)AlGltn-SLR4/1 and (P)HxAlGltn-SLR4/1 were implanted. (P)HxAlGltn had a large vascular hole area that was surrounded by α-SMA (Figure 4.10Bb). Many vascular regions formed around (P)HxAlGltn until 14 days after implantation (Figure 4.10Bc). (P)AlGltn showed a disadvantage with respect to number of vascular holes, vascular hole area, and α-SMA-positive area.

High expression of CD34 at an early stage and a wide vascular hole area with CD34 staining were observed over a 14-day period. These phenomena indicated that (P)HxAlGltn-SLR4/1 had the advantage of faster induction of infant vascular endothelial cells and faster formation of immature large vascular walls around the film. CD34 is a marker of immature cells; therefore, the sharp decline in the CD34-positive area after implantation from 7 to 14 days is consistent with the longer implantation period. The α-SMA-positive area of (P)HxAlGltn was larger than the CD34-positive area 14 days after implantation, indicating the promotion of mature endothelium formation. The proportional changes in the number of α-SMA-marked vascular regions and the α-SMA-marked vascular area indicate mature microvascular formation with congenial thickness around the porous films, especially around the (P)HxAlGltn-SLR4/1. There were large α-SMA-positive areas around (P)AlGltn-SLR4/1; however, few vascular holes formed around (P)AlGltn-SLR4/1, indicating that the angiogenic properties of (P)AlGltn-SLR4/1 were slower compared with those of (P)HxAlGltn-SLR4/1.

VEGF is secreted from various cells including fibroblasts to facilitate angiogenesis[49-51]. In the cell culture experiment, fibroblasts showed high cytocompatibility with (P)HxAlGltn-SLR4/1, and fibroblast-like cells around the (P)HxAlGltn-SLR4/1 produced VEGF and MMP to induce immature vascular endothelial cells and promoted microvascular maturation.

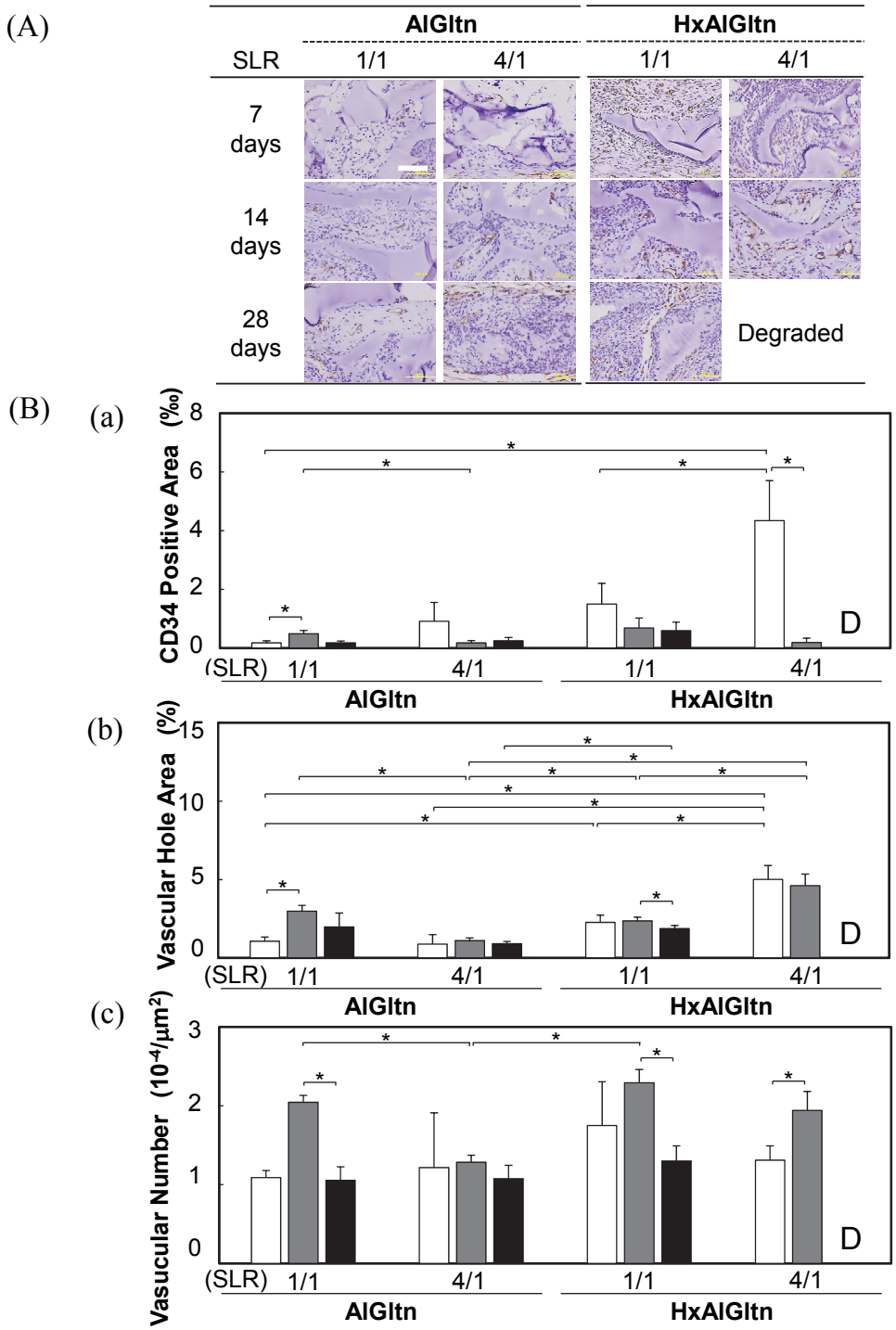

Figure 4.9. Angiogenesis analysis with CD34 staining. (A) Microscopic images of CD34-stained tissues and (P)AlGltns or (P)HxAlGltns fabricated with various solid-liquid ratios after subcutaneous implantation in rats for 7, 14, and 28 days. (B) Evaluation of angiogenesis based on the (a) CD34-positive area, (b) CD34-encircled vascular area, and (c) CD34-encircled vascular number. White column: 7 days, gray column: 14 days, black column: 28 days. D: completely degraded. Data are the means ± SD of three samples (n = 3), * $p < 0.05$. Scale bar: 100 μm.

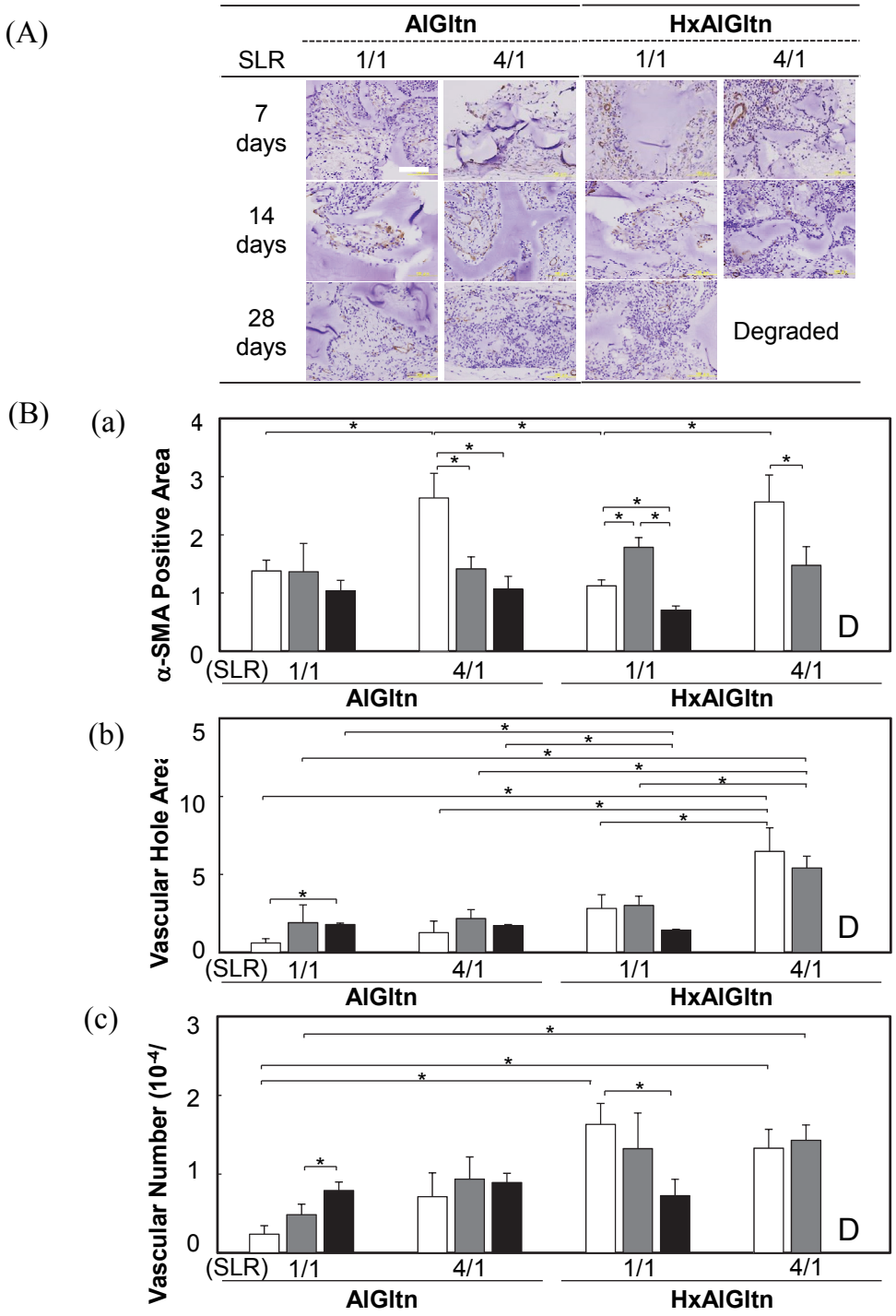

Figure 4.10. Angiogenesis analysis with α-SMA staining. (A) Microscopic images of α-smooth muscle actin (α-SMA)-stained tissues and (P)AlGltns or (P)HxAlGltns fabricated with various solid-liquid ratios after subcutaneous implantation in rats for 7, 14, and 28 days. (B) Evaluation of angiogenesis based on the (a) α-SMA-positive area, (b) α-SMA-encircled vascular area, and (c) α-SMA-encircled vascular number. White column: 7 days, gray column: 14 days, black column: 28 days. D: completely degraded. Data are the means ± SD of three samples (n = 3), * $p < 0.05$. Scale bar: 100 μm.

4.4.8. Fibronectin (FN), Basic Fibroblast Growth Factor (bFGF), and Vascular Endothelium Growth Factor (VEGF) Affinity with HxAlGltn

Fibronectin (FN) is a well-known cell adhesion protein owing to its arginine-glycine-asparagine (RGD) binding site residues. Furthermore, both basic fibroblast growth factor (bFGF) and vascular endothelium growth factor (VEGF) stimulate angiogenesis in vivo[25,28,42,43]. To clarify the angiogenesis mechanisms of (P)HxAlGltns, the affinity of these biofunctional proteins with (P)HxAlGltns was determined using surface plasmon resonance. Table 4.2 shows the dissociation constants (KD) for FN, bFGF, and VEGF from AlGltn or HxAlGltn molecules. The bFGF dissociation constant was smaller for AlGltn than HxAlGltn (HxAlGltn: 1.02×10^{-6}, AlGltn: 4.77×10^{-9}), indicating that AlGltn shows higher affinity for bFGF than does HxAlGltn. Both FN and VEGF demonstrated stronger binding to HxAlGltn molecules than to AlGltn molecules. In particular, the VEGF dissociation constant was 17.2 times smaller for AlGltn than HxAlGltn (HxAlGltn: 2.90×10^{-8}, AlGltn: 5.00×10^{-7}). Therefore, VEGF was more involved in angiogenesis after the implantation of (P)HxAlGltn.

Table 4.2. Dissociation constants of proteins from AlGltn/HxAlGltn

	Dissociation: K_D (M)		
	Fibronectin	**bFGF**	**VEGF**
AlGltn	6.38×10^{-6}	4.77×10^{-9}	5.00×10^{-7}
HxAlGltn	1.60×10^{-6}	1.02×10^{-6}	2.90×10^{-8}

The bFGF released from heparin is related to Hx-group modification[27]. Therefore, it can be hypothesized that angiogenesis factors including bFGF interact with HxAlGltn modified with the Hx group to facilitate angiogenesis. Unexpectedly, VEGF showed higher affinity to HxAlGltn than did bFGF. Therefore, angiogenesis around (P)HxAlGltn-SLR4/1 could largely depend on the capture and release of VEGF from HxAlGltn molecules. The mechanism of angiogenesis induced by HxAlGltn is follows. After implantation of (P)HxAlGltn, various types of inflammatory cells including macrophages infiltrate the (P)HxAlGltn. Then, cytokines and angiogenic factors including VEGF are released from inflammatory cells. As shown in Figure 4.11A, Hx group on the (P)HxAlGltn stimulates angiogenesis more than (P)AlGltn. And the Figure 4.11 shows, (P)HxAlGltns induce inflamation than (P)AlGltns. The released VEGF binds to (P)HxAlGltn. This VEGF binding behavior is expected based on the surface plasmon resonance analysis, as shown in Table 4.2. Inflammatory cells also release MMP[52-54]; therefore, VEGF bound to (P)HxAlGltn is released from the (P)HxAlGltn after the digestion of HxAlGltn. As a result, released VEGF bound to (P)HxAlGltn stimulates angiogenesis (Figure 4.11B).

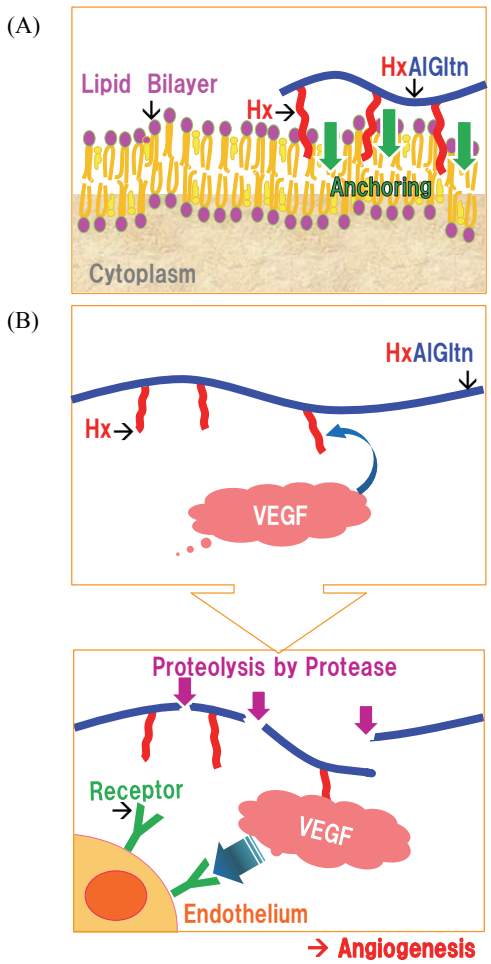

Figure 4.11. Bonding and angiogenesis mechanisms of (P)HxAlGltn. (A) The bonding mechanism of (P)HxAlGltn to soft tissue. The Hx group of HxAlGltn anchored to the lipid bilayer of the epithelium on the intestine surface. (B) Angiogenesis induction via (P)HxAlGltn. Secreted VEGF was bound to the HxAlGltn molecule subcutaneously, followed by HxAlGltn degradation via proteolysis with protease, and the VEGF-HxAlGltn moiety and endothelium interaction resulted in angiogenesis.

4.5. Conclusion

In conclusion, the bonding and angiogenic behavior of (P)HxAlGltns was evaluated. (P)HxAlGltns-SLR4/1 had superior bonding strength to the porcine intestine surface compared with (P)AlGltns. Angiogenic markers including CD34 and α-SMA were highly expressed around (P)HxAlGltn-SLR4/1 in all films. These results indicated that (P)HxAlGltns-SLR4/1, with a porosity of 62%, has potential for use as a tissue adhesive material as well as a scaffold for tissue engineering without the use of growth factors.

4.6. References

1. Rose, S. et al. Nanoparticle solutions as adhesives for gels and biological tissues. *Nature* **505**, 382-385 (2014).
2. Okamura, Y. et al. Fragmentation of poly(lactic acid) nanosheets and patchwork treatment for burn wounds. *Adv Mater* **25**, 545-551 (2012).
3. Lee, B. P., Messersmith, P. B., Israelachvili, J. N. & Waite, J. H. Mussel-inspired adhesives and coatings. *Ann Rev Mater Res* **41**, 99-132 (2011).
4. Lee, H., Dellatore, S. M., Miller, W. M. & Messersmith, P. B. Mussel-inspired surface chemistry for multifunctional coatings. *Science* **318**, 426-430 (2007).
5. Bartlett, M. D. et al. Looking beyond fibrillar features to scale gecko-like adhesion. *Adv Mater* **24**, 1078-1083 (2012).
6. Iwata, H., Matsuda, S., Mitsuhashi, K., Itoh, E. & Ikada, Y. A novel surgical glue composed of gelatin and N-hydroxysuccinimide activated poly(L-glutamic acid): Part 1. Synthesis of activated poly(L-glutamic acid) and its gelation with gelatin. *Biomaterials* 19, 1869-1876 (1998).
7. Cohen, B., Pinkas, O., Foox, M. & Zilberman, M. Gelatin-alginate novel tissue adhesives and their formulation-strength effects. *Acta Biomater* **9**, 9004-9011 (2013).
8. Taguchi, T., Saito, H., Iwasashi, M., Sakane, M. & Ochiai, N. Biodegradable adhesives composed of human serum albumin and organic acid-based crosslinkers with active ester groups. *J Bioact Compat Polym* **24**, 546-559 (2009).
9. Chao, H. & Torchiana, D. BioGlue: Albumin/glutaraldehyde sealant in cardiac surgery. *J Card Surg* **18**, 500-503 (2003).
10. Iwasashi, M. et al. In vivo evaluation of bonding ability and biocompatibility of a novel biodegradable glue consisting of tartaric acid derivative and human serum albumin. *J Biomed Mater Res A* **90** (2), 543-548 (2009).
11. Berchane, N. S., Andrews, M. J., Kerr, S., Slater, N. K. H. & Jebrail, F. F. On the mechanical properties of bovine serum albumin (BSA) adhesives. *J. Mater Sci Mater Medic* **19**, 1831–1838 (2008).
12. Lee, J. M. et al. Facile pore structure control of poly(ε-caprolactone) nano-fibrous scaffold by salt-dispenser aided electrospinning. *J Nanoeng Nanomanuf* **3**, 269-275 (2013).
13. Babensee, J. E., McIntire, L. V. & Mikos, A. G. Growth factor delivery for tissue engineering. *Pharmaceut Res* **17**, 497-504 (2000).
14. Boontheekul, T. & Mooney, D. J. Protein-based signaling systems in tissue engineering. *Curr Opin Biotech* **14**, 559-565 (2003).
15. Chen, R. R. & Mooney, D. J. Polymeric growth factor delivery strategies for tissue engineering. *Pharmaceut Res* **20**, 1103-1112 (2003).
16. Choi, J. S., Leong, K. W. & Yoo, H. S. In vivo wound healing of diabetic ulcers using electrospun nanofibers immobilized with human epidermal growth factor (EGF). *Biomaterials* **29**, 587-596 (2008).
17. Chwalek, K., Tsurkan, M. V., Freudenberg, U. & Werner, C. Glycosaminoglycan-based hydrogels to modulate heterocellular communication in in vitro angiogenesis models. *Sci Rep* **4**, 4414 (2014).

18. Lee, K., Silva, E. A. & Mooney, D. J. Growth factor delivery-based tissue engineering: general approaches and a review of recent developments. *J R Soc Interface/ R Soc* **8**, 153-170 (2011).
19. Richardson, T. P., Peters, M. C., Ennett, A. B. & Mooney, D. J. Polymeric system for dual growth factor delivery. *Nat Biotech* **19**, 1029-1034 (2001).
20. Sakiyama-Elbert, S. E., Panitch, A. & Hubbell, J. A. Development of growth factor fusion proteins for cell-triggered drug delivery. *FASEB J* **15**, 1300-1302 (2001).
21. Whitaker, M. J., Quirk, R. A., Howdle, S. M. & Shakesheff, K. M. Growth factor release from tissue engineering scaffolds. *J Pharm Pharmacol* **53**, 1427–1437 (2001).
22. Zisch, A. H., Lutolf, M. P. & Hubbell, J. A. Biopolymeric delivery matrices for angiogenic growth factors. *Cardiovasc Pathol* **12**, 295-310 (2003).
23. Fujisato, T., Sajiki, T., Liu, Q. & Ikada, Y. Effect of basic fibroblast growth factor on cartilage generation in chondrocyte-seeded collagen sponge scaffold. *Biomoterials* **17**, 155-162 (1996).
24. Jeon, E., Yun, Y. R., Kim, H. W. & Jang, J. H. Engineering and application of collagen-binding fibroblast growth factor 2 for sustained release. *J Biomed Mater Res A* **102**(1),1-7 (2014).
25. Numata, Y. et al. The accelerating effect of histamine on the cutaneous wound-healing process through the action of basic fibroblast growth factor. *J Invest Dermatol* **126**, 1403-1409 (2006).
26. Riboni, L., Viani, P., Bassi, R., Giussani, P. & Tettamanti, G. Basic fibroblast growth factor-induced proliferation of primary astrocytes. evidence for the involvement of sphingomyelin biosynthesis. *J Biolog Chem* **276**, 12797-12804 (2001).
27. Wissink, M. J. B. et al. Binding and release of basic fibroblast growth factor from heparinized collagen matrices. *Biomaterials* **22**, 2291-2299 (2001).
28. Sasaki, M., Inoue, M., Katada, Y. & Taguchi, T. The effect of VEGF-immobilized nickel-free high-nitrogen stainless steel on viability and proliferation of vascular endothelial cells. *Colloid Surface B* **92**, 1-8 (2012).
29. Zisch, A. H. et al. Cell-demanded release of VEGF from synthetic, biointeractive cell ingrowth matrices for vascularized tissue growth. *FASEB J* **17**, 2260-2262 (2003).
30. Zisch, A. H., Schenk, U., Schense, J. C., Sakiyama-Elbert, S. E. & Hubbell, J. A. Covalently conjugated VEGF–fibrin matrices for endothelialization. *J Cont Rel* **72**, 101–113 (2001).
31. Vempati, P., Mac Gabhann, F. & Popel, A. S. Quantifying the proteolytic release of extracellular matrix-sequestered VEGF with a computational model. *PLoS ONE* **5**, e11860 (2010).
32. Vempati, P., Popel, A. S. & Mac Gabhann, F. Extracellular regulation of VEGF: Isoforms, proteolysis, and vascular patterning. *Cytokine Growth Fact Rev* **25**, 1-19 (2013).
33. Tabata, Y., Nagano, A. & Ikada, Y. Biodegradation of hydrogel carrier incorporating fibroblast growth factor. *Tissue Eng* **5**, 127-138 (1999).
34. Tabata, Y. Tissue regeneration based on growth factor release. *Tissue Eng* **9**, S5-15 (2003).
35. Ishai-Michaeli, R. et al. Importance of size and sulfation of heparin in release of basic fibroblast growth-factor from the vascular endothelium and extracellular matrix. *Biochemistry* **31**, 2080-2088 (1992).
36. Matsuda, M. et al. Enhanced tissue penetration-induced high bonding strength of a novel tissue adhesive composed of cholesteryl group-modified gelatin and disuccinimidyl tartarate. *Colloid Surface B* **91**, 48-56 (2012).
37. Matsuda, M. & Taguchi, T. In vitro evaluation of tissue adhesives composed of hydrophobically modified

gelatins and disuccinimidyl tartrate. *Sci Technol Adv Mat* **13**, 064212 (2012).

38. Matsuda, M. et al. Enhanced tissue penetration-induced high bonding strength of a novel tissue adhesive composed of cholesteryl group-modified gelatin and disuccinimidyl tartarate. *Colloid Surface B* **91**, 48-56 (2012).
39. Yoshizawa, K. & Taguchi, T. Bonding behavior of hydrophobically modified gelatin films on the intestinal surface. *J Bioact Compat Polym* **29**, 560-571 (2014).
40. Yoshizawa, K. & Taguchi, T. Enhanced bonding strength of hydrophobically modified gelatin films on wet blood vessels. *Intn J Molecul Sci* **15**, 2142-2156 (2014).
41. Inoue, M., Sasaki, M., Nakasu, A., Takayanagi, M. & Taguchi, T. An antithrombogenic citric acid-crosslinked gelatin with endothelialization activity. *Adv Healthcare Mater* **1**, 573-581., 201200001 (2012).
42. Takayama, T. et al. The growth of a vascular network inside a collagen-citric acid derivative hydrogel in rats. *Biomaterials* **30**, 3580-3587 (2009).
43. Zeng, Z. & Zhu, B. H. Arnebin-1 promotes the angiogenesis of human umbilical vein endothelial cells and accelerates the wound healing process in diabetic rats. *J Ethnopharmacol* **154**, 653-662 (2014).
44. Murphy, C. M., O'Brien, F. J., Little, D. G. & Schindeler, A. Cell-scaffold interactions in the bone tissue engineering triad. *Eur Cells Mater* **26**, 120-132 (2013).
45. Murphy, C. M., Matsiko, A., Haugh, M. G., Gleeson, J. P. & O'Brien, F. J. Mesenchymal stem cell fate is regulated by the composition and mechanical properties of collagen–glycosaminoglycan scaffolds. *J Mechanic Behav Biomed Mater* **11**, 53-62 (2012).
46. Bellucci, C. et al. Differences in extracellular matrix production and basic fibroblast growth factor response in skin fibroblasts from sporadic and familial Alzheimer's disease. *Molecul Med* **13**, 542-550 (2007).
47. Kendall, R. T. & Feghali-Bostwick, C. A. Fibroblasts in fibrosis: novel roles and mediators. *Front Pharmacol* **5**, 123 (2014).
48. Bourget, J. M. et al. Human fibroblast-derived ECM as a scaffold for vascular tissue engineering. *Biomaterials* **33**, 9205-9213 (2012).
49. Ferrara, N. & Davis-Smyth, T. The biology of vascular endothelial growth factor. *Endocrine Rev* **18**, 4-25 (1997).
50. Yamamoto, T. et al. Expression of vascular endothelial growth factor in normal pituitary cells and pituitary adenomas producing adrenocorticotropic hormone. *Endocrine Pathol* **10**, 157-164 (1999).
51. Shifren, J. L., Doldi, N., Ferrara, N., Mesiano, S. & Jaffe, R. B. In the human fetus, vascular endothelial growth factor is expressed in epithelial cells and myocytes, but not vascular endothelium: implications for mode of action. *J Clin Endocrine Metabol* **79**, 316-322 (1994).
52. Parsons, S. L., Watson, S. A., Brown, P. D., Collins, H. M. & Steele, R. J. C. Matrix metalloproteinases. *Brit J Surg* **84**, 160-166 (1997).
53. Lin, T. et al. Neutrophil-mediated secretion and activation of matrix metalloproteinase-9 during cardiac surgery with cardiopulmonary bypass. *Anesth Analg* **100**, 1554-1560 (2005).
54. Ardi, V. C., Kupriyanova, T. A., Deryugina, E. I. & Quigley, J. P. Human neutrophils uniquely release TIMP-free MMP-9 to provide a potent catalytic stimulator of angiogenesis. *Proc Nation Acad Sci USA* **104**, 20262-20267 (2007).

55. Lang, G. Efficacy and safety of topical application of human fibrinogen/thrombin-coated collagen patch (TachoComb) for treatment of air leakage after standard lobectomy. *Eur J Cardio-thorac Surg* **25**, 160-166 (2004).
56. Matsuda, M., Inoue, M. & Taguchi, T. Enhanced bonding strength of a novel tissue adhesive consisting of cholesteryl group-modified gelatin and disuccinimidyl tartarate. *J Bioact Compat Polym* **27**, 31-44 (2012).
57. Morcol, T., Subramanian, A. & Velander, W. H. Dot-blot analysis of the degree of covalent modification of proteins and antibodies at amino groups. *J Immunol Met.* **203**, 45-53 (1997).
58. Taguchi, T. et al. Biocompatible high-strength glue consisting of citric acid derivative and collagen. *Mater Sci Eng C* **26**, 9-13 (2006).

Chapter 5

Pore Size Impact on Angiogenesis and Bonding Strength in Hexanoyl Group Modified Gelatin Adhesive Films

5.1. Summary

The relationship between wet tissue adhesion, the ability to stimulate angiogenesis and pore size of hexanoyl (Hx: C_6) group modified, alkaline-treated gelatin (HxAlGltn)-porous films ((P)HxAlGltn) was evaluated. (P)HxAlGltn was fabricated via salt-leaching using 43, 77, 156 or 375 μm diameter NaCl particles in a 4/1 (w/w)-solid-liquid ratio ((P43)-, (P77)-, (P156)-, and (P375)HxAlGltn). Among all (P)HxAlGltns and (P)AlGltns, (P77)HxAlGltn bound strongest to porcinal intestine, and showed the fastest water absorption out of the films evaluated. (P77)HxAlGltn also showed high cellular infiltration, and the fastest degradation out of the films tested when implanted in rat subcutaneous tissue. The infiltrated cells inside (P77)HxAlGltn showed much peroxidase expression. The (P43)HxAlGltn-tissue interface showed the largest CD34 positive area after 3 days implantation in rat subcutaneous tissue. These results indicate that strong bonding between (P)HxAlGltn and tissue is a result of body fluid absorption speed dependent on pore size and Hx group modification. Additionally, inflammatory reactions were found to be important in angiogenesis, and smaller pore sizes were found to induce mild inflammation and early angiogenesis.

5.2. Introduction

Materials that promote rapid wound healing without scar tissue formation are desperately needed in the clinic. For this purpose, several clinical adhesives have been investigated[1-4]. These adhesives, however, have poor bonding ability in wet tissues, forcing surgeons to rely on suturing to promote tissue healing. Suturing, however, wastes operation time and carries the possibility of infection[5,6]. It follows that adhesives with the ability to bond strongly to wet tissues with little to no inflammatory response could potentially supersede sutures.

These adhesives could potentially be effective scaffolds for tissue regeneration. Liquid type adhesives can be applied to any tissue surface morphology[7-9], however, premade adhesives are better suited for scaffolding[10-16]. There are now a number of biomaterials with internally connected spaces that have been designed as scaffolds to facilitate effective tissue regeneration[11,12,17-19]. In these scaffolds, material pore size is crucial to control of cytokine, antibody and cellular infiltration. The tissue regeneration is also depend on appropriate degradation, and it is crucial to control cells to produce growth factors and matrix proteases[20-22]. Therefore, sophisticated regulation of cellular regulation: appropriate inflammation, material degradation and angiogenesis is needed to allow for rapid tissue healing.

Angiogenesis regulation is another important factor for tissue regeneration[20-22]. Rapid angiogenesis results in favorable tissue regeneration in many organs and tissues[23-25]. In order to accelerate angiogenesis, biomaterials with angiogenic factors have been developed, but these factors are expensive, and there are problems regulating factor release[26-28].

We have previously developed a hydrophobically modified gelatin (hm-Gltn) adhesive for clinical use[29-34]. In liquid, solid, and film morphologies, hm-Gltn materials bond strongly to wet tissue surfaces as long as both adhesive and tissue interfaces react with hydrophobic groups anchored to the tissue surface. Alkaline-treated Gltn modified with hexanoyl group (Hx: C_6) (HxAlGltn) based highly porous films bound strongly to wet tissue. Moreover, we found that HxAlGltn had a high affinity to vascular endothelial growth factor (VEGF).

We hypothesized that the regulation of pore size in HxAlGltn based porous films can control wound healing via cellular infiltration and growth factor release to the porous film. Our aim in this study was to clarify the relationship between bonding strength and angiogenesis to HxAlGltn pore size. To accomplish this goal, bulk characterization, bonding strength, water absorbency measurements, and tissue reaction quantification of the porous film were completed.

5.3. Materials and Methods

5.3.1. Materials

BeMatrix®, or alkaline-treated gelatin (AlGltn) derived from porcine skin was kindly donated by Nitta Gelatin Inc. (Osaka, Japan). Ethanol (EtOH), dimethylsulfoxide (DMSO), triethylamine (TEA), 2,4,6-trinitorobenzoylsurfonic acid (TNBS), hydrochloric acid (HCl), sodium dodecyl sulfide (SDS), 10% formalin neutral buffer solution, tertially-buthylalcohol and sodium chloride (NaCl) were purchased from Wako Pure Chemical Industries, Ltd. (Osaka, Japan). Hexanoyl (Hx: C_6) chloride was purchased from Sigma Chemical Co. (St. Louis, MO, USA). Porcine intestine was purchased from Funakoshi Corporation (Tokyo, Japan). Phosphate buffered saline (PBS) was purchased from Lonza (Basel, Switzerland). 2-(2-methoxy-4-nitrophenyl)-3-(4-nitrophenyl)-5-(2,4-disulfophenyl)-2H-tetrazolium (WST-8) was purchased from Dojindo Laboratories (Kumamoto, Japan). All chemicals were used without further purification.

5.3.2. Synthesis and Characterization of HxAlGltn

Based on former reports[29-32], the Hx group introduced into the hm-AlGltn (HxAlGltn) was prepared by reaction between Hx chloride and the primary amino groups of AlGltn. First, AlGltn (10 g) was fully dissolved into 99 mL of dehydrated DMSO at 80℃. Following this step, one mL of hexanoyl chloride was added into the AlGltn/DMSO solution to obtain 100 mL of 10 w/v% AlGltn/DMSO solution under a dry N_2 atmosphere at room temperature. Triethylamine (TEA) was subsequently added to the AlGltn solution and was stirred for 17h at room temperature. The resulting HxAlGltn/DMSO solution was then poured into 300 mL of cold EtOH and stirred for 1 h. Subsequently, the HxAlGltn precipitate was washed twice with 300 mL of cold EtOH followed by evaporation under vacuum. Yields were then calculated.

The modification ratio of Hx groups in HxAlGltn was quantified by the method previously reported using 2,4,6-trinitrobenzensulfonicacid (TNBS)29-32,42. Briefly, HxAlGltns or original AlGltn was dissolved into DMSO to obtain 0.05 w/v% solutions. After this, 100 μL of 0.1 v/v% TEA/DMSO, 50 μL of 0.1 w/v% SDS/DMSO and 100 μL of 0.1 w/v% TNBS/DMSO were added to 100 μL of HxAlGltn or AlGltn/DMSO solution followed by incubation at 37℃ for 2h under light shielding conditions. Following this, 50 μL of 2 N-HCl/DMSO was added to quench the reaction. Finally, light absorbance intensity was measured spectrophotometrically at 340 nm using a microplate-reader (GENios A-5082, Tecan Japan Kanagawa, Japan). The substitution percentage of amino groups with Hx chloride was then calculated from the intensities of HxAlGltn compared with the original AlGltn.

5.3.3. Preparation and Characterization of (P)HxAlGltns and (P)AlGltns

HxAlGltn was first dissolved in DMSO to prepare a 25 w/v% solution. Required amounts of TSC were then added into 10 mL HxAlGltn/DMSO solution, and the TSC-HxAlGltn/DMSO was stirred quickly. NaCl particles were sieved into 5 sizes: 43, 77, 156 and 375 μm in diameter. The required amount of NaCl (the liquid-solid ratio was 4/1) was added to the solution and mixed, allowing for uniform NaCl dispersion. The solution was then packed into a zipper bag (Unipack, Seisannipponsha ltd, Tokyo, Japan) and the HxAlGltn solution including NaCl were put between glass plates with 1 mm thick silicone spacers. After overnight cross-linking, the NaCl-HxAlGltn gels were immersed into 4℃ ultra-pure water for 3 days with frequent water changing to remove DMSO, NaCl, unreacted TSC and side products including n-hydroxysuccinimide (NHS). The hydrogels were frozen at -80℃, and were lyophilized for 3 days to obtain a (P)HxAlGltn film. AlGltn was used to fabricate (P)AlGltn films using the same technique as described above.

5.3.4. Measurement of the Mechanical Strength of (P)HxAlGltns

Each film was cut out into 5 mm × 1 mm shapes, and both sides were bonded on 5 mm × 1 cm plastic sheets by GelBoy (LOCTITE, Japan Henkel, Japan) in a 2.5 mm × 5 mm area. After drying at room temperature, both plastic ends were clipped by probes, and tensile tests at 10 mm/minute speed were performed for all samples before and after 37℃ –water immersion (n = 3).

5.3.5. Measurement of Bonding Strength Between Intestine and (P)HxAlGltns and (P)AlGltns and Observation of the Peeling Interfaces

The following measurement method was applied as previously reported[33,34]. Porcinal intestine was dissected with a dermal punch into disks of 4 mm in diameter. The dissected intestine was bonded onto a probe with GelBoy®. The porous films were also punched out into a 7 mm diameter circle shape, and placed on a heated plate at 37℃. They were then fixed with scotch tape (3M, Tokyo, Japan) with a hole of 4 mm diameter. The bonding strength was then measured using a Texture Analyzer (TA-XT2i, Stable Microsystems, UK) (n = 3) using the following parameters: 180 seconds contact time, 40 g/mm^2 pressure and 10 mm/minute tracking speed.

After the bonding strength measurement, each sample was fixed with 10% formalin neutral buffer solution followed by hematoxylin and eosin (H&E) staining. Each cross-section of the stained samples was observed with an optical microscope (BX51, Olympus, Tokyo, Japan).

5.3.6. Water Absorption Speed of the (P)HxAlGltns and (P)AlGltns

Two μL of ultra-pure water was placed on the porous films at room temperature. The complete water absorption time (T_a) was determined, and the appearance of water on the films at each period was taken using a contact angle meter (DM800, Kyowa Interface Science Co. Ltd., Saitama, Japan) and FAMAS software (Kyowa Interface Science Co., Ltd.). The absorption speed of each film (S_a) was calculated by the following equation (n = 3).

$$S_a = 1/T_a$$

5.3.7. Biodegradability and Tissue Infiltration Observation of the (P)HxAlGltns and (P)AlGltns Under Rat Subcutaneous Tissue

Each porous film was punched into 1 cm diameter disks, and sterilized with ethylene-oxide gas. The disks were implanted under rat subcutaneous tissue (Wister, 7weeks old, male) for 3, 7 and 14 days. After this period, each tissue including the porous film disk was removed. The amount of biodegradation in each film was examined by sight. The tissues-film compounds were then fixed in 10% formalin neutral buffer solution, and stained by H&E followed by light microscope observation.

5.3.8. Inflammatory Evaluation of (P)HxAlGltns Under Rat Subcutaneous Implantation

After 10% formalin buffer fixation, the implanted (P)HxAlGltn and surrounding tissue were peroxidase stained. The peroxidase positive cells that infiltrated into the porous films were quantified by cellular counting under light microscopic observation (X51, Olympus). The areas infiltrated by cells were quantified with the ImageJ image analysis tool.

5.3.9. Angiogenesis Evaluation Around (P)HxAlGltns and (P)AlGltns by CD34 and α-SMA Immunostaining

The 10% formalin neutral buffer solution fixed samples were immunostained using CD34 and α-SMA after 3, 7 and 14 days implantation. The CD34 or α-SMA density per unit area was calculated by ImageJ imaging analysis. The applied gray scale value for CD34 expression quantification was under 100 and that for α-SMA was under 170 (n = 3) , which gray scale value range was lower than that of nuclei and darker than that of other extra cellular matrix.

5.3.10. Statistical Analysis

Statistical analysis was carried out using Aspin-Welch's t-test. Data are the means ± SD of three samples ($n = 3$). Statistically significant differences were accepted when $p < 0.05$.

5.4. Results and Discussion

5.4.1. Preparation and Characterization of (P)HxAlGltns and (P)AlGltns with Regulated Pore Size

We previously reported that hexanoyl (Hx) chloride successfully reacts with the amino groups of the AlGltn molecules (Figure 5.1A). The number of amino groups substituted with Hx chlorides was determined using the 2,4,6-trinitrobenzensulfonicacid (TNBS) method. The Hx group modification ratio was 34%. (P)HxAlGltns, were fabricated through the use of salt leaching with 43, 77, 156, and 375 μm-diameter NaCl combined with HxAlGltn films. The 34% modification ratio was reduced to a modification ratio of 25% by diluting HxAlGltn with AlGltn. The HxAlGltn molecule was then chemically cross-linked with a citrate acid derived cross-linker or trisuccinimidyl citrate (TSC) to make it water-insoluble. Finally, we obtained (P)HxAlGltns with each pore size: (P43)HxAlGltn, (P77)HxAlGltn, (P156)HxAlGltn, and (P375)HxAlGltn (Figure 5.1B). Figure 5.1C shows the cross sections of each dried porous film. The pore sizes were the almost same size within each film, and the pores were interconnected with the other pores. (P43)AlGltn, (P77)AlGltn, (P156)AlGltn, and (P375)AlGltn were also successfully fabricated using the same technique as (P)HxAlGltns fabrication.

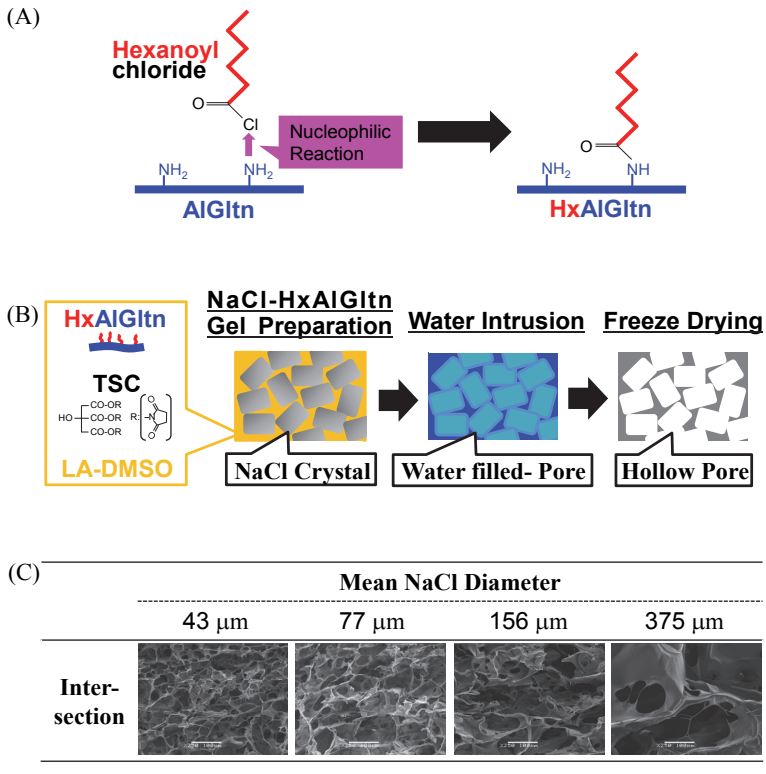

Figure 5.1. Synthesis of HxAlGltn (A).Fabrication of the (P)HxAlGltns with each pore sizes by salt-leaching method (B). SEM images of the porous films with each pore size in dried state (C).

The pore size inside the porous films was dependent on the NaCl particle sizes used during salt-leaching. The solid-liquid ratio (SLR) remained 4/1 (w/w), and each NaCl-HxAlGltn gel was fabricated in a 1 mm thick mold followed by water immersion and lyophilize. Therefore, only NaCl particle size was responsible for pore size of the porous films.

5.4.2. Mechanical Strength of (P)HxAlGltns (P)AlGltns

The mechanical strengths of the dry and wet porous films were measured. The strength of the dried (P)HxAlGltns film drastically decreased from 77 to 156 μm NaCl size (Figure 5.2A). The strength of the wet (P)HxAlGltns, however, showed different behavior. In these films, (P77)HxAlGltn was strongest(Figure 5.2B). On the other hand, (P)AlGltns behaved very differently from (P)HxAlGltns in terms of strength. The (P77)AlGltn was the weakest in all the (P)AlGltns under dry conditions while (P156)AlGltn was the weakest under wet conditions.

Larger pores inside solid materials like ceramics weaken mechanical stability (pore size: 6 to 490 μm)[35]. On the other hand, larger pores inside soft materials like hyaluronan-collagen tend to improve mechanical stability (pore size: 123 to 182 μm[36] or 302.5 to 525 μm[37]). Further, other research groups have found that the polymer composition significantly affects polymer strength for each porous body[38]. It can be hypothesized that (P)HxAlGltn and (P)AlGltn behaved differently due to the Hx group. In the dry state, (P)HxAlGltn showed solid material like mechanical strength due to its inner Hx group aggregation. On the other hand, (P)AlGltn without hydrophobic aggregation behaved like a softer material.

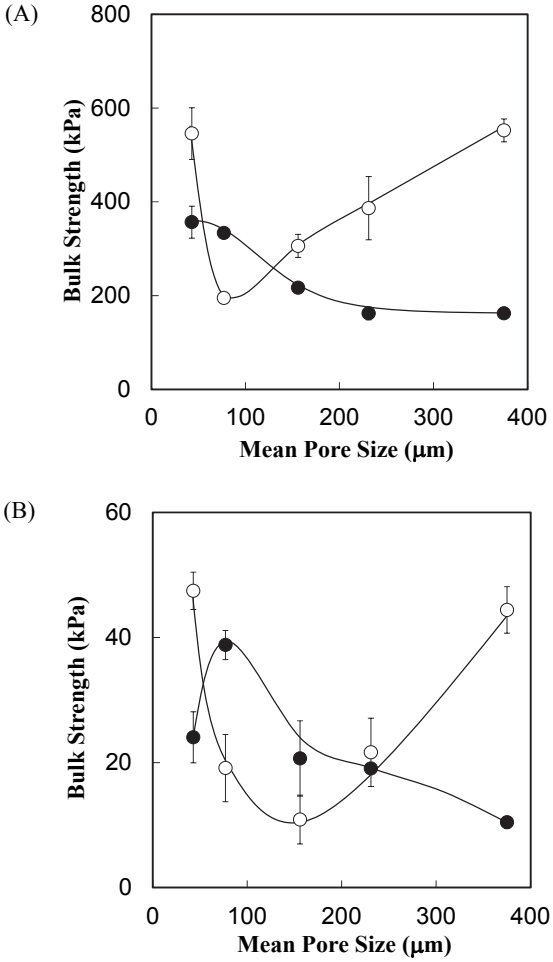

Figure 5.2. Bulk strength of (A) dry and (B) wet (P)HxAlGltns (●) and (P)AlGltn (○) . N=3.

5.4.3. Bonding Strength Measurements and Peeling Surface Observation between Porcinal Intestine and (P)HxAlGltns/(P)AlGltns

(P77)HxAlGltn bound strongest to wet porcinal intestine out of the (P)HxAlGltns and the (P)AlGltns films. Further, (P)HxAlGltn bonding strengths were more than 1.7 times greater than the bonding strength of (P)AlGltns (Figure 5.3A). However, the strength of (P)AlGltn decreased with pore size increases. After the measurement, tissue that adhered to the film, and film that adhered to the tissue were observed. Tissue with high cellularity adhered to (P77)HxAlGltn, (P43)HxAlGltn, and (P375)HxAlGltn. (P43)HxAlGltn and (P77)HxAlGltn film remnants remained on the tissue. Tissue remnants with low cellularity remained on the (P43)AlGltn and (P375)AlGltn films while (P156)AlGltn remnants remained on the tissue.

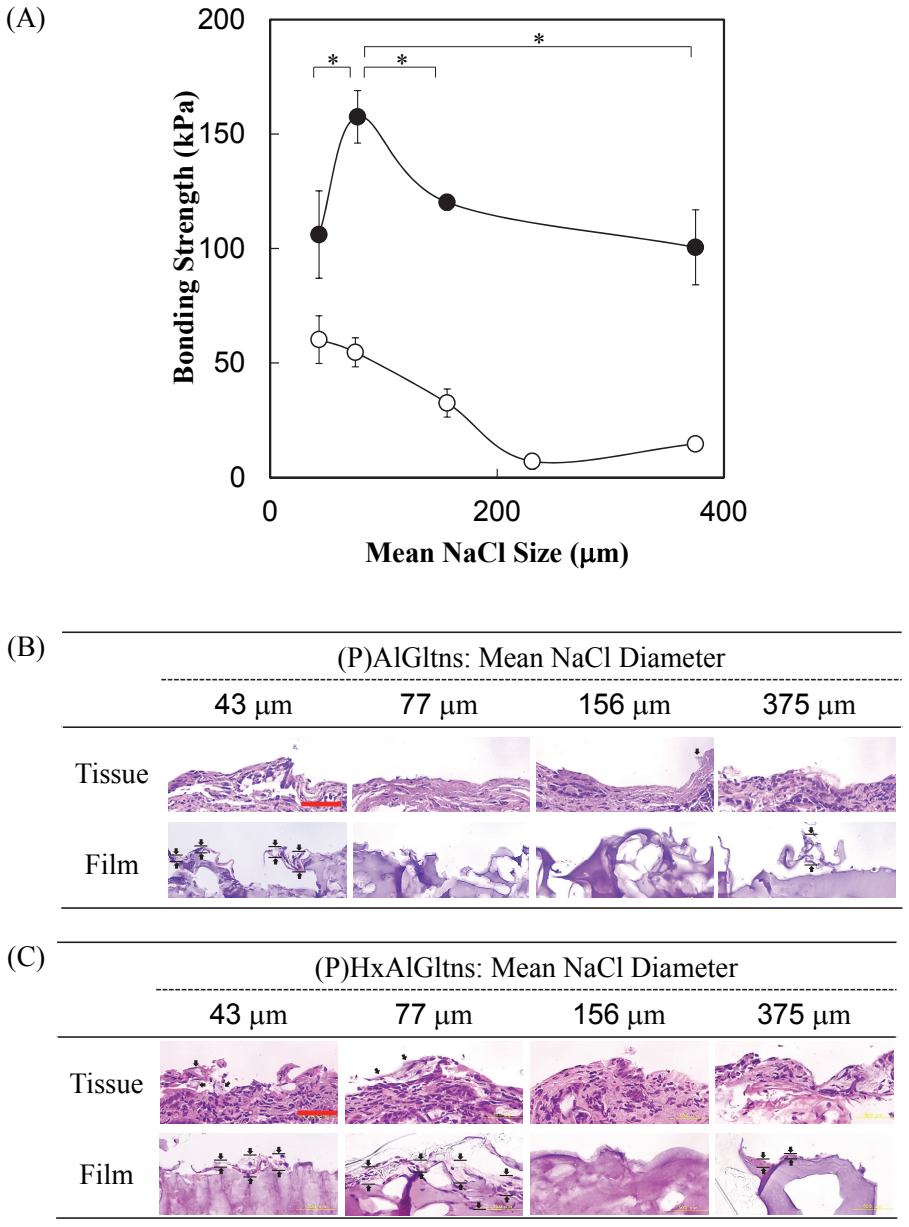

Figure 5.3. (A) Bonding strength between porcinal intestine and (P)HxAlGltn (●) or (P)AlGltn (○) with each pore size. (B) Tissue-(P)AlGltn interfaces after bonding strength measurement. (C) Tissue-(P)HxAlGltn interfaces after bonding strength measurement. Arrows: film or tissue remained on the surface. N=3, * $p < 0.05$, bar: 50 μm.

The above result suggests that Hx group anchoring into the tissue surface is important for tissue:(P)HxAlGltn binding. In addition to the effect of Hx anchoring, the bulk strength of the films could also affect bonding strength. Therefore, we evaluated the bulk strength of the films in both the wet and dry state. In the dry condition, both (P43)AlGltn and (P43)HxAlGltn showed higher bulk strength (Figure 5.2A). However, in the wet condition, (P77)HxAlGltn showed the highest bulk strength in the (P)HxAlGltns while (P43)AlGltn showed the highest bulk strength in all the (P)AlGltns (Figure 5.2B). It can be hypothesized that the tissue-porous film interface was wet while the film body distant from the interface was dry. (P77)HxAlGltn had a high bulk strength in both the wet and dry state. Therefore, (P77)HxAlGltn had the strongest bonding strength compared with the other (P)HxAlGltns.

5.4.4. Water Absorption Speed of (P)HxAlGltns and (P)AlGltns

(P)HxAlGltns absorbed water much faster than the (P)AlGltns (Figure 5.4A). The water absorption speed of (P77)HxAlGltn was the greatest out of all films tested followed by (P43)HxAlGltn, (P156)HxAlGltn, (P231)HxAlGltn, and (P375)HxAlGltn in that order. The water absorption speed of (P)AlGltns decreased inversely with pore size.

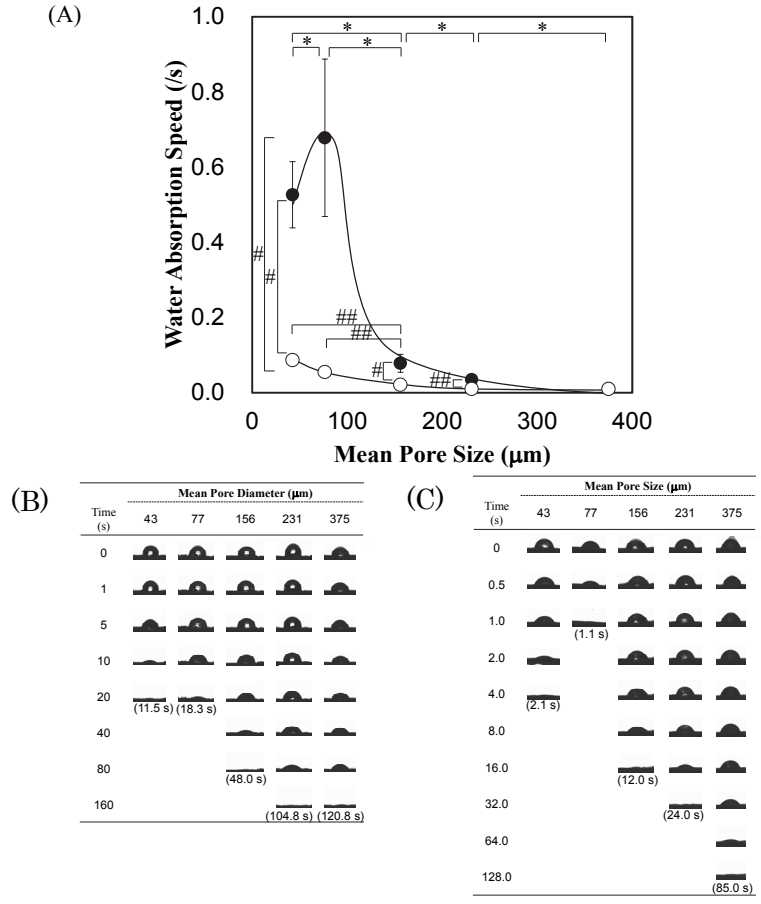

Figure 5.4. (A) Water absorption speed of (P)HxAlGltns (●) and (P)AlGltns (○) with each pore size. Pictures of water drop on (P)AlGltns (B) or (P)HxAlGltns (C) at each measuring time point. The parenthetic values are the complete water absorption time. N = 3, *p < 0.05, #p < 0.05, ##p > 0.05.

It is well known that the capillary phenomenon impacts rapid liquid absorption. The rapid water absorption seen with (P77)HxAlGltn may have come from the bivalent hydrophilicity of HxAlGltn or the hydrophobically modified gelatin molecule. Hydrophilic polymers easily absorb water, but do not allow for the diffusion of water. On the other hand, hydrophobic polymers have a difficult time absorbing water, but have little problem allowing for the diffusion of water. And the application of those polymers properties in moisture permeable membrane is the combination of such. Those properties of the hydrophilic and hydrophobic polymers have been applied in moisture permeable membranes, or water vapor permeability studies[39,40]. In this study, simultaneous water flux in and out in the (P)HxAlGltns could potentially have facilitated optimal water absorption resulting in much faster absorption speed compared to the (P)AlGltns.

5.4.5. Biodegradability and Tissue Infiltration in (P)HxAlGltns Implants under Rat Subcutaneous Tissue

(P)HxAlGltn was punched 1 cm diameter disc, and each disc was implanted under rat subcutaneous tissue for 3, 7 and 14 days as three separate experiments (n=3). (P43)-, (P77)-, and (P156)HxAlGltn were smaller than (P375)HxAlGltn at 7 days implantation. (P375)HxAlGltn was still present at 14 days implantation, however no (P43)-, (P77)-, (P156)-HxAlGltn was left at this time point. (Figure 5.5A).

Based on complete (P43)-, (P77)-, and (P156)HxAlGltns degradation after 14 days implantation, tissue infiltration and tissue-(P)HxAlGltn integration were observed after histological H&E staining (Figure 5.5B). At day 3, (P43)-, (P77)-, and (P156)HxAlGltn were easily distinguished from the rat subcutaneous tissue with clearly visible interfaces. By day 7, however, the tissue-(P)HxAlGltn interfaces were unclear and difficult to define.

Those results indicate that (P)HxAlGltn requires certain degree of fine pore for faster biodegradation/integration to circumference.

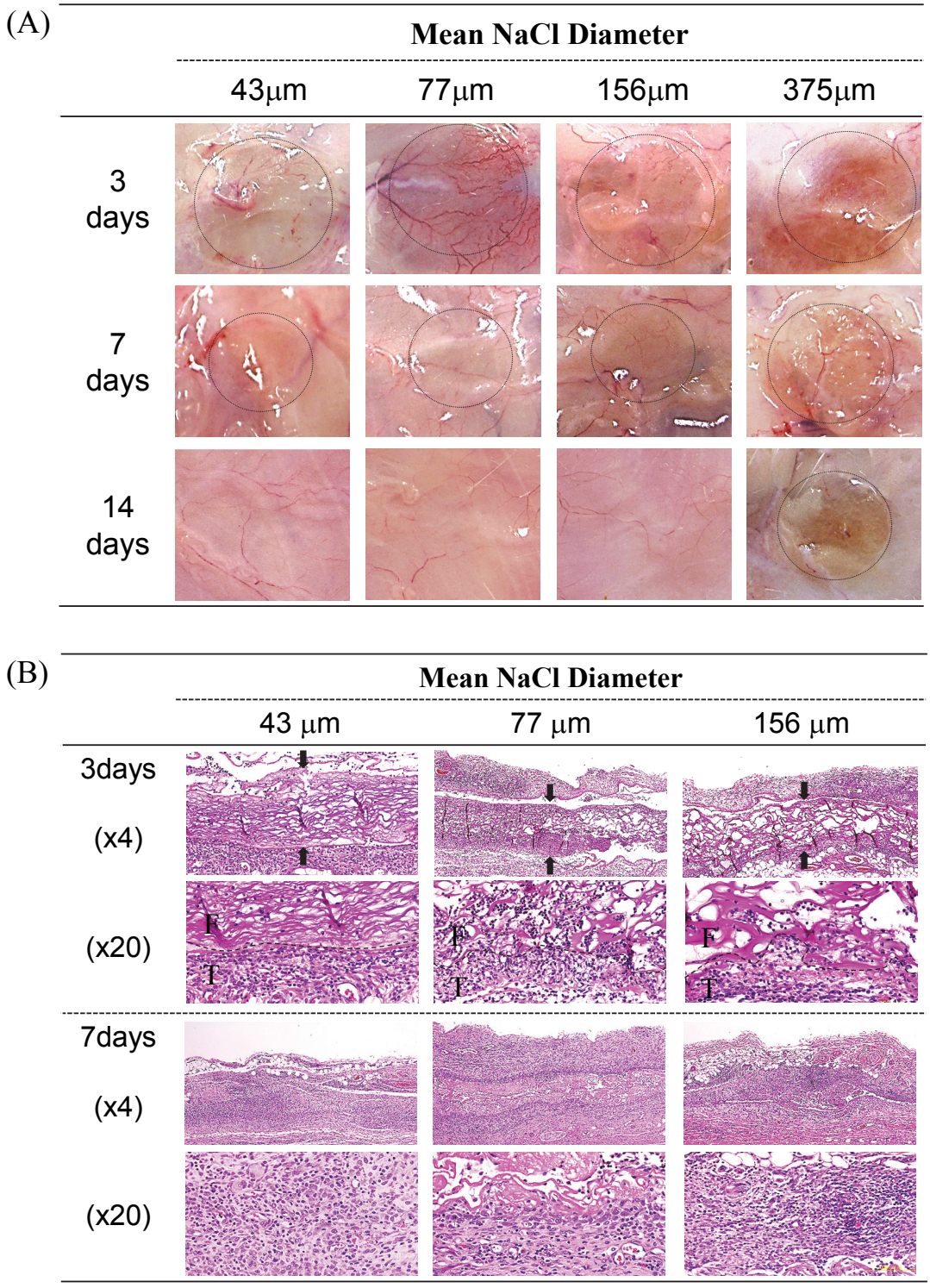

Figure 5.5. (A) Biodegradation of (P)HxAlGltns with each pore size under rat subcutaneous. (B) H&E stained (P)HxAlGltns and the surrounding tissue after rat subcutaneous implantation. Arrows: porous film between rat subcutaneous tissue. Dashed line: interface of the porous film and the rat subcutaneous tissue. F: porous film, T: subcutaneous tissue.

5.4.6. Cell Infiltration in (P)HxAlGltns Implanted under Rat Subcutaneous Tissue

Many cells was observed at sight in the (P77)HxAlGltn pores 3 days post-implantation (Figure 5.6). Further, it is possible that (P)HxAlGltn degradation speed was related to cellular infiltration. We, therefore, counted cell numbers in the pores. The greatest number of the cells infiltrated into (P77)HxAlGltn (5.46×10^3 mm^{-2}) followed by (P156)- (2.82×10^3 mm^{-2}) and (P44)HxAlGltn (0.65×10^3 mm^{-2}) (Figure 5.7B).

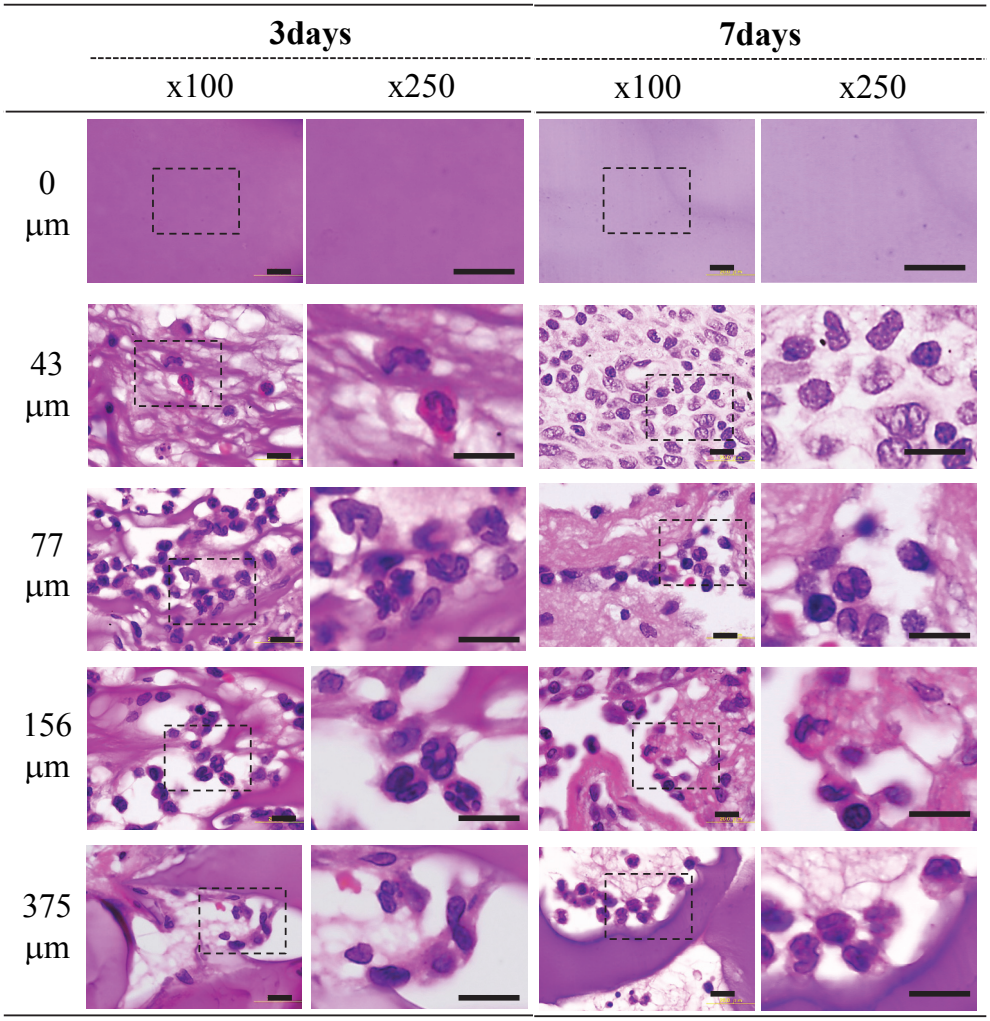

Figure 5.6. Cells infiltrated into the porous cells under rat subcutaneous. H&E staining, dashed block: the magnified part, scale bar: 10 μm.

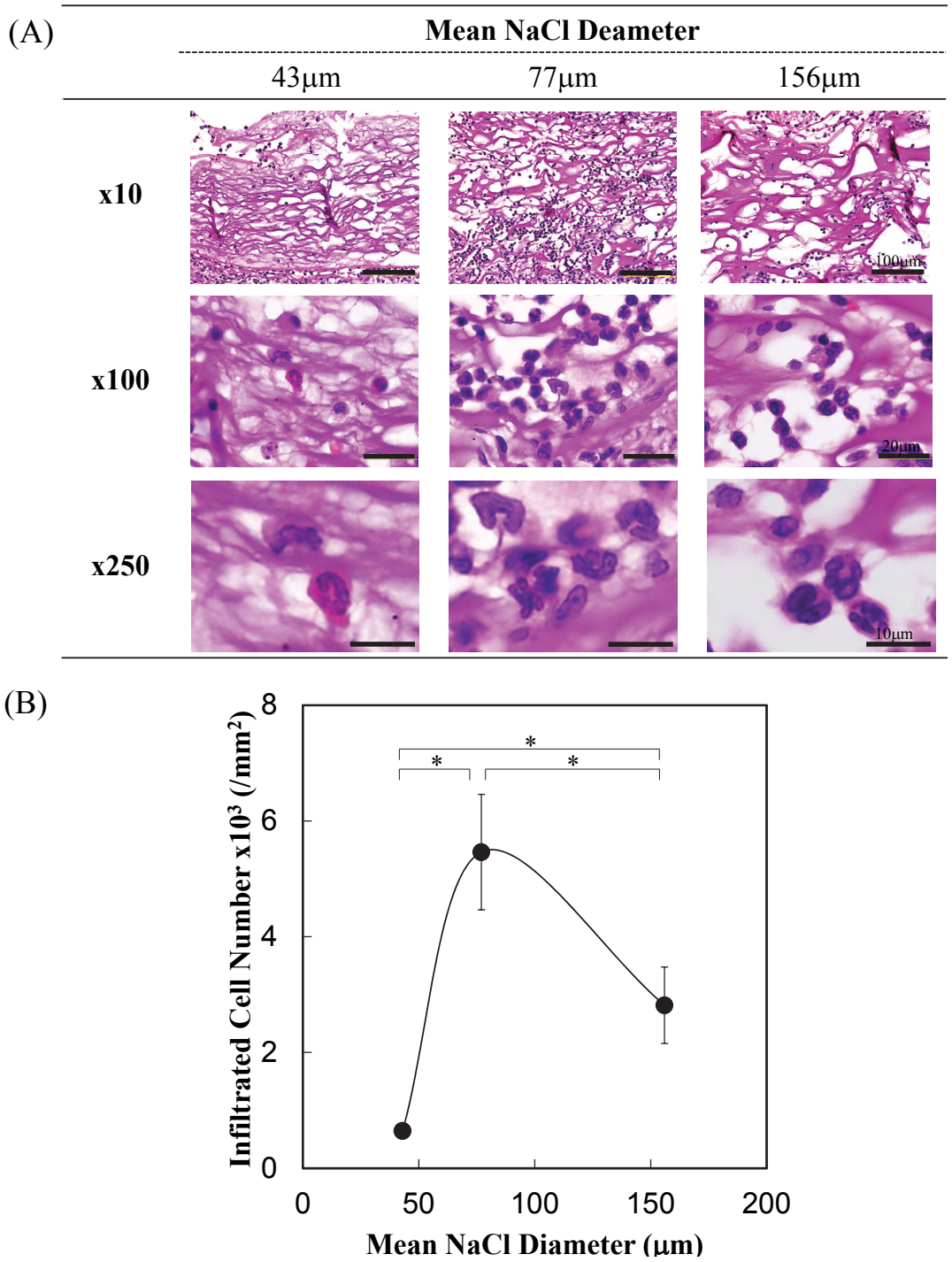

Figure 5.7. H&E stained (P)HxAlGltns with cellular infiltration inside of the pore (A) and the cell numbers in the pore (B) after 3 days' rat subcutaneous implantation. N = 3, *p < 0.05.

Cells can pass through holes depending on cell size and hole diameter[41]. The cellular infiltration tendency in this study can be related to the pore size of each film. The cells are approximately 10 μm in diameter. The size of through hole connecting each pores of (P43)HxAlGltn was too small for cell infiltration. On the other hand, the through hole in (P156)HxAlGltn compared with (P43)- and (P77)HxAlGltn could be much larger than the cell diameter. (P77)HxAlGltn had the most appropriate through hole size as significant cellular infiltration occurred in this film. Many of the cells had segment-shaped nuclei, and thus were likely neutrophils suggesting an inflammatory immune response. We immunostained the gels to verify this hypothesis.

5.4.7. Inflammatory Evaluation of (P)HxAlGltns Implants under Rat Subcutaneous Tissue

For evaluation of the inflammation inside the porous films, formalin fixed (P)HxAlGltns were treated with peroxidase post rat subcutaneous implantation. Figure 5.8A showed that there were more peroxidase positive cells that infiltrated (P77)HxAlGltn compared with (P43)HxAlGltn and (P156)HxAlGltn. Cell number quantification also found that the number of peroxidase positive cells was significant in (P77)HxAlGltn compared to (P43)HxAlGltn and (P156)HxAlGltn (Figure 5.8B). In addition, the cells around those films showed similar tendency as inside the films (data is not shown). This indicated that (P77)HxAlGltn was highly inflammatory compared to the other (P)HxAlGltns. These results suggest that in (P77)HxAlGltn, cells easily moved into the pores. These cells infiltrated in the (P77)HxAlGltn contacted with the surrounding film walls and the neighboring cells facilitated much crosstalk resulted in much more peroxidase production.

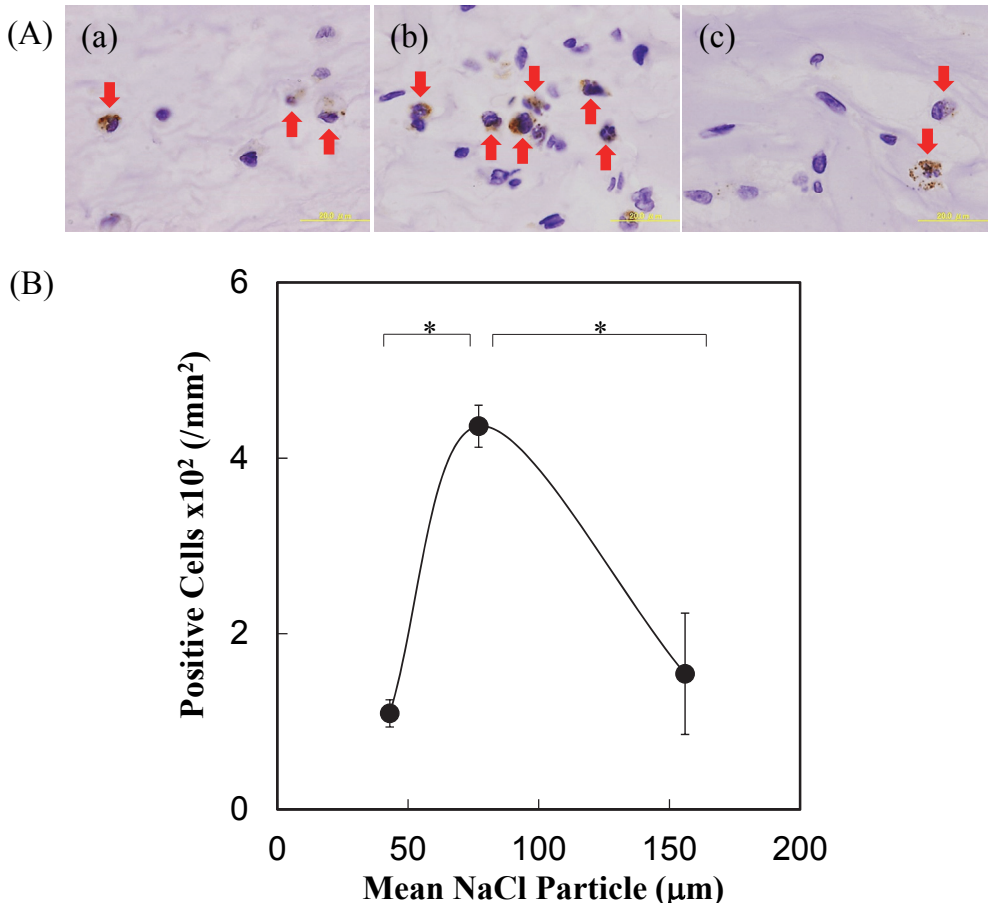

Figure 5.8. Inflammatory evaluation with peroxidase staining inside each (P)HxAlGltn. (A) Microscopic images of cells inside the (a) (P43)HxAlGltn, (b) (P77)HxAlGltn or (c) (P156)HxAlGltn. Cells colored brown (red arrows) are peroxidase positive. (B) Peroxidase positive cells inside the (P)HxAlGltns. *$p < 0.05$, $n = 5$.

5.4.8. Angiogenesis Evaluation around (P)HxAlGltns Implants by CD34 and α-SMA Immunostaining under Rat Subcutaneous Tissue

Microvasculature may have developed during the process of cellular and tissue infiltration into the (P)HxAlGltns. Therefore, we stained for CD34 and α-SMA in order to see whether angiogenesis had occurred in and around the (P)HxAlGltns after rat subcutaneous implantation. CD34 is an immature endothelial cell marker, and α-SMA is a mature endothelial cell marker. With the use of these two markers, early angiogenesis and the establishment of mature vasculature can be investigated.

At day 3, (P43)HxAlGltn was rich in CD34 compared with (P77)- and (P156)HxAlGltn. At day 7, the CD34 area in and around (P43)HxAlGltn decreased. Meanwhile, no significant differences in α-SMA area between the three (P)HxAlGltns through 3 to 7 days implantation were found. It was natural that CD34 decreased with time because immature endothelial were abundant during the early angiogenesis stage (Figure 5.9B)

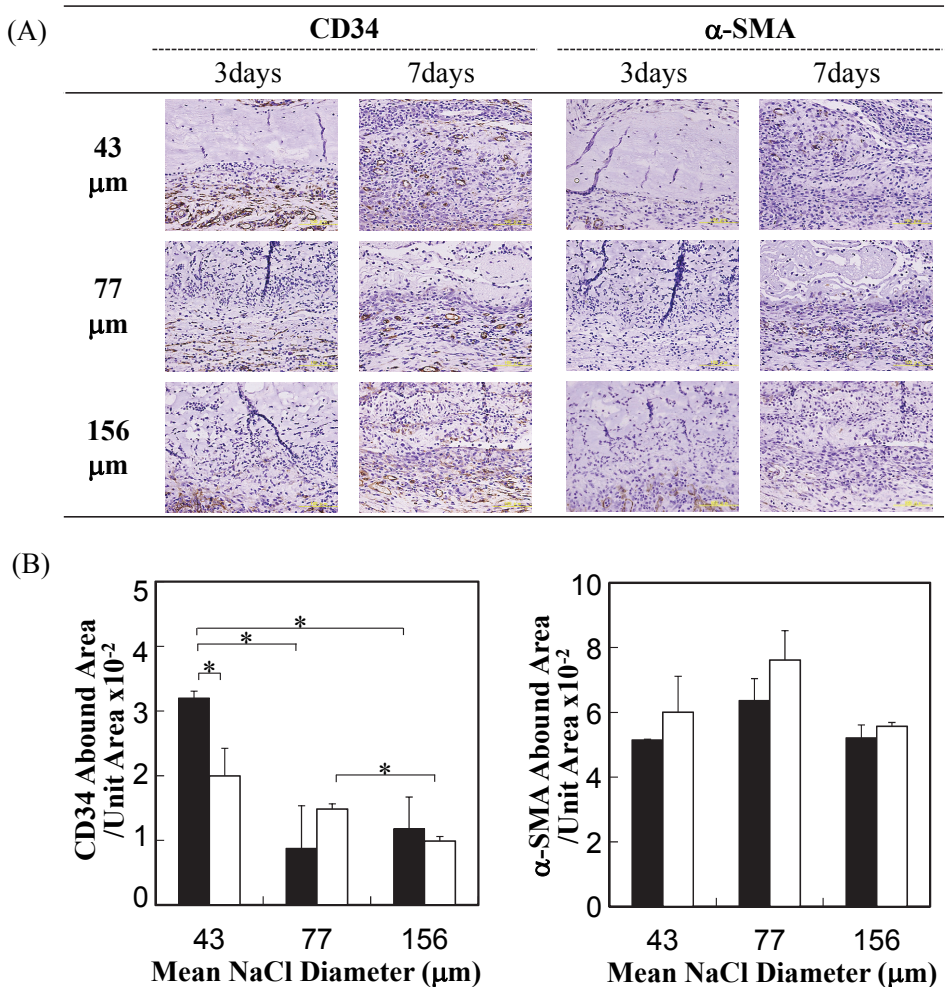

Figure 5.9. CD34 and a-SMA expression around the tissue-(P)HxAlGltns interface after rat subcutaneous implantation. (A) 20 times magnified images. (B) CD34 or a-SMA abound area around each tissue-(P)HxAlGltn interfaces, black: 3 days implantation, white: 7 days implantation, n = 3, *p < 0.05.

Contrary to CD34, there was no significant difference in α-SMA expression in and around the three (P)HxAlGltns through day 3 to 7 post implantation. However, the value at day 7 was a little greater in and around each (P)HxAlGltn, although the difference was not statistically significant ($p > 0.05$). A few immature endothelial turned into mature endothelial to express α-SMA. However, mature endothelial expressing α-SMA already existed prior to (P)HxAlGltn implantation making. The slight increase in α-SMA expression from 3 to 7 days post implantation may have indicated immature to mature endothelial transition, and pre-existed micro vascular got matured.

(P)HxAlGltns films bonded stronger than all (P)AlGltns to wet porcinal intestine. This indicated that the Hx group on the (P)HxAlGltns surface strengthens the film-tissue interface interaction. This film-tissue interaction is likely mediated through hydrophobic bonding with the extra-cellular matrix and the lipid bilayer of cells. In addition, (P77)HxAlGltn showed the strongest bonding to the wet tissue surface among all porous films tested. Further, (P77)HxAlGltn had the fastest water absorption rate showing that body fluid absorption speed controlled by pore size is important for strong adhesion (Figure 5.10A and B).

On the other hand, many neutrophil-like cells and peroxidase positive neutrophil-like cells, which reacted more inflammatory than peroxidase negative neutrophil-like cells, in the (P77)HxAlGltn indicated that the inflammation level was higher in (P77)HxAlGltn than (P43)- and (P156)HxAlGltn. The infiltrated cells were around 10 μm in diameter, and the through holes which connecting each pore in the (P77)HxAlGltn could be around 10 μm. Each infiltrated cell was adjacent to the other cells in (P77)HxAlGltn pores (Figure 5.6 and 5.7A). Cell to (P)HxAlGltn wall and cell to cell contact increased the immune response and brought about peroxidase production (Figure 5.10C and D).

CD34 expression around (P43)HxAlGltn at 3 days posts implantation indicated that smaller pores were better for early angiogenesis. In addition, there were fewer peroxidase positive cells in (P43)HxAlGltn than in (P77)- and (P156)HxAlGltn. These results suggest the initiation of angiogenesis is inversely related to the inflammatory properties of (P)HxAlGltns (Figure 5.10C and D). The infiltrated cell number in (P43)HxAlGltn was smaller than (P156)HxAlGltn, while, the numbers of peroxidase positive cells in (P43)- and (P156) were similar. However, the (P)HxAlGltn contact area of the cells in (P43)HxAlGltn was much larger than those in (P156)HxAlGltn. Each infiltrated cell in the (P43)HxAlGltn hardly contacted other cells (Figure 5.7A and 5.8Aa). On the other hand, cells that infiltrated the (P156)HxAlGltn film could contact other infiltrated cells. Those differences resulted in inflammation level and following angiogenesis extent.

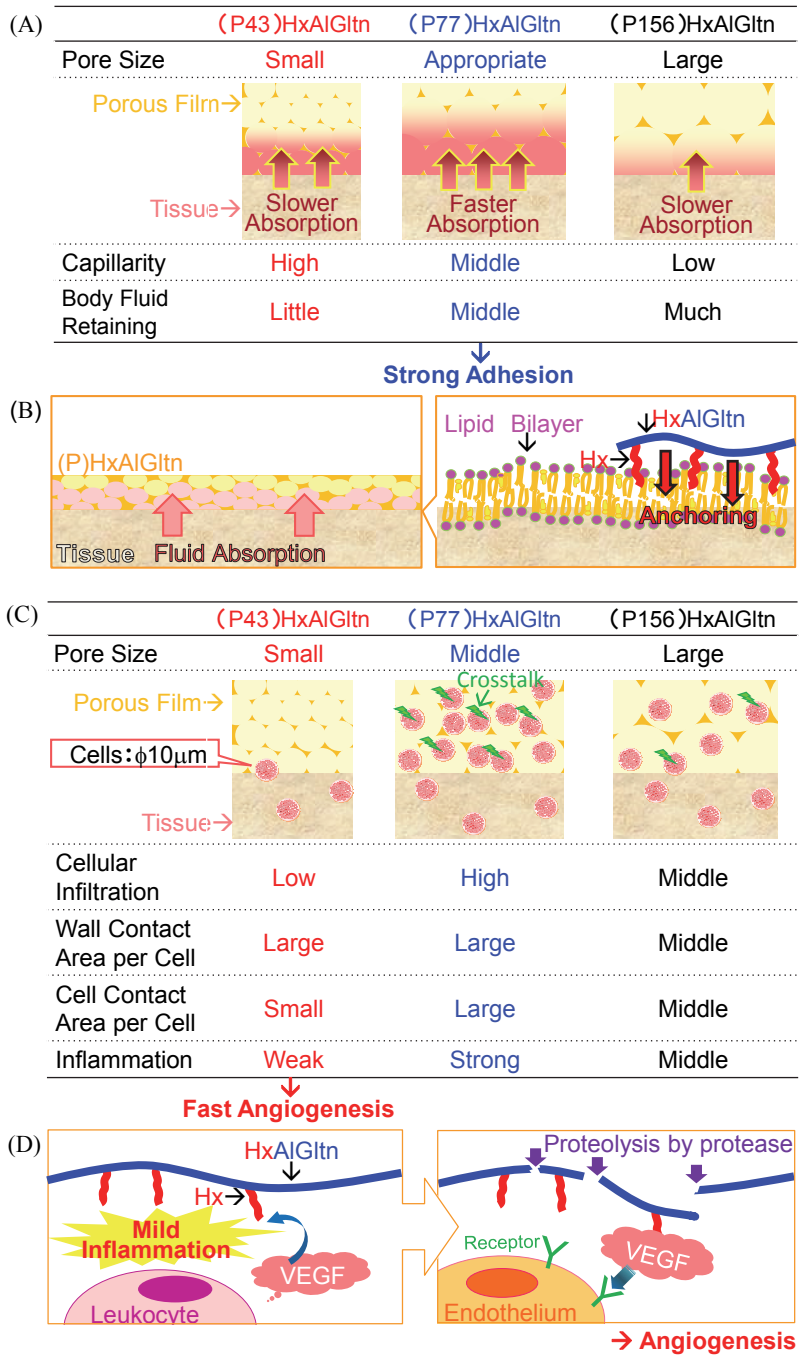

Figure 5.10. The mechanism of strong binding between (P)HxAlGltn and intestine tissue surface as well as angiogenesis facilitation by (P)HxAlGltn. (A) Relationship between NaCl particle sizes and body fluid absorption. (B) Effects of (P)HxAlGltn strong binding to intestine. (C) Relationship between NaCl particle sizes and angiogenesis. (D) Mechanism for angiogenesis after (P)HxAlGltn implantation.

5.5. Conclusion

Porous Hx (C_6) group modified AlGltn film adhesives ((P)HxAlGltns) were fabricated with NaCl particles that were 43, 77, 156, or 375 μm in diameter ((P43)-, (P77)-, (P156)-, and (P375)HxAlGltn). (P)HxAlGltns, especially (P77)HxAlGltn, bound stronger than (P)AlGltns to the wet intestine surface. Further, (P77)HxAlGltn showed a number of advantages in terms of water absorption speed, cellular infiltration and biodegradation. The cells that infiltrated the film were neutrophils that were identified through their segment shaped nuclei. In addition to the neutrophils, many more peroxidase positive cells found in the (P77)HxAlGltn film than in (P43)- and (P156)HxAlGltns films. Significantly more CD34 expression was identified around (P43)HxAlGltns-tissue interface compared to (P77)- and (P156)HxAlGltn after 3 days rat subcutaneous implantation. These results indicate that bonding strength between (P)HxAlGltn depends on tissue fluid absorption while early angiogenesis depends on mild inflammation caused by cellular infiltration.

5.6. References

1. Suzuki, M., Uchiyama, T., M., O., Takemura, S. & Matusno, S. Clinical application of GRF glue adhesive in liver surgery. *Jpn J Gastroenterol Surg* **33**, 18-24 (2000).
2. Bouten, P. J. M. et al. The chemistry of tissue adhesive materials. *Prog Polym Sci* **39**, 1375–1405 (2014).
3. Peng, H. T. & Shek, P. N. Novel wound sealants: biomaterials and applications. *Exp Rev Med Dev* **7**, 639-659 (2010).
4. Ryou, M. & Thompson, C. C. Tissue adhesives: a review. *Tech Gastroint Endoscopy* **8**, 33-37 (2006).
5. Edmiston, C. E. et al. Bacterial adherence to surgical sutures: can antibacterial-coated sutures reduce the risk of microbial contamination? *J Am College Surg* **203**, 481-489 (2006).
6. Katz, S., Izhar, M. & Mirelman, D. Bacterial adherence to surgical sutures. A possible factor in suture induced infection. *Ann Surg* **194**, 35-41 (1981).
7. Chao, H. H. & Torchiana, D. F. BioGlue: albumin/glutaraldehyde sealant in cardiac surgery. *J Cardiac Surg* **18**, 500-503 (2003).
8. Leonard, F., Kulkarni, R. K., Nelson, J. & Brandes, G. Tissue Adhesives and hemostasis-inducing compounds. The alkyl cyanoacrylates. *J Biomed Mater Res* **1**, 3-9 (1967).
9. Fukunaga, S. et al. The use of gelatin-resorcin-formalin glue in acute aortic dissection type A. *Eur J Cardiothorac Surg* **15**, 564-570 (1999).
10. Das, S. et al. Enhanced redifferentiation of chondrocytes on microperiodic silk/gelatin scaffolds: toward tailor-made tissue engineering. *Biomacromolecules* **14**, 311-321 (2013).
11. Santamaria, V. A. et al. Influence of the macro and micro-porous structure on the mechanical behavior of poly(L-lactic acid) scaffolds. *J Non-Crystal Solids* **358**, 3141-3149 (2012).
12. Lawrence, B. J. & Madihally, S. V. Cell colonization in degradable 3D porous matrices. *Cell Adhes Migrat* **2**, 9-16 (2008).
13. Yao, X. et al. Adaptive fluid-infused porous films with tunable transparency and wettability. *Nat Mat*er **12**, 259-534 (2013).
14. Wang, S., Zhang, Y., Wang, H., Yin, G. & Dong, Z. Fabrication and properties of the electrospun polylactide/silk fibroin-gelatin composite tubular scaffold. *Biomacromolecules* **10**, 2240-2244 (2009).
15. Sisson, K., Zhang, C., Farach-Carson, M. C., Chase, D. B. & Rabolt, J. F. Evaluation of cross-linking methods for electrospun gelatin on cell growth and viability. *Biomacromolecules* **10**, 1675-1680 (2009).
16. Han, J. et al. Co-electrospun blends of PLGA, gelatin, and elastin as potential nonthrombogenic scaffolds for vascular tissue engineering. *Biomacromolecules* **12**, 399-408 (2011).
17. Han, J. et al. Co-electrospun blends of PLGA, gelatin, and elastin as potential nonthrombogenic scaffolds for vascular tissue engineering. *Biomacromolecules* **12**, 399-408 (2011).
18. Li, C. Q. et al. Construction of collagen II/hyaluronate/chondroitin-6-sulfate tri-copolymer scaffold for nucleus pulposus tissue engineering and preliminary analysis of its physico-chemical properties and biocompatibility. *J Mater Sci Mater Med* **21**, 741-751 (2010).
19. Messias, A. D., Lucchesi, C., Coraça-Huber, D. C., Filho, A. P. & Duek, E. A. R. Lithograph-moulded poly-L-co-D,L lactide porous membranes for osteoblastic culture. *Mater Res* **17**, 7-15 (2014).

20. Guo, S. & Dipietro, L. A. Factors affecting wound healing. *J Dent Res* **89**, 219-229 (2010).
21. Velnar, T., Bailey, T. & Smrkolj, V. The wound healing process: an overview of the cellular and molecular mechanisms. *J Intn Med Res* **37**, 1528-1542 (2009).
22. Diegelmann, R. F. & Evans, M. C. Wound healing: an overview of acute, fibrotic and delayed healing. Frontiers in bioscience. *J Virtual Library* **9**, 283-289 (2004).
23. Tonnesen, M. G., Feng, X. & Clark, R. A. Angiogenesis in wound healing. *J Invest Dermatol Symp Proc / Soc Invest Dermatol* **5**, 40-46 (2000).
24. Madeddu, P. Therapeutic angiogenesis and vasculogenesis for tissue regeneration. *Exp Physiol* **90**, 315-326 (2005).
25. Nucera, S., Biziato, D. & De Palma, M. The interplay between macrophages and angiogenesis in development, tissue injury and regeneration. *Intn J Develop Biol* **55**, 495-503 (2011).
26. Tabata, Y., Nagano, A. & Ikada, Y. Biodegradation of hydrogel carrier incorporating fibroblast growth factor. *Tissue Eng* **5**, 127-138 (1999).
27. Ikada, Y. & Tabata, Y. Protein release from gelatin matrices. *Adv Drug Deliv Rev* **31**, 287-301 (1998).
28. Tabata, Y. Tissue regeneration based on growth factor release. *Tissue Eng* **9** Suppl 1, S5-S15 (2003).
29. Lang, G. Efficacy and safety of topical application of human fibrinogen/thrombin-coated collagen patch (TachoComb) for treatment of air leakage after standard lobectomy. *Eur J Cardio-thorac Surg* **25**, 160-166 (2004).
30. Creton, C. & Hooker, J. Bulk and interfacial contributions to the debonding mechanisms of soft adhesives: extension to large strains. *Langmuir* **17**, 4948-4954 (2001).
31. Matsuda, M. et al. Enhanced tissue penetration-induced high bonding strength of a novel tissue adhesive composed of cholesteryl group-modified gelatin and disuccinimidyl tartarate. *Colloid Surface B* **91**, 48-56 (2012).
32. Matsuda, M. & Taguchi, T. In vitroevaluation of tissue adhesives composed of hydrophobically modified gelatins and disuccinimidyl tartrate. *Sci Technol Adv Mater* **13**, 064212 (2012).
33. Yoshizawa, K. & Taguchi, T. Bonding behavior of hydrophobically modified gelatin films on the intestinal surface. *J Bioact Compat Polym* **29**, 560-571 (2014).
34. Yoshizawa, K. & Taguchi, T. Enhanced bonding strength of hydrophobically modified gelatin films on wet blood vessels. *Intn J Molecul Sci* **15**, 2142-2156 (2014).
35. Yoshida, K., Tsukidate, H., Murakami, A. & Miyata, H. Influence of pore size on fracture strength of porous ceramics. *J Solid Mechan Mater Eng* **2**, 1060-1069 (2008).
36. Lin, Y. C., Tan, F. J., Marra, K. G., Jan, S. S. & Liu, D. C. Synthesis and characterization of collagen/hyaluronan/chitosan composite sponges for potential biomedical applications. *Acta Biomater* **5**, 2591-2600 (2009).
37. Al-Munajjed, A. A., Hien, M., Kujat, R., Gleeson, J. P. & Hammer, J. Influence of pore size on tensile strength, permeability and porosity of hyaluronan-collagen scaffolds. *J Mater Sci Mater Med* **19**, 2859-2864 (2008).
38. Lanasa, S. M., Hoffecker, I. T. & Bryant, S. J. Presence of pores and hydrogel composition influence tensile properties of scaffolds fabricated from well-defined sphere templates. *J Biomed Mater Res B* **96**, 294-302 (2011).

39. Matsuno, I., Takizawa, A., Kinoshita, T. & Tsujita, Y. Water vapor permeability through laminated membrane composed of hydrophilic and hydrophobic layers. *Sen'i Gakkaishi* **43**, 578-586 (1987).
40. Hirata, Y., Marais, S. & Nguyen, Q. T. Relationship between the gas and liquid water permeabilities and membrane structure in homogeneous and pseudo-bilayer membranes based on partially hydrolyzed poly(ethylene-co-vinyl acetate). *J Membrane Sci* **256**, 7-17 (2005).
41. Higuchi, A. & Tsukamoto, Y. Cell separation of hepatocytes and fibroblasts through surface-modified polyurethane membranes. *J Biomed Mater Res A* **71**, 470-479 (2004).
42. Morcol, T., Subramanian, A. & Velander, W. H. Dot-blot analysis of the degree of covalent modification of proteins and antibodies at amino groups. *J Immunol Met* **203**, 45-53 (1997).

Chapter 6

Concluding Remarks and Future Directions

6.1. Concluding Remarks

This research focused on determining the wet tissue-bonding ability of adhesive films fabricated by hydrophobically modified alkali-treated porcine gelatin (hm-AlGltn). First, hm-AlGltn modified with each alkyl group and with each modification ratio was synthesized. The bonding between wet tissue and the hm-AlGltn flat films fabricated by the casting method was examined. The bonding between wet tissue and mechanically strengthened hm-AlGltn flat films by simple thermal crosslinking without any crosslinker was investigated. How the effects of porosity on porous hm-AlGltn films crosslinked by citrate-derived crosslinker affected binding to wet tissue, biodegradability, and angiogenesis were determined.

Chapter 1 introduces the background about adhesives and discusses the elements crucial for adhesive design. The adhesive location as a kind of wound dressings, the bonding mechanisms, and the adhesive styles are described. Citing previous literature and current research, we clarified the objectives of this study.

Chapter 2 described the effect of hydrophobic modification of flat film shaped gelatin on wet tissue bonding strength. Each alkyl group with each chain length was introduced into AlGltn to synthesize hydrophobically modified AlGltns. Then plane flat films were fabricated by the mold casting method without any crosslinking to clarify the molecular interaction/effect on wet tissue bonding strength without any mechanical interaction such as the effects of bulk strength. The shortest alkyl group or hexanoyl group modified AlGltn: HxAlGltn film bonded most strongly onto porcine intestine among all hm-AlGltn films, and we discovered that the modification ratio of Hx group affected the burst strength of wet porcinal intestine. These results indicate that shorter alkyl groups and greater modification ratios cause strong bonding to the intestine surface. Additionally, the hm-AlGltn film bonding to wet tissue was directly strengthened by hydrophobic group modification.

Chapter 3 describes the relation between wet tissue-bonding strength and alkyl chain length/modification ratio of hm-AlGltn mechanically strengthened flat film by thermal crosslinking. In this experiment, the physical strengthening of the hm-AlGltn film relied on thermal crosslinking. The thermal crosslinking was intended to clarify the effect of hydrophobic group modification on bonding strength even under mechanically strengthened state, If chemically crosslinked, the crosslinker composition/compounds should have some effect on the hm-AlGltn films and the tissue interaction. To begin, thermally crosslinked hm-AlGltn films (t-hm-AlGltns) were fabricated by original AlGltn and hm-AlGltns with each alkyl group modification. Even with thermal crosslinking, HxAlGltn film (tHxAlGltn) with the greater modification ratio bonded most strongly to wet tissue. Furthermore, fibroblasts spread out a great deal on tHxAlGltn at early bonding stage. These results indicate that the hm-AlGltn film-wet tissue bonding strength and cellular reaction could be attributed to the shorter alkyl group modification and its greater modification ratio.

Chapter 4 describes the porosity effects of porous hm-AlGltn films crosslinked by citrate-derived crosslinker on the wet tissue bonding effect and on tissue reaction. As described above, the HxAlGltn flat film with/without thermal crosslinking bonded the strongest to wet tissue. Therefore, the effect of the porous structure of HxAlGltn film on wet tissue bonding and tissue reaction were examined. There are two properties in a porous body: porosity and pore size, and in this chapter, we focused on porosity with a constant pore size. At the beginning, porous hm-AlGltn films were fabricated by AlGltns or HxAlGltns ((P)AlGltns or (P)HxAlGltns) by a salt leaching method using 375-μm NaCl particle with each solid-liquid ratio (SLR): 0/1, 1/1, 2/1, 3/1, 4/1 and 5/1 (w/w). The (P)HxAlGltn fabricated with 4/1 w/w SLR ((P)HxAlGltn-SLR4/1) bonded most strongly to wet porcine intestine among all the porous films. (P)HxAlGltn-SLR4/1 demonstrated the fast tissue infiltration, fast biodegradability, and great angiogenesis properties in the absence of growth factor additives. Moreover, compared with AlGltn, the HxAlGltn molecule showed high affinity to vascular endothelial growth factor (VEGF), indicating the competence of HxAlGltn in angiogenesis facilitation by growth factor attraction. These results suggested that (P)HxAlGltn with great porosity is superior in wet tissue bonding and tissue regeneration ability.

Chapter 5 describes the pore size effect of (P)HxAlGltns to wet tissue-bonding effect and tissue reaction. In Chapter 4, the porosity effects of (P)HxAlGltn in wet tissue bonding strength and tissue reaction were determined. To examine the porous effect, porous size effect on bonding strength and angiogenesis should be also elucidated. On the other hand, it is well known that capillarity depends on the pore size and that body fluid absorption is responsible for porous film adhesivity. Therefore, (P)HxAlGltns and (P)AlGltn with each pore size were prepared by a salt leaching method with 43, 77, 156, or 375-μm NaCl particle in 4/1 w/w SLR. All the (P)HxAlGltns at each pore size showed greater water absorption speed, especially, (P77)HxAlGltn absorbed the quickest indicating its superiority in 77-μm pore size and Hx group modification. In wet tissue bonding strength measurement, (P)HxAlGltns, especially (P77)HxAlGltn, demonstrated advantages in bonding strength. (P)HxAlGltns with small pores degraded faster under rat subcutaneous tissue, and the greatest cellular number was counted in (P77)HxAlGltn pore at an early stage *in vivo*. However, (P)HxAlGltn with smaller pore size facilitated angiogenesis at an early stage *in vivo*. These results suggested that both pore size and Hx group modification of (P)HxAlGltn are responsible for strong bonding to wet tissue and facilitate angiogenesis.

In conclusion, an hm-AlGltn film with advantages of wet tissue bonding and tissue reaction was developed in this study. The length and the modification ratio of the hydrophobic group on hm-AlGltn were directly related to the bonding strength. In addition, the constitution of the material affected the wet tissue bonding strength, tissue infiltration, biodegradation, and angiogenesis *in vivo*. This study determined that the shorter alkyl group-modified hm-AlGltns like ProAlGltn and HxAlGltn were more effective in wet tissue bonding, biodegradability, and angiogenesis. Among the (P)HxAlGltn film constitutions, SLR4/1 and 77 μm pore size were the most effective in wet tissue bonding while 43 μm pore size was the most effective for early stage angiogenesis *in vivo*. Regulation of the hydrophobic modification and the porous constitution will also be applied for adhesives to allow further control of bonding strength and tissue regeneration.

6.2. Future Directions

In this study, the effects of hydrophobic modification and porous constitution on wet tissue bonding and on tissue reaction were investigated, and it was determined that the bonding strength and tissue reaction can be controlled by the modification and constitution conditions. A current prospective application of this hm-AlGltn film is for use during surgery involving wound closure and for wound dressing with smooth continuous tissue reconstruction that leaves no scars.

However, the angiogenesis facilitation ability of porous hm-AlGltn film by growth factor attraction suggested the modifications and the constitution could regulate other cytokines *in vivo*. Therefore, further modifications of gelatin molecules and the adhesive constitution could induce reactions including angiogenesis, rejuvenation, or cancer cell apoptosis.

The porous hm-AlGltn films can be used in drug delivery. Medication control is crucial in some diseases like cancer, and intravenous drips, frequent injections, and frequent oral medications are time consuming, hard to precisely control, and are not ideal for the patient's quality of life. Thus, medicine combined with adhesives to control its gradual release could be used in treatment.

The porous (P)hm-AlGltns can be applied for tissue engineering. The present study shows that the scaffold affects cellular differentiation. Some cells are difficult to retain at the unusual part, in other words, different tissues are difficult to connect in some cases. The adhesion property should be able to address those tissues. In addition, the (P)hm-AlGltn films provide an appropriate barrier with proper 3D environment for smooth connection of those tissues. The interconnected pores would provide smoother integration between tissues composed of cells with/without adhesiveness.

Above all, adhesive biomaterials with specific molecular design and with regulated constitution are the future of efficient wound care/cure and novel tissue engineering (Figure 6.1)

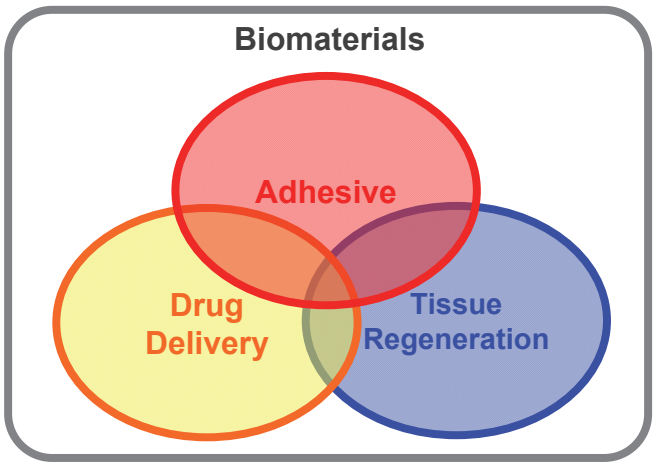

Figure 6.1. Adhesive application with drug delivery and tissue regeneration property.

List of Publications

1. Keiko Yoshizawa and Tetsushi Taguchi. Enhanced Bonding Strength of Hydrophobically Modified Gelatin Films on Wet Blood Vessels. *Int J Molecul Sci* 2014, **15**, 2142-2156.

2. Keiko Yoshizawa and Tetsushi Taguchi. Bonding Behavior of Hydrophobically Modified Gelatin Films on the Intestinal Surface. *J Bioact Compat Polym* 2014, **29**(6), 560-571.

3. Keiko Yoshizawa, Ryo Mizuta and Tetsushi Taguchi. Enhanced Angiogenesis of Growth Factor-Free Porous Biodegradable Adhesive Made with Hexanoyl Group-Modified Gelatin. Submitted.

4. Keiko Yoshizawa and Tetsushi Taguchi. Pore Size Impact on Angiogenesis and Bonding Strength in Hexanoyl Group Modified Gelatin Adhesive Films. To be submitted

5. Keiko Yoshizawa and Tetsushi Taguchi. Side Chain Length Effect on Bonding Behavior and Angiogenesis of Hydrophobically Modified Gelatin Porous Films on Wet Tissue. To be submitted

List of Presentations

International Conferences

1. Yoshizawa K. and Taguchi T., "Enhanced bonding strength of hydrophobically-modified gelatin films to soft tissues under wet condition", 2nd International Conference on Biomaterials Science in Tsukuba (ICBS2013), March 19-22, 2013, Tsukuba, Japan. (Poster)

2. Yoshizawa K. and Taguchi T., "Bonding behavior of film adhesive composed with hydrophobically-modified gelatin under wet condition", Tsukuba International Conference on Materials Science (TICMS2013), August 29-30, 2013, Tsukuba, Japan. (Poster)

3. Yoshizawa K, and Taguchi T., "Adhesion behavior of hydrophobically-modified gelatin films to soft tissues under wet condition", 25th European Conference on Biomaterials, October 8-12, 2013, Madrid, Spain. (Oral)

4. Yoshizawa K., Ito T., Mizuta R. and Taguchi T., "Stimulation of angiogenesis by growth factor-free porous adhesive films fabricated with hexanoyl group modified gelatin", NIMS Conference 2014, July 1-3, 2014, Ibaraki, Japan. (Poster)

5. Yoshizawa K. and Taguchi T., "Stimulation of angiogenesis by growth factor-free porous adhesive films made by hexanoyl group modified gelatin", 26th European Conference on Biomaterials, August 31- September 3, 2014, Liverpool, UK. (Oral)

6. Yoshizawa K., Mizuta R. and Taguchi T., "Adhesion behavior of porous adhesive films composed with hexanoyl groups modified gelatin under wet condition", WCARP-5, September 7-11, 2014, Nara, Japan. (Oral)

7. Yoshizawa K., Mizuta R. and Taguchi T., "Growth factor free porous adhesive films prepared by hydrophobically modified gelatin facilitating angiogenesis", PN&G, October 10-14, 2014, Tokyo, Japan. (Poster)

8. Yoshizawa K., Mizuta R. and Taguchi T., "Growth factor-free, porous tissue adhesive films with angiogenic activity", IPC2014, December 2-5, 2014, Ibaraki, Japan. (Poster)

9. Yoshizawa K., Mizuta R. and Taguchi T., "Growth factor-free, porous Tissue Adhesive Films With Angiogenic Activity Fabricated By Hexanoyl Group Modified Gelatin", MANA/NIMS-SACE/KNU Workshop on Nanostructured and Advanced Functional Materials, January 19, 2015, Tsukuba, Japan. (Oral)

Domestic Conferences

1. 吉澤恵子、井上元基、田口哲志 「組織接着性を有する生体吸収性フィルムの創製」
第 34 回日本バイオマテリアル学会大会、2012 年 11 月 26-27 日、仙台 (Oral)

2. 吉澤恵子、田口哲志 「湿潤組織接着性を示す疎水化ゼラチンフィルムの創製」
新宿バイオマテリアルの会、2013 年 1 月 21 日、東京 (Oral)

3. 吉澤恵子、井上元基、田口哲志 「湿潤環境下で組織接着能を有する分解性フィルムの創製」
つくば医工連携フォーラム 2013、2013 年 1 月 29 日、茨城 (Oral)

4. 吉澤恵子、田口哲志 「湿潤組織に接着する架橋剤フリー疎水化ゼラチンフィルムの創製」
第 62 回高分子学会年次大会、2013 年 5 月 29-31 日、仙台 (Oral)

5. 吉澤恵子、田口哲志 「湿潤環境下において組織との接着能を向上させた疎水化ゼラチンフィルム」
日本接着学会年次大会、2013 年 6 月 20-21 日、東京 (Oral)

6. 吉澤恵子、田口哲志 「疎水基導入ゼラチンフィルムの湿潤組織に対する接着効果」
第 35 回日本バイオマテリアル学会大会、2013 年 11 月 25-26 日、東京 (Oral)

7. 吉澤恵子、田口哲志 「疎水化ゼラチン多孔質膜の調製と軟組織接着性評価」
第 35 回日本バイオマテリアル学会、2013 年 11 月 25-26 日、東京 (Poster)

8. 吉澤恵子、田口哲志 「湿潤組織接着性を有する疎水化ゼラチン多孔膜の開発」
第 63 回高分子学会年次大会、2014 年 5 月 28-30 日、東京 (Oral)

9. 吉澤恵子、田口哲志 「組織接着性を有する疎水化ゼラチン多孔膜の開発」
つくば医工連携フォーラム 2014、2014 年 1 月 28 日、茨城 (Poster)

10. 吉澤恵子、田口哲志 「血管新生能と組織接着能を併せ持つ疎水化ゼラチン多孔質フィルムの創製」
第 36 回日本バイオマテリアル学会、2014 年 11 月 17-18 日、東京 (Oral)

11. 吉澤恵子、水田亮、田口哲志 「血管新生能と組織接着能を有する成長因子フリー吸収性多孔膜」
つくば医工連携フォーラム 2015、2015 年 1 月 23 日、茨城 (Poster)

Awards

1. ICBS 2013 TravelAward

2. 第 35 回日本バイオマテリアル学会大会ハイライト公演
   (田口哲志、伊藤典明、水田亮、吉澤恵子、秋山利正、神谷勝弘)

3. つくば医工連携フォーラム 2015　研究奨励賞

Acknowledgements

First of all, I thank my supervisor Prof. Tetsushi Taguchi for directing me in a conscientious and sophisticated manner during the course of my doctoral research. His dedicated teaching and training, not only in experiments, but also in consideration and presentation, improved my abilities. He inspires me to get up and talk. I follow his superb example and his sincere manner. I learned the attitude required to be a scientist from him.

I am also extremely grateful for Prof. Takao Aoyagi, Prof. Guopin Chen, and Prof. Seiya Tsujimura. Their advice helped to steer this project in the right direction. I could not have completed my thesis without them. They have encouraged me, both in and outside of research.

I thank Dr. Yasuyuki Katada, Dr. Kousaku Kawakami, Dr. Sachiko Hiromoto, and Dr. Yoko Shirai. Dr. Katada advised to study with a warm heart, and Dr. Kawakami helped me solve my difficulties. Dr. Hiromoto gave much wisdom and smiles, and Dr. Shirai provided great insight for my animal experiments.

I must acknowledge the people who supported me during my four years in Tsukuba. Dr. Miyuki Matsuda, Dr. Motoki Inoue, and Dr. Makoto Sasaki always offered a helping hand. I could not have completed this work without them. Ms. Tomoka Kojima and Ms. Ayako Tsubokawa kindly and politely supported me. Ms. Masami Ueno always gave helpful advice. Mr. Yoshiaki Endo, Mr. Temmei Ito, and Mr. Ryo Mizuta took valuable time from their work to help me. Ms. Hiroko Imai, Ms. Toshiko Ishizuka Ms. Sanae Sugita, Ms. Yukari Kurihara and Ms. Mayumi Katano always helped and encouraged me.

Finally, I'd like to thank my grandparents, my family, my friends, and all the people who have always supported me with a warm heart. My career in research would be nothing without them.

I also wish to extend my sincere appreciation to all the people who supported me throughout my life.